KU LEUVEN

FACULTEIT WETENSCHAPPEN

Unraveling the *in vivo* role of MMP-2 and MT1-MMP in mammalian axonal regeneration

Lien ANDRIES

Promotor: Prof. Dr. Lieve Moons

Begeleider: Dr. Manuel Salinas-Navarro

Begeleidster: Lies De Groef

Proefschrift ingediend tot het
behalen van de graad van
Master of Science in Biochemie & Biotechnologie

Departement Biologie, Dierenfysiologie en Neurobiologie
KU Leuven, Naamsestraat 61 3000 Leuven, België

Academiejaar 2014-2015

ACKNOWLEDGMENTS

Over the past year, I have worked on investigating the effect of matrix metalloproteinases on axonal regeneration. This research project would not have been possible without the support of many people. I would like to take this opportunity to thank them for their support, commitment and confidence.

I'm especially grateful to professor Dr. Lieve Moons, my promoter, for given me the opportunity to perform my thesis at the laboratory of 'Neural Circuit Development and Regeneration' and despite her busy schedule, she has not declined giving me invaluable assistance, guidance and support in the research field.

I also want to thank Dr. Manuel Salinas-Navarro, my supervisor, for helping me with my research project.

Manuel, gracias por revisar mis informes y presentaciones, por contestar todas mis preguntas y por compartir su competencia, lo que ha contribuído a mi propia experiencia.

Gracias por su apoyo en todas las fases de mi proyecto de investigación.

I want to thank Lies De Groef for the guidance, for reviewing my reports and presentations, and for the interest she showed in my project. Although she was not my supervisor from the start, her understanding and patience added a lot to my experience. I'm also grateful for all I have learned from her and for the continuous help regardless of her own work for her thesis.

I must also acknowledge all the PhD students of the laboratory of 'Neural Circuit Development and Regeneration' and of the laboratory of 'Comparative Endocrinology' for answering all my questions and always being prepared to help when needed. I especially want to thank Lut Noterdaeme for her technical support and for her assistance and advice in the lab.

Special thanks goes out to my fellow thesis students, An, Claudia, Isabelle, Julie, Jurgen, Laetitia, Sarah and Valerie, for all the memorable moments, in and outside the lab. I also want to thank my friends, especially Julie, for their support and friendship.

Family, you don't choose and that is why I know how lucky I am. I am grateful to my parents for giving me the chance to realize this thesis at the end of these 5 years of studying. Bedankt mama en papa voor een zorgeloze jeugd, voor jullie liefde, jullie steun, jullie goede raad, jullie genegenheid en jullie begrip. Bedankt om altijd klaar te staan voor mij!

I am proud to say my experience in the Laboratory of Neural Circuit Development and Regeneration was intellectually exciting and fun, and has energized me to continue in academic research.

LIST OF ABBREVIATIONS

3D	Three-dimensional
3DISCO	Three-dimensional imaging of solvent-cleared organs
AAV	Adeno-associated virus
AD	Aqua destillata
ADP	Adenine diphosphate
Akt	Protein kinase B or PKB
ANOVA	Analysis of variance
AP-1	Activator protein 1
BABB	Benylalcohol benzylbenzoaat
Bcl-2	B-cell lymphoma 2
BDNF	Brain-derived neurotrophic factor
bp	Base pair
BSA	Bovine serum albumin
C	Central
C-terminal	Carboxy-terminal
cAMP	Cyclic adenosine monophosphate
cGMP	Cyclic guanosine monophosphate
CNS	Central nervous system
CNTF	Ciliary neurotrophic factor
CPT	Chlorophenylthio
Cre	Causes recombination
CREB	cAMP respons element binding protein
CSPG	Chondroitin sulphate proteoglycan
CTB	Cholera toxin subunit B
DAPI	4',6-diamidino-2-phenylindole
DMSO	Dimethylsulfoxide
DNA	Deoxyribonucleic acid
dpi	Days post injury
DPX	Depex
e.g.	Exempli gratia, for example
E11	Embryonic age of 11 days
ECL	Enhanced chemiluminiscence
ECM	Extracellular matrix
EGF	Epithelial growth factor
ELM	External limiting membrane
ER	Estrogen receptor
F-actin	Actin filament

Fc region	Fragment crystallizable region
FG	Fluorogold
GAP-43	Growth associated protein 43
GAR	Goat anti-rabbit
GCL	Ganglion cell layer
GDi	Guanine nucleotide displacement factor
GDNF	Glial-derived neurotrophic factor
GFP	Green fluorescent protein
GLAST	Glutamate aspartate transporter
GLP	Good laboratory practices
GTPase	Guanosine triphosphatase
H&E	Hematoxylin and eosin
HRP	Horse radish peroxidase
hsp	Heat shock protein
i.e.	id est
i.p.	Intraperitoneal
Ig	Immunoglobulin
IHC	Immunohistochemistry
ILM	Inner limiting membrane
INL	Inner nuclear layer
IPL	Inner plexiform layer
JAK	Janus kinase
KB	Koninklijk besluit
kDa	Kilodalton
LDS	Lithium dodecyl sodium
LGN	Lateral geniculate nucleus
LINGO	LRR and Ig domain-containing Nogo receptor interacting protein
LoxP	Locus of X-over P1
LRR	Leucine-rich repeat
MAG	Myelin-associated glycoprotein
MMP	Matrix metalloproteinase
MQ	Milli-Q
MT	Microtubule
MT-MMP	Membrane-type matrix metalloproteinase
mTOR	Mammalian target of rapamycin
MW	Molecular weight
N-terminal	Amino-terminal
NFL	Nerve fiber layer
NgR	Nogo receptor

NHR	Nuclear hormone receptor
Nogo	Neurite outgrowth inhibitor
OCT	Optical coherence tomography
OD	Oculus dexter
OMgp	Oligodendrocyte-myelin glycoprotein
ON	Optic nerve
ONC	Optic nerve crush
ONH	Optic nerve head
ONL	Outer nuclear layer
OPL	Outer plexiform layer
OS	Oculus sinister
OS	Outer segment
P	Peripheral
P2	Postnatal age of 2 days
$p75^{NTR}$	Neurotrophin receptor p75
PAGE	Polyacrylamide gelelectrophorese
PBS	Phosphate buffered saline
PFA	Paraformaldehyde
PI	Phosphatidylinositol
PID/G/R	Pre-immuun donkey/goat/rabbit
PIP_2	Phosphatidylinositol (4,5)-diphosphate
PIP_3	Phosphatidylinositol (3,4,5)-triphosphate
PKC	Protein kinase C
PNG	Peripheral nerve graft
PNS	Peripheral nervous system
PTEN	Phosphatase and tensin homolog
PVDF	Polyvinylidene fluoride
RGC	Retinal ganglion cell
RhoA	Ras homolog gene family, member A
RI	Refractive index
RISC	RNA induced silencing complex
RNA	Ribonucleic acid
RNAi	RNA interference
ROCK	Rho kinase
RONC	Regenerative optic nerve crush
RPBMS	RNA-binding protein with multiple splicing
RPE	Retinal pigmented epithelium
rpm	Routs per minute
RT	Room temperature

SC	Superior colliculus
SCN	Suprachiasmatic nucleus
SEM	Mean values ± standard error
siRNA	Small interfering (short interfering; silencing) RNA
SOCS3	Suppressor of cytokine signaling 3
STAT	Signal transducer and activator of transcription
T	Transition
TBS	Tris-buffered saline
TGF	Transforming growth factor
THF	Tetrahydrofuraan
Thy1	Thymocyte antigen 1
TIMP	Tissue inhibitor of metalloproteinases
TNB	Tris-sodiumchloride blocking buffer
TNF-α	Tumor necrosis factor alpha
TROY	Related protein of TNFα receptor family
TSA	Tyramide signal amplification
TXF	Tamoxifen
V1	Primary visual cortex
WT	Wild-type
YFP	Yellow fluorescent protein

LIST OF FIGURES

CONTENTS

SUMMARY

Adult mammals lack the robust capacity to regenerate damaged neurons, which makes investigating new regeneration-inducing molecules essential. Matrix metalloproteinases (MMPs) are Zn^{2+}-dependent endopeptidases, that can modify the structure and activity of many substrates, including proteinases, growth factors, signaling molecules, cell surface receptors, and even intracellular targets. Deregulated MMP activity is common to many neurodegenerative disorders but, MMPs also have an important function in the developing and the adult central nervous system (CNS). Therefore, balanced MMP activity is essential.

The working hypothesis of the present study was that MMP-2 and MT1-MMP have a beneficial role on retinal ganglion cell (RGC) axonal regeneration, which was investigated using a regenerative optic nerve crush (RONC) model.

First, the RONC model and the methodology for axonal tracing on optic nerve (ON) sections were optimized. As a high inter-animal variability was experienced, the first steps towards optical clearing and three-dimensional imaging were taken. In a second part, axonal regeneration was compared in wild-type *versus* *Mmp-2*$^{-/-}$ mice and this revealed a reduced number of regenerating axons in the ON upon *Mmp-2 deletion*. Whether this was related to an altered RGC survival in the retinas of *Mmp-2*$^{-/-}$ mice remained obscure.

Additional immunohistochemical studies on retinal sections further indicated an upregulation of MMP-2 expression at 7 days post RONC and an accumulation of MMP-2 immunopositive inflammatory cells in the vitreous.

In a final set of experiments, axonal regeneration was evaluated in *Mt1-mmp*$^{flox/flox}$*;GLAST-CreER*$^{+/-}$ and the accompanying control mice. This indicated that the number of regenerating axons was decreased upon *Mt1-mmp* deletion, although the effect was less pronounced as compared to that seen in *MMP-2*$^{-/-}$ mice.

Taken together, evidence has been provided that MMP-2 as well as MT1-MMP play a beneficial role in axonal regeneration after optic nerve crush.

SAMENVATTING

Volwassen zoogdieren missen de capaciteit om beschadigde neuronen te regenereren, wat onderzoek naar nieuwe regeneratie-inducerende moleculen essentieel maakt. Matrix metalloproteinasen (MMPs) zijn Zn^{2+}-afhankelijke endopeptidasen, die de structuur en de activiteit van vele substraten, waaronder proteïnasen, groeifactoren, signaalmoleculen, celoppervlaktereceptoren, en zelfs intracellulaire doelwitten, kunnen wijzigen. Abnormale MMP activiteit is kenmerkend voor vele neurodegeneratieve aandoeningen maar MMPs zijn ook belangrijke spelers in zowel het ontwikkelend als het volwassen CNS. Daarom is een gebalanceerde MMP activiteit essentieel.

De werkhypothese van dit onderzoek was dat MMP-2 en MT1-MMP een gunstige rol in de axonale regeneratie van retinale ganglion cellen (RGC) hebben. Dit werd onderzocht met behulp van een muismodel waarbij regeneratie van de oogzenuw na beschadiging wordt geïnduceerd (*regenerative optic nerve crush*; RONC).

In het eerste deel werden het RONC model en de methodologie voor het merken van axonen in coupes van de optische zenuw geoptimaliseerd. Omdat er een hoge variabiliteit aanwezig was tussen de proefdieren, werden de eerste stappen richting *optical clearing* en driedimensionale beeldvorming genomen. In een tweede deel werd de axonale regeneratie bij wild-type *versus* *Mmp-2*$^{-/-}$ muizen vergeleken waarbij een verlaagd aantal regenererende axonen in de optische zenuw van muizen met een *Mmp-2* deletie werd vastgesteld. Of dit gerelateerd was met een wijziging in het overleven van RGCs bleef onduidelijk. Bijkomende immunohistochemische studies op retinale coupes wezen op een verhoogde MMP-2 expressie 7 dagen na RONC en op een accumulatie van MMP-2 immunopositieve inflammatoire cellen in het glasachtig lichaam.

In een laatste reeks van experimenten werd de axonale regeneratie geëvalueerd in *Mt1-mmp*$^{flox/flox}$*;GLAST-CreER*$^{+/-}$ en hun controle muizen. Dit gaf een verlaagd aantal regenererende axonen in de optische zenuw van muizen met een *Mt1-mmp* deletie aan, hoewel het effect minder uitgesproken was in vergelijking met dat waargenomen in *Mmp-2*$^{-/-}$ muizen .

Hierbij is het bewijs geleverd dat zowel MMP-2 als MT1-MMP een positieve rol spelen in de axonale regeneratie van de optische zenuw na beschadiging.

1 INTRODUCTION

1.1 STUDY RATIONALE

In contrast to the peripheral nervous system (PNS) (Schwob, 2002; Czaja *et al*, 2012), the central nervous system (CNS) of adult mammals lacks the robust capacity to replace lost neurons (*de novo* neurogenesis) or to repair injured axons (axonal regeneration) (Yin *et al*, 2009; Kurimoto *et al*, 2013; Benowitz & Popovich, 2011). Damage to the CNS after injury or in neurodegenerative diseases is often characterized by axonal degeneration, followed by progressive neuronal death. Neurotrauma or degeneration drastically diminishes life quality in our aging society and leads to severe impairments. Over the last decades, the repair of long neuronal pathways, such as the optic nerve (ON), has gone from strongly contested to being recognized as a potential clinical challenge (Thanos *et al*, 2012). In order to establish successful and novel regenerative therapies promoting neuronal repair, our knowledge about the molecules and mechanisms underlying axonal outgrowth and navigation has to be expanded. However, despite intensive research efforts, complete restoration of neuronal function and induction of axonal regeneration and proper guidance to achieve subsequent functional recovery of the injured mammalian CNS remain a challenge. This makes the search for new molecules involved in axonal outgrowth and navigation indispensable. Using the visual system as a model, considerable progress has been made towards the identification of multifactorial causes underlying the restricted regeneration potential of the mammalian CNS. The visual system is the most accessible part of the CNS and therefore forms a powerful model to improve our understanding (Benowitz & Yin, 2008). The morphology and functionality of the retina is well-characterized, the axons of the ON arise from a single neuronal cell population, the retinal ganglion cells (RGCs) can be experimentally manipulated with minimal surgery, the typical organization of glial cells facilitates the study of glial reactivity after damage (Berry *et al*, 2008), while the vitreous can be used as a reservoir for certain drugs, molecules and genes (Benowitz & Yin, 2008).

1.2 AXONAL REGENERATION IN THE ADULT CNS

1.2.1 THE VISUAL SYSTEM

The visual system consists of the retina, the ON, the optic chiasm, the optic tract and the target areas in the brain, like the nuclei in the thalamic midbrain and the primary visual cortex (V1). It all begins with the eyes, which extract information from the environment via detection of light within the retina. In the neuroretina, the incoming photons are translated into electrical signals by the photoreceptors. These pass on the signals through the axons of the RGCs to the brain where the information is further processed in the superior colliculus (SC), the lateral geniculate nucleus (LGN) and V1 (Bear *et al*, 2006; Remington, 2011).

1.2.1.1 ANATOMY OF THE EYE

The eye is fixed in his bony orbit by the conjunctiva and consists of three layers, the fibrous layer, the vascular layer and the inner layer (figure 1) (Bear *et al*, 2006; Martini *et al*, 2014; Purves *et al*, 2004).

The outer fibrous layer involves the cornea and the sclera, which is the white coat that protects and supports the eye. Three pairs of extraocular muscles attached to the sclera control the eye movements. The sclera is continuous with the cornea, the glassy transparent external surface of the eye. The cornea covers the iris and pupil and exists of multiple layers of collagen fibers, organized to not interfere with the passage of light. The limbus is the site where the sclera merges with the cornea (Bear *et al*, 2006; Martini *et al*, 2014; Purves *et al*, 2004).

The vascular layer is the middle layer that consists of the iris, the ciliary bodies and muscles and the choroid. The ciliary bodies are responsible for the secretion of the aqueous humor, while the capillary network in the choroid delivers nutrients and oxygen to the retina. The pupil is a circular opening in the iris, a colored smooth muscle that acts as a diaphragm to ensure optimal light exposure to the retina. The ciliary muscles attached to the zonule fibers, allow the lens to change its shape, which is an essential part of the focusing process (Bear *et al*, 2006; Martini *et al*, 2014; Purves *et al*, 2004).

Finally, the light is focused on the inner layer or retina that receives the photons (Bear *et al*, 2006; Martini *et al*, 2014; Purves *et al*, 2004).

The lens is located behind the pupil, dividing the eye into an anterior and a posterior segment. It is composed of concentric layers of lens fibers, which are made up of transparent proteins, called crystallins. These proteins give the lens both its clarity and its focusing power (Bear *et al*, 2006).

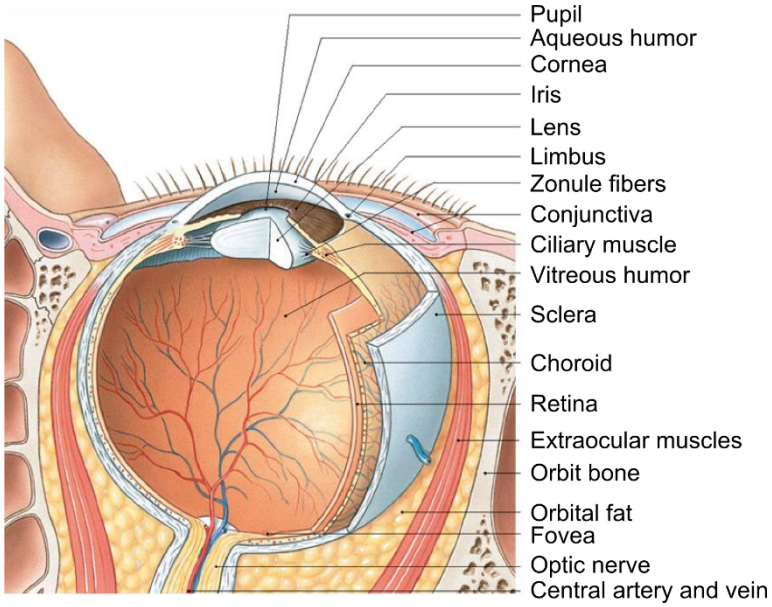

Figure 1: Cross section of a human eye. The posterior segment of the human eye is made up of three layers, the outer layer is called the sclera, the middle layer is the choroid and the inner layer is called the retina. The retina is specialized to convert light energy into neuronal activity. Several other structures of the eye regulate the amount of light that reaches the retina and result in light refracting onto the retina. Reproduced from (Martini *et al*, 2014).

The anterior segment of the eye can be divided into two chambers, the anterior chamber between the cornea and the iris and the posterior chamber between the iris and the lens. The fluid in the anterior segment, which flows from the posterior chamber to the anterior chamber, is termed the aqueous humor and is responsible for generating the intraocular pressure. Reabsorption of the aqueous humor occurs mainly in the anterior chamber of the eye via the trabecular meshwork and the canal of Schlemm. The fluid in the posterior segment between the lens and the retina, is called the vitreous humor and has a more gelatinous consistency, which helps maintaining the shape of the eye (Bear *et al*, 2006; Martini *et al*, 2014; Purves *et al*, 2004).

1.2.1.2 ANATOMY OF THE RETINA

The retina is composed of five neuronal cell types: photoreceptors, bipolar cells, RGCs, horizontal cells and amacrine cells (figure 2A). These cell types have a laminar organization (figure 2B). The layer of the outer segments (OS) of the photoreceptors contains the light sensitive elements of the retina and is separated from the outer nuclear layer (ONL), which holds the cell bodies of the photoreceptors, by the external limiting membrane (ELM). The outer plexiform layer (OPL) where the photoreceptors make contact with bipolar and horizontal cells, follows the ONL. The cell bodies of bipolar cells, as well as the cell bodies of horizontal cells and amacrine cells, are located in the inner nuclear layer (INL). In the inner plexiform layer (IPL), bipolar cells connect with amacrine cells and RGCs (Bear *et al*, 2006; Martini *et al*, 2014; Hildebrand & Fielder, 2011). Next, the ganglion cell layer (GCL) contains the cell bodies of the RGCs and the displaced amacrine cells. (Hildebrand & Fielder, 2011;

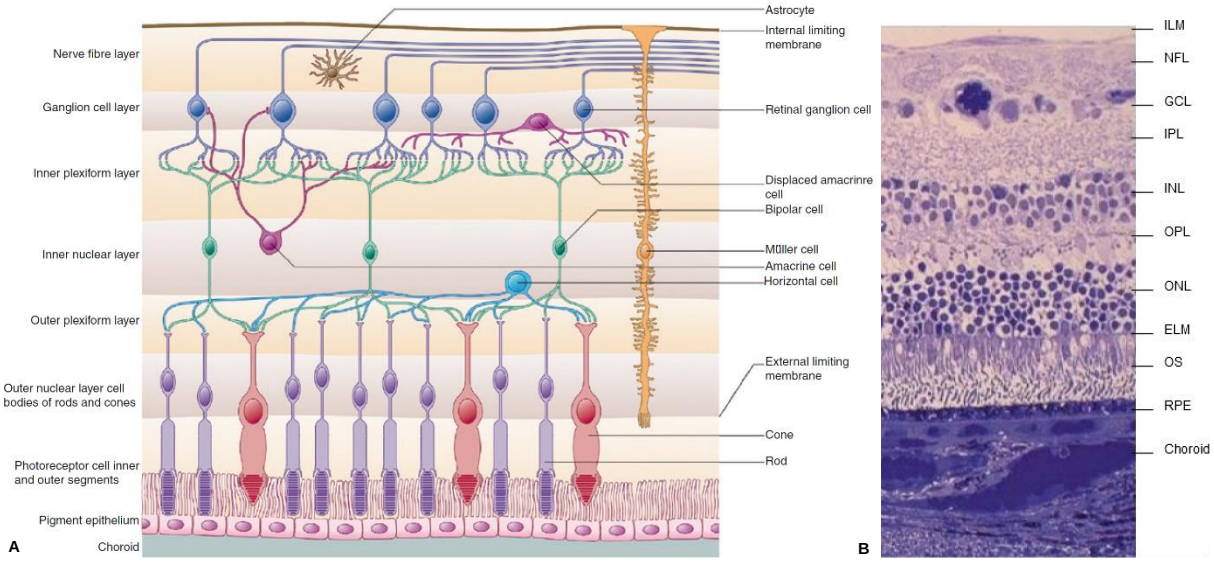

Figure 2: A) The different cell types and laminar organization of the retina. The direct pathway of information processing in the eye is from photoreceptors (purple/red) to bipolar cells (green) to ganglion cells (dark blue). The indirect pathways involve the horizontal cells (light blue) and the amacrine cells (magenta), which modify the responses of bipolar cells and ganglion cells via lateral connections. The ganglion cells project axons out of the eye in the ON. The five different cell types are organized in layers in such way that light must pass through all cell layers of the neuroretina before it reaches the photoreceptors. The Müller cells (orange) and astrocytes (brown) are also present in the retina. **B) Hematoxylin and eosin staining of a transverse section of the retina and the choroid showing the different layers**. Reproduced from (Standring, 2008).

Standring, 2008). At last, there is the nerve fiber layer (NFL) including the axons of the RGCs and covered by the inner limiting membrane (ILM). This laminar organization implies that light has to pass from the vitreous humor through two nuclear and two plexiform layers before it reaches the photoreceptors. The direct pathway for visual information to leave the eye is from photoreceptors to bipolar cells to RGCs. The latter are the only source of output from the retina. The RGC axons leave the eye at the optic nerve head (ONH) and are collected in a bundle called the ON. This pathway can be influenced by two additional cell types or interneurons. The horizontal cells receive input from photoreceptors and influence surrounding bipolar cells and photoreceptors. Amacrine cells receive input from bipolar cells and influence surrounding RGCs, bipolar cells and other amacrine cells (Bear *et al*, 2006; Martini *et al*, 2014; Purves *et al*, 2004). The fovea is a thinning of the retina due to the lateral displacement of the cells above the photoreceptors, allowing the light to strike the photoreceptors without passing through the other layers of the retina. In humans, the fovea can be used as an anatomical reference point. The part closer to the nose is the nasal retina and the part closer to the ear is the temporal retina. The superior and inferior retina are located respectively above and below the fovea.

Besides the neuronal cells, there are several glial cell types present in the retina. The Müller glia support and protect the neurons. Their perikarya are mainly found in the INL with cell processes that span the entire neuroretina. Astrocytes are macroglia derived from stem cells in the ON and control the chemical environment of the neurons. The microglia are resident macrophages of the retina and act as the first and main form of active immune defense in the CNS. Upon injury, other macrophages can be recruited from the circulation (Bear *et al*, 2006). The axons of the RGCs are myelinated in the ON by brain-derived oligodendrocytes (Benowitz & Yin, 2008; Hildebrand & Fielder, 2011). Finally, the retinal pigmented epithelium (RPE) forms the outermost rim around the neuroretina that plays a critical role in the maintenance of the photoreceptors and photopigments. The RPE absorbs light that passes entirely through the retina to prevent scattering in the eye (Bear *et al*, 2006; Martini *et al*, 2014; Purves *et al*, 2004).

1.2.1.3 RETINOFUGAL PROJECTION

At the optic chiasm, partial decussation of RGC axons takes place (figure 3A). In humans, approximately 50% of the axons remain ipsilateral, while the other 50% project contralateral. As such, information about the left visual hemifield is projected via the right optic tract to the right brain hemisphere, whereas axons from RGCs gathering information from the right visual hemifield project axons into the left optic tract and to the left brain hemisphere. The RGC axons first reach the suprachiasmatic nucleus (SCN) before innervating the SC (~10) and the LGN (90%), which are the key targets of the optic tract (figure 3B). The SC coordinates the eye and head movements, the so-called saccadic eye movements. The LGN is a relay station for the axons that are projecting to V1 via optic radiation (Bear *et al*, 2006).

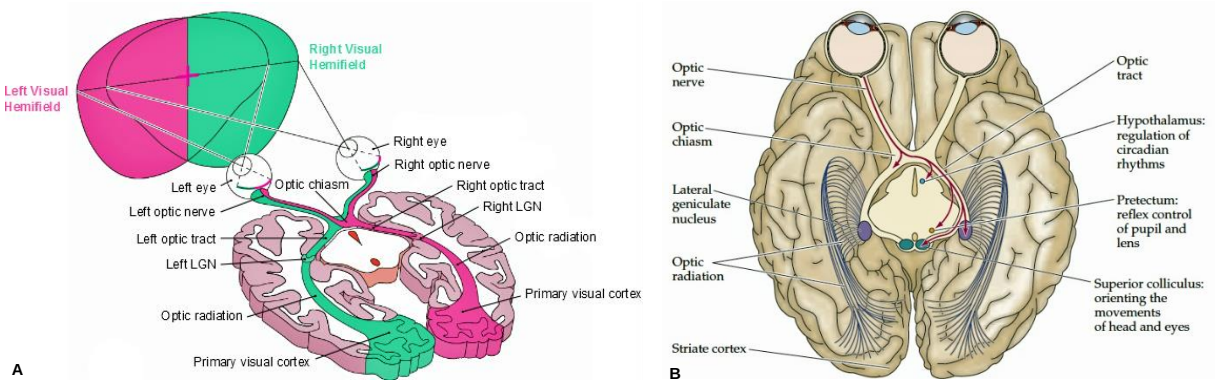

Figure 3: A) The retinofugal pathway from retina to V1. Light enters the eye via the pupil and the retina converts photons into electrical signals. These are transduced via the optic nerve, the optic chiasm and the optic tract to the LGN. The axons project into the V1 via optic radiation. The complete left visual hemifield is viewed by the right hemisphere of the brains and the complete right visual hemifield is viewed by the left hemisphere of the brains. **B) Target areas in the brain of the RGCs.** In addition to the LGN, the axons of RGCs also project in the SC, the pretectum, and the SCN. Reproduced from (Bear *et al*, 2006; Purves *et al*, 2004).

1.2.1.4 COMPARISON WITH VISUAL SYSTEM OF THE MOUSE

The visual system in most mammals is similar in structure and function (Levkovitch-Verbin, 2004; Tkatchenko *et al*, 2010; Waterston *et al*, 2002). Therefore, adult rodents are frequently used as experimental animal models despite the fact that there are some differences compared to humans. Thanks to these model organisms, our knowledge of the biology of human diseases is expanding and potential therapies to be used in humans can be evaluated (Levkovitch-Verbin, 2004).

In rodents, approximately 60% of the neuronal population in the RGC layer consists of displaced amacrine cells (Perry, 1981; Jeon *et al*, 1998) whereas in humans, this is 3% of the neuronal population in the central and 80% of the neuronal population in the far peripheral retina (Curcio & Allen, 1990). The majority of rodent RGCs projects their axon to the SC (98%) and only 2% projects to other targets like the LGN or the SCN, whereas in humans this is ~10% *versus* 90%, respectively. Due to the lateral displacement of the eyes, the mouse has a larger visual field but a smaller binocular visual field. As a consequence, over 90% of the axons decussates at the optic chiasm, unlike humans where only 50% decussates (Levkovitch-Verbin, 2004; Hübener, 2003; Erskine & Herrera, 2007; Salinas-Navarro *et al*, 2009; Lambot *et al*, 2005). Other differences are that the lenses of rodents are rounder, less flexible and occupy a larger portion of the eye, and that no fovea is present. In addition, 97% of the photoreceptors in the retina are rods, which adjust the visual system of rodents to their nightlife (Tkatchenko *et al*, 2010).

1.2.2 GENERATION AND REGENERATION OF AXONS

1.2.2.1 AXON GROWTH

The capacity of axons to grow and navigate is mediated by the growth cone, a specialized and highly dynamic structure that is located at the distal tip of the growing axon (figure 4A). The tip of the growth cone consists of two types of structures, thin finger-like filopodia that are separated by veil-like lamellipodia. Based on the cytoskeletal distribution, the growth cone is divided into three domains. The peripheral (P-) domain contains the filopodia, consisting of long bundled actin filaments (F-actin bundles), and the lamellipodia, which are characterized by F-actin networks. Thanks to their highly dynamic microtubules (MTs), the filopodia can continuously protrude and retract, and as such explore the extracellular environment. The central (C-) domain is a thicker region, containing multiple organelle and stable, bundled MTs that enter the growth cone from the axon shaft. The transition (T-) zone is located at the interface of the P- and C-domain and consists of the actomyosin contractile structures called actin-arcs (Lowery & Van Vactor, 2009; Dent & Gertler, 2003; Erskine & Herrera, 2007).

The dynamics of these cytoskeleton elements determines the shape and movement of the growth cone (Lowery & Van Vactor, 2009).

To form new axon segments, growth cones progress through three morphologically distinct stages termed protrusion, engorgement and consolidation. First, during the protrusion phase, when the distal end of the growth cone has encountered an attractive or repellant, the adhesive substrate binds to the growth cone receptors (figure 4Ba). This will activate intracellular signaling cascades and will lead to the formation of a mechanical complex that

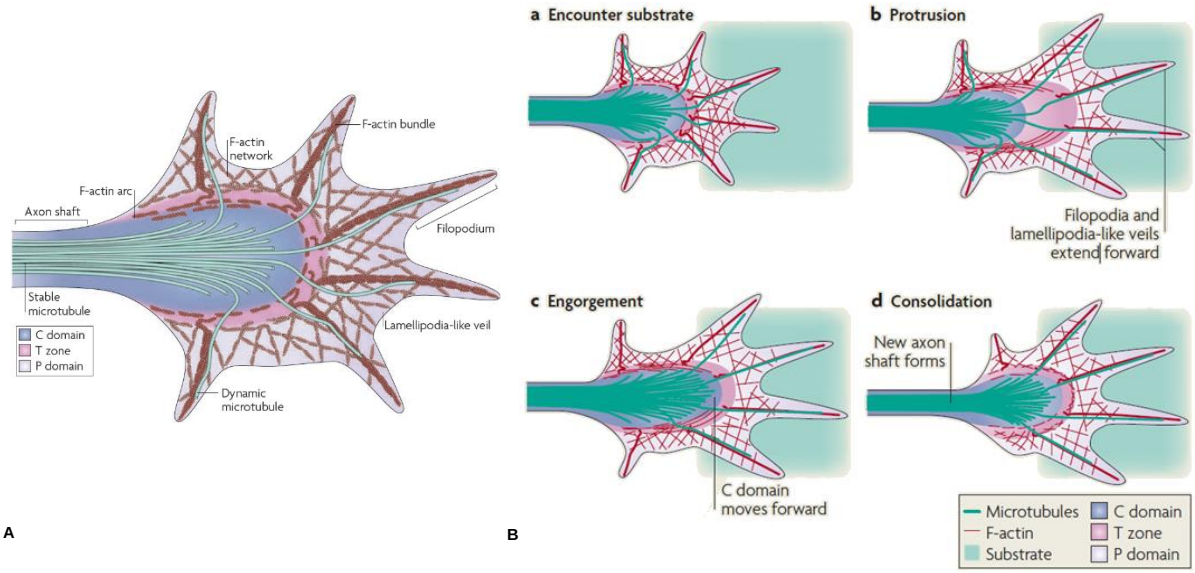

Figure 4: A) Structure of the growth cone. The structure of the growth cone is essential to its function. Changes in the cytoskeleton of the growth cone determine axon growth and navigation. **B) Stages of axon outgrowth.** The axonal outgrowth is divided into three stages: protrusion, engorgement and consolidation. a) Encounter substrate: the distal end of the growth cone contacts with an adhesive substrate. b) Protrusion: lamellipodia and filopodia move forward to extend their leading edge. c) Engorgement: the C-domain moves forward. d) Consolidation: the neck of the growth cone compacts to form a new segment of axon shaft. Reproduced from (Lowery & Van Vactor, 2009).

acts as a molecular clutch, coupling the substrate and the actin cytoskeleton. Next, as F-actin polymerization occurs, the clutch is strengthened and the lamellipodia and filopodia of the P-domain move forward to extend on the adhesive substrate (figure 4Bb). The phase of engorgement starts after the disappearance of F-actin between the adhesion site and the C-domain and the reorientation of the F-actin arcs from the C-domain towards the site of new growth. Eventually, the C-domain MTs are guided by the T-zone actin arcs to further invade the growth cone, fixing the axonal growth direction and resulting in a forward movement towards the adhesive site (figure 4Bc). Finally, axon shaft consolidation of the recently advanced C-domain occurs, as the contractile actin arcs compact the MTs to form a cylindrical axon shaft into the newly localized C-domain. Finally, the novel axon segment is further stabilized by MT-associated proteins and filopodia activity is suppressed in this region in order to promote axon shaft consolidation (figure 4Bd) (Lowery & Van Vactor, 2009; Dent & Gertler, 2003).

1.2.2.2 AXON NAVIGATION

The rate and direction of axon extension are controlled by the interaction of growth cones with their extracellular environment. Growth cones carry molecular receptors to direct them to their destination by responding to gradients of navigation cues in the extracellular matrix (ECM). The growth of the axon in a certain direction is stimulated (promoting growth towards a specific region) or inhibited (preventing growth in a particular direction) depending on the attractive or repulsive signals. These molecules can be associated with the ECM and work in a contact-dependent fashion or act at a distance via secreted diffusible factors. The same signal can provoke different responses depending on the type of neurons, and different cues can influence each other via interactions at the cell membrane and complicated networks of intracellular signaling cascades. There are four well-characterized families of axon guidance molecules: ephrins, semaphorins, netrins and Robos/Slits. However, many other molecules controlling axon navigation have been identified over the past decades (Lowery & Van Vactor, 2009; Erskine & Herrera, 2007; Chilton, 2006; Dickson, 2002; Huber *et al*, 2003; Dent & Gertler, 2003).

By binding to their receptors present on the growth cone, these axon guidance molecules activate intracellular signal cascades that induce changes in the cytoskeleton, resulting in altering the direction and rate of the growth cone (Erskine & Herrera, 2007).

During development, *de novo* neurogenesis results in the formation of newborn neurons, from which newly formed axons have to extend and navigate to reach their targets. As animals enlarge their body size during postnatal and adolescent stages, the distance from neuron to target increases. By consequence, damaged axons in the adult CNS have to overcome much longer distances than those travelled by the initial, *de novo* growing axons in the developing CNS. Moreover, a high level of morphological specialization and cellular complexity is present in the mammalian adult neural circuits, which makes it even more

difficult for the axons to reach their proper targets. During regeneration of the RGCs, these neurons have to extend their axons over considerable distances with a multitude of potential targets presented on route before they reach, recognize and form synapses with the appropriate target cells (Erskine & Herrera, 2007).

Visual information is relayed from the eye to the brain via the axons of the RGCs. In the retina, the axons of the RGCs extend into the NFL at the inner surface of the retina, where they grow towards their exit point out of the eye, the ONH, and form the ON. The ONs of the left and right eye meet at the optic chiasm where the axons choose the right direction (ipsilateral or contralateral) and project their axons within the optic tracts towards their targets in the brain e.g., the SC (in the midbrain), the LGN (in the thalamus) or the SCN (in the hypothalamus) (figure 3B). Despite differences in organization of the RGC axons in different organisms, studies reveal a high degree of conservation in the underlying navigation mechanisms (Erskine & Herrera, 2007; Herrera *et al*, 2003; Nakagawa *et al*, 2000; Haupt & Huber, 2008; Lowery & Van Vactor, 2009).

1.2.2.3 AXONAL REGENERATION

In non-mammals, robust axonal regeneration is observed in the injured CNS, however, adult mammals seem to have lost this capability. Indeed, although the damaged axons in their CNS do exhibit an early growth response, this response is abortive and does not lead to the complete repair of the axons. Instead, this sprouting response is followed by axonal degeneration and ultimately even neuronal cell death. On the contrary, axonal regeneration does occur in the mammalian PNS. One of the reasons underlying the lack of robust regeneration in the mammalian CNS, can therefore be deduced from the major difference between the CNS and PNS, the strong inhibitory glial environment present in the CNS (Goldberg *et al*, 2002). Prior to myelination, injured axons in the CNS can regrow, but after myelination, post-injury axonal growth is inhibited. Macrophages and Schwann cells in the PNS rapidly clear myelin after injury and downregulate all myelin proteins and their debris. In the CNS, oligodendrocytes only provide minimal growth support or phagocytic activity and even tend to undergo apoptosis (Filbin, 2003; Benowitz & Yin, 2010).

The inability of damaged CNS axons to regenerate is thus largely due to several inhibitory signals present in the ECM like myelin- and glial scar-derived inhibitory factors. The lack of neurotrophic support also contributes to the reduced regeneration capacity of the CNS in mammals. In addition, adult neurons have a low intrinsic potential to regenerate their axons. By consequence, substantial levels of *in vivo* axonal regeneration would require combinatorial treatments that counteract extrinsic inhibitors and activate the intrinsic growth state of neurons at the same time (Benowitz & Yin, 2007, 2008, 2010; Fitch & Silver, 2008; Filbin, 2003; Domeniconi *et al*, 2002).

1.2.2.3.1 EXTRINSIC INHIBITION

Myelin-derived inhibitory factors

Inhibitors of axonal regeneration present in myelin prevent recovery of the injured adult mammalian CNS. Three myelin proteins, neurite outgrowth inhibitor (Nogo) A, oligodendrocyte-myelin glycoprotein (OMgp) and myelin-associated glycoprotein (MAG), all found in the myelin membrane immediately adjacent to the axon, inhibit axon growth through the same receptor complex (figure 5). NogoA is a splice variant of a reticulon protein that is produced by the oligodendrocytes and is usually associated with the endoplasmatic reticulum (Prinjha *et al*, 2000; Chen *et al*, 2000; Grandpré *et al*, 2000; Benowitz & Yin, 2007, 2008; Filbin, 2003). However, it is also found on the oligodendrocyte surface and on the innermost loop of the myelin membrane, where it can make contact with the axon. The 66 amino acid region at the C-terminus of NogoA is one of the inhibitory domains that binds with high affinity to the Nogo receptor (NgR) (Benowitz & Yin, 2007; Fournier *et al*, 2001; Huber *et al*, 2002; Filbin, 2003). The other inhibitors of axon growth are OMgp and MAG, though in some cases the latter can promote axon growth in immature neurons. OMgp is a glycosyl phosphatidylinositol (PI)-linked protein and is expressed by both oligodendrocytes and neurons. MAG is a member of the immunoglobulin super family and is a sialic acid-binding protein (Benowitz & Yin, 2007; Cai *et al*, 2001; Filbin, 2003). Although there is no obvious sequence or domain similarity between NogoA, MAG and OMgp, they use the same receptor complex to induce growth cone collapse and inhibit axon outgrowth. Nevertheless, other receptors may be involved as well, because after enzymatic cleavage or genetic deletion of NgR, neurons continue to respond to inhibitory myelin proteins. This competition for binding

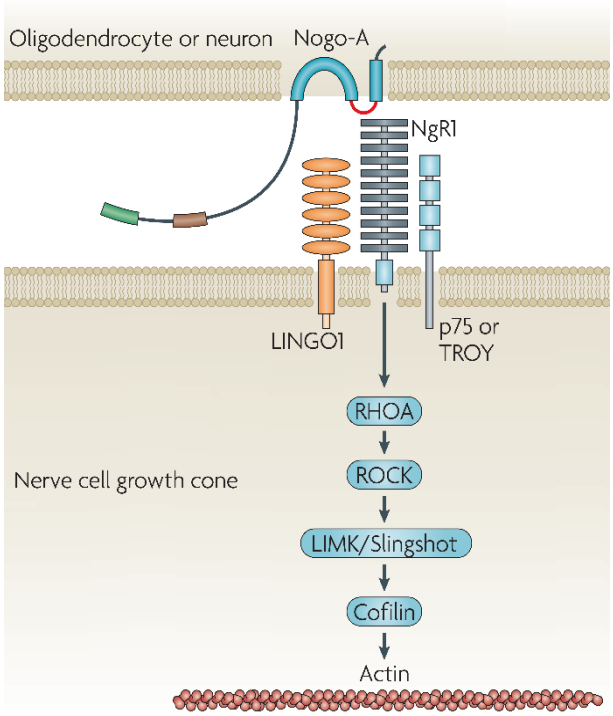

Figure 5: Inhibitory pathway of NogoA. NogoA interacts with the phosphatidylinositol-linked NgR to inhibit axon outgrowth. NgR interacts with LINGO1 and $p75^{NTR}$/TROY to transduce the signal across the membrane and activate RhoA to bring about inhibition. OMgp and MAG can use the same inhibition pathway. Reproduced from (Schwab, 2010) .

the same receptor may explain the redundancy observed when a single inhibitory component is blocked *in vivo* (Domeniconi *et al*, 2002; Liu *et al*, 2002; Venkatesh *et al*, 2005; Wang *et al*, 2002; Zheng *et al*, 2005).

NgR is a PI-linked protein without a transmembrane domain. It has to form a complex with two other proteins to transduce the inhibitory signal across the membrane of the neurons. One of these is LINGO (LRR (leucine-rich repeat) and Ig (immunoglobulin) domain-containing, Nogo Receptor interacting protein), the second is either the neurotrophin receptor p75 ($p75^{NTR}$) or TROY (a related protein of the TNFα receptor family). These receptors play an important role in cell death, migration of Schwann cells, modulation of synaptic transmission and functional regulation of sensory neurons and axon elongation. All of these processes are mediated by the activity of Ras homolog gene family, member A (RhoA), that is modulated by the NgR-LINGO-$p75^{NTR}$/TROY complex. RhoA is a guanosine triphosphatase (GTPase) that regulates the state of actin polymerization via a guanine nucleotide displacement factor (Rho-GDi). When ligand is bound to the NgR-LINGO-$p75^{NTR}$/TROY complex, Rho-GDi associates with $p75^{NTR}$, enabling RhoA to be converted to its active state. Activated RhoA binds to GTP, activating his downstream effector, Rho kinase (ROCK), which results in rigidificiation of the actin cytoskeleton and growth cone collapse, thereby terminating the elongation of the axons. Matrix metalloproteinases (MMPs) have the capacity to degrade many of these myelin-derived inhibitory factors (Yamashita & Tohyama, 2003; Benowitz & Yin, 2008; De Groef *et al*, 2014).

Glial scar-derived inhibitory factors

In addition to myelin, the scar tissue that forms at the site of neuronal injury (gliosis) is a major barrier to axonal regeneration in the CNS. Regenerating axons that cross such a glial scar, undergo dystrophy of the end bulbs and cannot elongate. The scar mainly consists of reactive astrocytes which change their morphology to become a physical barrier to axonal regrowth and upregulate several ECM-associated inhibitors of regeneration. Proteoglycans, like chondroitin sulphate proteoglycan (CSPG), are also present in the glial scar. CSPGs inhibit axon growth in the adult CNS through the activation of RhoA and ROCK. In addition, CSPGs are also known to be present outside the glial scar, e.g., to limit axonal growth, to repel axons from inappropriate regions and to restrict structural plasticity during CNS development. Also the glial scar-derived factors can be degraded by MMPs (Benowitz & Yin, 2007, 2008; Wehrle *et al*, 2005; Ahmed *et al*, 2005; De Groef *et al*, 2014).

Counteracting extrinsic inhibitors

During the last decennia, researchers have tried to produce extensive RGC regeneration in the ON by counteracting inhibitory signaling. Methods to inhibit the activity of NogoA have been the administration of antibodies against NogoA or introducing a dominant-negative form of the NgR in the genomes of RGCs. Another way to overcome inhibitory signals is to interfere with RhoA, which is inactivated by C3 ribosyltransferase. These approaches had

little success. A possible reason is that even when overcoming one of the major inhibitors, other ones are still in place. Another plausible argument is that even when all inhibitory signals are neutralized, the axons still need to be stimulated to a growth-enabled state. So, it is important that when one wants to stimulate robust axonal regeneration, one should focus on both extrinsic inhibitors and the intrinsic growth capacity of the neurons. Without taking the intrinsic state of the neuron into account, one will never observe more than a moderate effect of axonal regeneration (Benowitz & Yin, 2007, 2008, 2010; Fischer *et al*, 2004a).

1.2.2.3.2 INTRINSIC GROWTH POTENTIAL

In addition to the extrinsic inhibitors, a strong intrinsic neuronal growth capacity is elementary for the regeneration of axons. RGCs undergo a marked shift in their intrinsic growth state and experience different growth stages during the course of development. RGCs are derived from retinal progenitor cells. In mice, RGCs differentiate between the embryonic age of 11 to 19 days (E11-E19). Once differentiated, they begin to form axons and show rapid axon elongation. After birth, axon growth gradually slows down. The axons reach the SC between birth and 6 days postnatal (P0-P6). RGCs in mice older than P2 exhibit slow axon growth and switch to prolific dendritic differentiation (Sernagor *et al*, 2001; Dallimore *et al*, 2002). The intrinsic growth state of the RGCs appears not to change cell-autonomously but requires direct contact with the amacrine cells. Adult RGCs can be programmed to undergo a shift in growth potential that resembles the growth stages during development.

To achieve this switch, the signaling pathways that regulate RGC survival and RGC axonal outgrowth need some adjustments. Reports have implicated the involvement of two well-known signaling pathways utilizing cyclic adenosine monophosphate (cAMP) response element binding protein (CREB) and signal transducer and activator of transcription 3 (STAT3). Recent findings also associate protein kinase C (PKC), B-cell lymphoma 2 (Bcl-2) and integrins with neuronal regeneration (Teng & Tang, 2006). Studies show that there are dramatic changes in gene expression when RGCs are stimulated to regenerate their axons. For example, enhanced neurotrophins, in the form of brain-derived neurotrophic factors (BDNFs) and glia-derived neurotrophic factors (GDNFs), could block the growth inhibitory effects of the CNS neurite growth inhibitor MAG by elevating cAMP levels. These alterations resemble those seen in axons of the PNS undergoing regeneration. As an example, some of the major known molecules like growth associated protein (GAP) -43, cAMP and Bcl-2 are mentioned in following paragraphs (Goldberg *et al*, 2002; Benowitz & Yin, 2007; Teng & Tang, 2006).

GAP-43

Proteins expressed by RGCs, which are forming axons and synapses, become downregulated in adult stages. An example is GAP-43, which is a membrane phosphoprotein that is present in high concentrations when RGCs are extending their axons and synaptogenesis is ongoing, but becomes downregulated to almost undetectable levels in

adult stages. The RGCs that experience damage show only a small, transient upregulation. However, GAP-43 levels are strongly upregulated in RGCs that are stimulated to regenerate their axons (Benowitz & Yin, 2007; Fischer *et al*, 2004b).

cAMP

Small intracellular messenger molecules play a crucial role in the signaling cascades that translate extracellular signals into axonal elongation, navigation and synaptogenesis. For example, the response of the axon to an axon guidance molecule is strongly determined by the intracellular concentration of cAMP ($[cAMP]_i$). Elevated $[cAMP]_i$ facilitates axon growth in several ways. In general, $[cAMP]_i$ elevation is required for RGCs to respond to most factors that support cell survival and axon outgrowth. It induces the growth factor receptors to translocate from the cytoplasm to the cell membrane. $[cAMP]_i$ levels also determine whether growth cones are attracted or repelled by various guidance molecules. Indeed, signals that normally repel axons can become attractive in the presence of cAMP. For example, MAG stimulates the growing RGCs, which are featured by an elevated ratio of $[cAMP]_i$ to cyclic guanosine monophosphate (cGMP), and inhibits adult RGCs, which are featured by a low ratio of $[cAMP]_i$ to cGMP. Finally, cAMP mediates the 'priming' effect of trophic factors for overcoming extrinsic growth inhibitors. $[cAMP]_i$ has a relatively modest effect on enabling axon outgrowth into the ON, though excessive high $[cAMP]_i$ can work counterproductive (Cai *et al*, 2001; Benowitz & Yin, 2007).

Bcl-2

RGCs of which the axons are damaged normally endure apoptosis due to energy depletion or trophic factor withdrawal. This results in the activation of an intracellular signaling cascade, involving immediate early genes, pro- and anti-apoptotic members of the Bcl-2 family, and caspases. This process can be prevented by overexpression of anti-apoptotic proteins of the Bcl-2 family. Although the survival of the damaged axons is essentially complete, they will not regenerate into the ON. Axonal regeneration clearly requires RGCs to remain viable but RGC survival alone is clearly not sufficient to induce axon outgrowth. It seems that RGC cell survival and RGC axonal outgrowth rely on different intracellular signaling pathways (Bähr, 2000).

1.2.2.3.3 NEUROTROPHIC SUPPORT

In addition to the decrease in intrinsic growth capability and presence of extrinsic inhibitors, the injured CNS becomes deprived of neurotrophic factors. These factors are responsible for the growth and survival of developing neurons and the maintenance of mature neurons. Neurotrophic factors like ciliary neurotrophic factor (CNTF) and BDNF are capable of supporting the survival of injured CNS neurons both *in vitro* and *in vivo*. They also stimulate neurite outgrowth, needed for reorganization of the injured CNS, and the expression of key enzymes for neurotransmitter synthesis that may need to be upregulated to compensate for reduced innervation (Deister & Schmidt, 2006).

1.2.3 Recent strategies to Induce Long-Distance RGC Axonal Regeneration

Over the past years, many studies identified several strategies to induce long-distance axonal regeneration in the ON. The extracellular inhibitors and the factors that influence the intracellular growth capacity of the axons mentioned in previous paragraphs can all be targets for therapies to induce axonal regeneration. The most important methods, currently used to induce RGC regeneration, are peripheral nerve grafting (Yin *et al*, 2009), administration of neurotrophins such as CNTF (Pernet *et al*, 2013a; Leaver *et al*, 2006), deletion of genes such as phosphatase and tensin homologue (*Pten*) and/or suppressor of cytokine signaling 3 (*Socs3*) (Sun *et al*, 2011) and administration of ROCK inhibitors (Pernet *et al*, 2013b). Within the optic system, partial axonal regeneration can also be obtained via induction of controlled inflammation and glial reactivity. In addition, combinations of these methods can also be used to induce even more regeneration (Benowitz & Popovich, 2011; Lorber *et al*, 2012).

1.2.3.1 Peripheral nerve grafting

Cajal's student, Tello, provided the first piece of evidence that mature neurons of the CNS retain some capacity to regenerate their axons (Benowitz & Yin, 2008, 2007). He discovered that, in rats, if the ON is cut and given the opportunity to grow into a peripheral nerve graft (PNG), approximately 5% of the RGCs can regenerate their axons into the graft. Some of them get all the way through the PNG, which extends from the eye to the SC, and form synapses in the correct retinal recipient layers of the SC. These results are probably obtained due to the more permissive environment of the PNS *versus* the CNS environment. In addition, these transplants appear to contain a higher level of growth-permissive factors (e.g., laminin and GAP-43) and a lower concentration in growth inhibiting factors (e.g., NogoA). The PNG provides essential neurotrophic factors and activates macrophages that are believed to be responsible for the axon growth promoting effect (Benowitz & Yin, 2008, 2007, 2010).

1.2.3.2 Neurotrophic factors

In mice, the effects of intraocular injections of the recombinant CNTF peptide are probably restricted in time because of the short half-life of this recombinant peptide and the negative feedback control mediated by the upregulation of SOCS3. To sustain CNTF delivery, adeno-associated virus (AAV) vectors, which encode a modified secretory form of CNTF and selectively infect RGCs, are injected intravitreally. This promotes the survival of adult RGCs (neuroprotection) and stimulates the regeneration of many RGC axons across the ON crush site, some growing as far as the optic chiasm (Pernet *et al*, 2013a). In addition, many regenerating axons showed sharp U-turns and aberrant axonal sprouting at the inner surface of the retina, suggesting that guidance cues are missing and that the distance of axonal

regeneration is decreased by the return of the growing axons towards the retina. After AAV-CNTF-GFP injections and PNG, about 25% of adult RGCs remained viable at 7 weeks post peripheral nerve transplantation and about half of these cells regenerated axons 1-1,5cm into the autologous PNG. Again, axonal misguidance is a key limiting factor for long-distance axonal regeneration with this approach (Leaver *et al*, 2006; Smith *et al*, 2009).

Intravitreal AAV-BDNF-GFP injections also enhanced RGC survival at 7 weeks after optic nerve crush (ONC). Although many axons were seen proximal to the injury, there was no significant regeneration into the distal ON in these animals (Leaver *et al*, 2006).

1.2.3.3 PTEN AND SOCS3

Deleting genes that encode suppressors of the intrinsic growth control pathways is a possible strategy to induce long-distance axonal regeneration (Sun *et al*, 2011).

PTEN acts as a phosphatase to dephosphorylate phosphatidylinositol (3,4,5)-triphosphate (PIP_3), resulting in phosphatidylinositol (4,5)-biphosphate (PIP_2). Inactivation of PTEN results in the accumulation of PIP_3 and the activation of the Akt (protein kinase B) signaling pathway. SOCS3 is a negative regulator of the Janus kinase (JAK)/STAT pathway by inhibiting the phosphorylation of STAT (Smith *et al*, 2009). Downstream effectors of these pathways, like mammalian target of rapamycin (mTOR), in neuronal somata and axon terminals might coordinate different steps of axon growth during development and injury induced axonal regeneration (Park *et al*, 2008, 2010).

The injured ON did undergo significant axonal regeneration after conditional deletion of *Pten* or *Socs3* in adult RGCs, but the regrowth only occurred during the first 2 weeks. Simultaneous deletion of both *Pten* and *Socs3* enabled robust and sustained axonal regeneration. Concurrent activation of mTOR and STAT3 pathways are revealed to be essential for sustaining long-distance axonal regeneration in adult CNS, which is a crucial step towards functional recovery (Park *et al*, 2008; Sun *et al*, 2011; Smith *et al*, 2009).

1.2.3.4 ROCK INHIBITORS

One key mediator of growth inhibitory signaling is ROCK, which has been shown to modulate growth cone stability by regulation of actin dynamics. To test the role of myelin associated inhibitors, many of which act via the Rho/ROCK pathway, ROCK was blocked pharmacologically. This ROCK blockade, along with the AAV2.STAT3-ca stimulation, was recently shown to promote extension of much longer and straighter axons and decreased the frequency of axonal misnavigation (Pernet *et al*, 2013b).

1.2.3.5 INDUCTION OF INFLAMMATION

Partial axonal regeneration can also be obtained via induction of inflammation and glial reactivity in the eye (Benowitz & Popovich, 2011; Lorber *et al*, 2012; Kurimoto *et al*, 2013; de Lima *et al*, 2012). The paradigm that, under certain circumstances, inflammation can produce factors that promote CNS regeneration, has been confirmed in a variety of species

(Benowitz & Yin, 2008; Lorber *et al*, 2005; Okada *et al*, 2005; Pernet & Polo, 2006). It has been shown that factors secreted by reactive astrocytes, Müller cells, infiltrating macrophages and resident microglia play a significant role in the partial reversal of the inability of mature RGCs to regenerate their axons following ON injury. Although, current knowledge about the identity of these growth factors is very limited, one evolutionarily conserved 12 kilodalton (kDa) Ca^{2+} binding protein has been identified as a macrophage-derived growth factor, namely oncomodulin. In the presence of elevated $[cAMP]_i$, oncomodulin can stimulate extensive axonal regeneration in the mature ON. No other known trophic factor (e.g., BDNF or CNTF) is able to stimulate such a strong axon outgrowth (Benowitz & Yin, 2007; Yin *et al*, 2006).

Controlled ocular inflammation can be invoked either via lens injury or via pharmalogical treatment, e.g., via the intravitreal injection of zymosan. Zymosan is a yeast cell wall extract that induces restricted ocular inflammation, which results in the influx of neutrophils and activated macrophages (Benowitz & Yin, 2007, 2008, 2010; Yin *et al*, 2003, 2006; Cui *et al*, 2009; Leon *et al*, 2000). Using zymosan, macrophage activation caused more regeneration than lens injury or a PNG (Benowitz & Yin, 2008; Leon *et al*, 2000; Yin *et al*, 2003). When combined with *Pten* deletion, it leads to a dramatic increase in axonal regeneration and even to a limited re-innervation of thalamic neurons in the brain (figure 6) (Kurimoto *et al*, 2010; Benowitz & Popovich, 2011; Lorber *et al*, 2012; Kurimoto *et al*, 2013; Ahmed *et al*, 2010; Leibinger *et al*, 2009; Cui *et al*, 2009; Lorber *et al*, 2009).

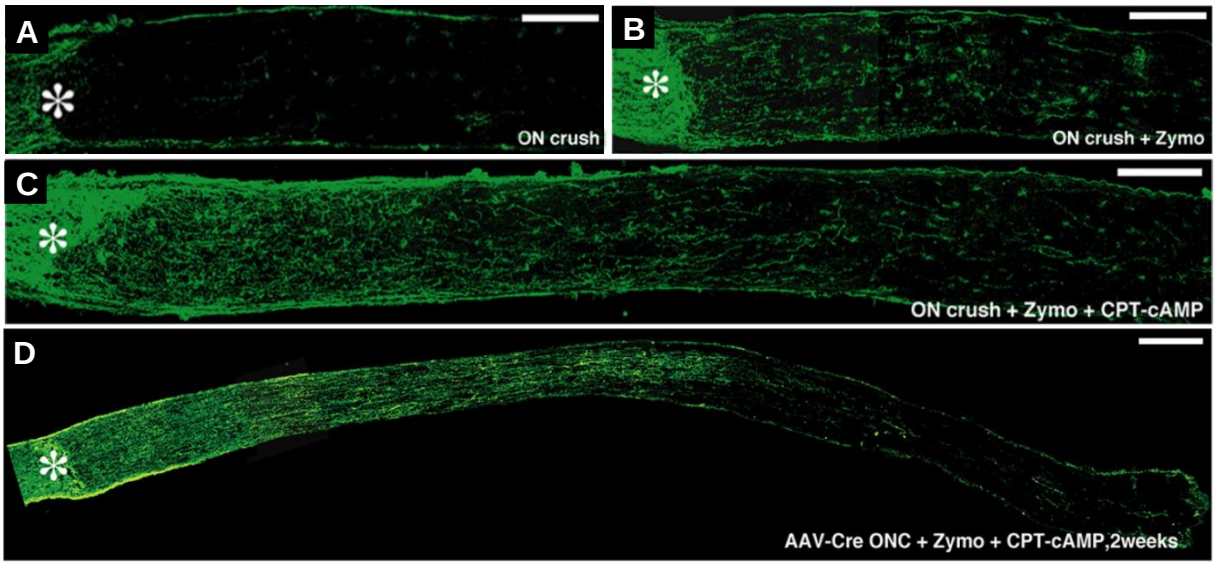

Figure 6: Effects of intraocular inflammation, cAMP and *Pten* deletion. A-D) Longitudinal sections through the ON showing GAP-43$^+$ axons distal to the ONC denoted with asterisks. A) Absence of regeneration after surgery alone. B) Increased regeneration after intraocular injection of zymosan alone. C) Extensive regeneration induced by zymosan and CPT-cAMP. D) Combination of *Pten* deletion, zymosan and CPT-cAMP resulted in far greater regeneration than any other treatment. Scale bar, 200µm. Reproduced from (Kurimoto *et al*, 2010).

1.3 MATRIX METALLOPROTEINASES IN AXONAL REGENERATION

1.3.1 FAMILY OF MMPS

The founding member of the MMP family, MMP-1, was identified in 1962 by Gross and Lapiere (Gross & Lapiere, 1962). Further research led to the discovery of structurally related proteinases. The MMPs constitute a family of over 20 proteolytic enzymes (Sternlicht & Werb, 2001). Together, these proteinases can degrade virtually all constituents of the ECM (Page-McCaw *et al*, 2007; Yong *et al*, 2001).

Proteolytic enzymes are classified in two groups: exopeptidases and endopeptidases, based on whether they cleave the terminal or the internal peptide bonds (figure 7). Depending on their catalytic mechanism and inhibitor sensitivities, the endopeptidases are divided into serine-, cysteine-, aspartic- or metalloproteinases. The latter are further separated into five superfamilies, based on their sequence. The metzincin superfamily is then further subdivided into multigene families: the serralysins, astacins, adamalysins and MMPs. The group of MMPs owes its name to its dependence on metal ions for catalytic activity, its capability to degrade structural proteins of the ECM and its specific sequence that distinguishes it from the other closely related metalloproteinases (Sternlicht & Werb, 2001). MMP family members have been categorized into subgroups including gelatinases, stromelysins, collagenases and membrane-type (MT)-MMPs (Yong *et al*, 2001).

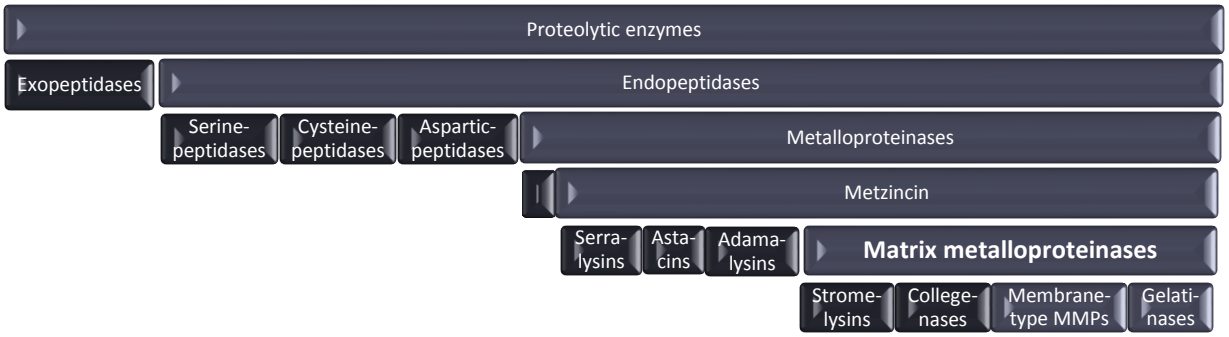

Figure 7: Classification of the proteolytic enzymes. The MMPs are endopeptidases that belong to the metalloproteinases and more specifically to the metzincin family because they use zinc in their catalytic domain. Reproduced from (Sternlicht & Werb, 2001).

1.3.2 STRUCTURE OF MMPS

MMPs are members of the zinc-dependent metalloproteinases called metzincins. They share a zinc-binding motif, containing three histidine residues (HExxHxxGxxHS) in their active site to bind the zinc ion. The conserved methionine residue or 'Met turn' (xxMxP) delineates a distinct beta-turn at the active site and seems essential for activity. Moreover, MMPs have additional stretches of sequence homology, which gives them a fairly conserved structure (figure 8) (Sternlicht & Werb, 2001; Page-McCaw *et al*, 2007; Yong *et al*, 2001).

All MMPs have a short amino (N)-terminal signal sequence (pre-domain) that is removed when travelling to the cell surface. Most of the MMPs are secreted, but six of them display transmembrane domains and are called MT-MMPs. These do not lose their pre-domain in the endoplasmatic reticulum and are expressed as membrane-bound enzymes. In mammalian MMPs, the pre-domain is followed by a conserved domain structure that consists of a N-terminal autoinhibitory pro-domain and a N-terminal catalytic domain. The pro-domain contains a conserved cysteine residue that coordinates the zinc ion at the active site to inhibit catalysis and to maintain the latency of the enzyme until the pro-domain is removed or disrupted. When the pro-domain is destabilized or removed, the active site becomes available to cleave substrates. The catalytic domain has a zinc-binding region and is localized after the pro-domain. It determines where the MMPs cleave their substrate. Most of the members of the MMP family also contain a hemopexin-like domain. It is attached to the catalytic domain by a flexible hinge region, which is short in the collagenases and longer in all other MMPs. This hemopexin domain mediates protein-protein interactions, substrate recognition, activation of the enzyme, protease localization, internalization and degradation and also affects the binding of inhibitors and substrates (Sternlicht & Werb, 2001; Page-McCaw *et al*, 2007; Yong *et al*, 2001).

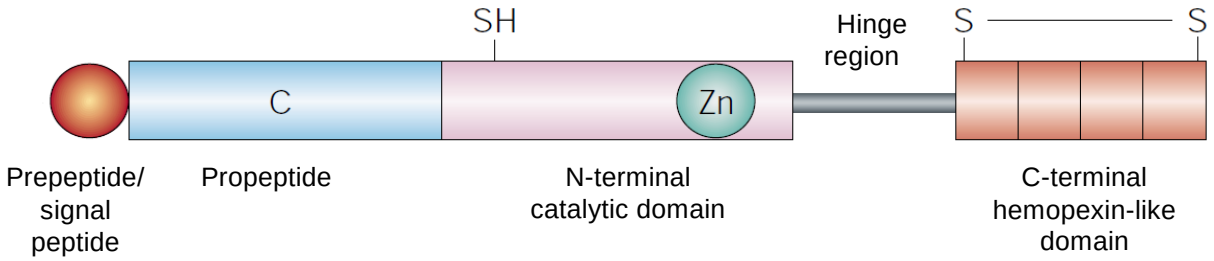

Figure 8: General domain structure of MMPs. All MMPs consist of an amino-terminal signal prepeptide (orange), an amino-terminal propeptide (blue) and catalytic domain (pink) that contains a zinc molecule (green). Most of them have a carboxy (C)-terminal hemopexin-like domain (red) connected to the N-terminal domains by a hinge region (grey). The MT-MMPs have a transmembrane domain at the C-terminal. Reproduced from (Yong *et al*, 2001).

1.3.3 FUNCTION OF MMPS

Historically, MMPs were considered to function mainly as enzymes that degrade structural components of the ECM. However, MMPs can regulate cell behavior in numerous ways, by cleaving other signaling molecules with independent biological activity such as receptors, cytokines, adhesion molecules and growth factors. Most of the MMPs carry out their function extracellularly. However, some MMPs, like MMP-2, also fulfill a role intracellularly e.g., in the nuclei of neurons and glial cells (Page-McCaw *et al*, 2007; Sternlicht & Werb, 2001; Rivera *et al*, 2010).

Because of their diversity in substrates and their expression by different cell types and tissues all over the body, MMPs can accomplish important functions in a wide range of physiological processes including ovulation, wound healing, cell migration, cell shape, cell movement, differentiation, growth, inflammatory processes, apoptosis, angiogenesis, embryonic development and bone development *etc*. In addition to the positive effects, MMPs

can also have some negative influences in pathological conditions. The increased expression of MMPs is characteristic for several diseases like Alzheimer's disease, multiple sclerosis, chronic rheumatoid arthritis or cancer. Thus, it is essential to keep in mind the importance of balancing the potential favorable and detrimental effects of MMPs (Duchossoy *et al*, 2001; Mccurley & Callard, 2010; Yong *et al*, 2001; Sternlicht & Werb, 2001; Agrawal *et al*, 2008; Page-McCaw *et al*, 2007; Verslegers *et al*, 2013).

In the CNS, MMPs have a fundamental function in development but they are also indispensable in the adult CNS. There, they play a role in synaptic plasticity and turnover of myelin, inflammation, cell death, demyelination, learning and memory.

1.3.4 Regulation of MMPs

The important functions of MMPs and their capacity to alter cell fate and developmental outcomes implies that their expression and activity must be highly regulated (Yong *et al*, 2001). This regulation is controlled at the following levels: transcription of MMP genes, zymogen activation, MMP inhibition, degradation or clearance and the compartmentalization of MMPs on or near the cell surface (Ethell & Ethell, 2007).

The expression of MMP genes is, to a large extent, regulated by the *cis*-elements in the promoter that are activated or inhibited by their corresponding *trans*-activators. Different response elements in the promoter, e.g., the TATA-box or the activator protein (AP)-1 binding site, render these genes responsive for changes in the amount or activity of a large variety of cytokines or growth factors including interleukins, interferons, epithelial growth factor (EGF), tumor necrosis factor (TNF)-α and transforming growth factor (TGF)-β. A number of MMP promoters share common structural features and therefore are co-regulated in their expression to some extent. (Sternlicht & Werb, 2001; Yan & Boyd, 2006).

Furthermore, MMPs are produced as zymogens (inactive pro-enzymes). They are maintained in a latent conformation by the cysteine switch (PRCGxPD). This is an unpaired cysteine sulfhydryl group near the carboxy (C)-terminal end of the pro-domain, that acts as a fourth ligand for the zinc ion in the catalytic site. Activation of MMPs requires enzymatic splicing of this cysteine switch through proteolytic removal of the pro-domain by other MMPs or serine proteases or through ectopic perturbation of the cysteine to zinc interaction. When MMPs are activated, the zinc ion becomes available to attack the peptide bonds of MMP substrates (Sternlicht & Werb, 2001; Nagase *et al*, 2006).

Once MMPs are activated, there are several physiological inhibitors that can block their activity. In circulation, MMPs are inhibited by alpha2-macroglobuline, but in tissues, inhibition is mainly accomplished by the four mammalian tissue inhibitors of metalloproteinases (TIMP-1-4) that bind reversibly to MMPs. MMPs are inhibited by interaction of the N-terminal domain of the TIMPs with the catalytic domain of the MMPs. Individual TIMPs differ in their capacity to inhibit various MMPs and in terms of their gene regulation and tissue specific patters of gene expression (Sternlicht & Werb, 2001; Yong *et al*, 2001; Baker *et al*, 2002).

Another way to regulate and inactivate MMPs is via autoproteolysis, degradation and clearance. Although little is known about MMP degradation, some cleavages that inactivate MMPs have been identified, whereas others generate truncated enzymes with altered substrate specificities and reduced affinity for their TIMPs. Thus, proteases that influence MMP degradation can at the same time alter their concentrations, their substrate specificities, their localization and their capacity to be activated or inhibited. Moreover, clearance of the intact enzymes can regulate extracellular MMP levels. For example, MMPs can cleave the bait region of alpha2-macroglobulin thereby initiating a conformational change of alpha2-macroglobulin that irreversibly traps the MMPs. The complex is eventually removed by endocytosis. Thrombospondin-2 has also been implicated in the clearance of MMPs (Sternlicht & Werb, 2001).

In addition to these main mechanisms for regulation, there is also MMP internalization or secretion. Several molecules can regulate whether the synthesized MMPs are taken up or released. For example, in macrophages, plasmin and thrombin induce the secretion of MMP-12 but do not alter the rate of transcription. Furthermore, activity of MMPs can be regulated by post-translational modification, storage of MMPs in granules and neutrophils and compartmentalization of the available substrates. The latter is a form of spatial regulation in which MMPs are attached to cells via specific interactions with membrane proteins. Cells also rely on surface receptors to detect the presence and location of specific substrates (Sternlicht & Werb, 2001).

The multiplicity of MMPs with distinct but somewhat overlapping functions probably acts as a safeguard against any losses of regulatory control. Because of this overlap of specificities, the biological function of individual MMPs is largely dictated by their differential patterns of expression. Overall, the MMPs have to be in the right cell type, at the right time, in the correct amount and be appropriately activated or inhibited (Sternlicht & Werb, 2001).

1.3.5 MMPS IN AXONAL REGENERATION

As mentioned before, diminished growth capacity of the adult CNS, reduced neurotrophic factors and formation of a physicochemical barrier adds to the failure of the mammalian CNS to regenerate axons. MMPs have been suggested to have an essential role in successful axonal regeneration for several reasons. First, MMPs add to the clearance of cellular and matrix debris at the site of injury. Second, all key components of the glial scar are substrates of one or multiple MMPs. Increased MMP activity decreases the formation of a glial scar and the associated inhibitory signals. This is particularly true for CSPGs, that have a strong inhibitory effect on axonal regeneration and are substrates of MMPs. Third, MMPs are also able to degrade myelin-derived inhibitory factors that are released by degenerating axons in the CNS. Fourth, MMPs can unmask, activate, or release other factors that have a beneficial effect on CNS repair. They can indirectly provide neurotrophic support to regenerating axons via release of sequestered growth factors or the conversion of inactive pro-growth factors to

their active forms. Fifth, MMPs can invoke 'focalized' proteolysis at the growth cone, thereby reorganizing the ECM to facilitate attachment and motility of the growing axon. Notably, stimulation of axonal regeneration after ON transection in rats by PNG, coincides with significantly enhanced MMP activity in the regenerating ON as compared with the non-regenerating ON (De Groef *et al*, 2014).

1.3.6 MMP-2 AND MT1-MMP

The focus of this thesis lies on MMP-2 (EC 3 4 24 24) and MT1-MMP (EC 3 4 24 80). MMP-2 is also known as gelatinase A or 72kDa type IV collagenase, which belongs to the gelatinase subgroup of the MMPs (figure 7). MMP-14 or MT1-MMP is a member of the membrane-type MMPs. The overall structure, function and regulation of MMP-2 and MT1-MMP are similar to what has been described above with a few exceptions (Sternlicht & Werb, 2001).

1.3.6.1 STRUCTURE OF MMP-2 AND MT1-MMP

Gelatinases, like MMP-2, and transmembrane MMPs, like MT1-MMP, have the general structure of MMPs with some additional features. Gelatinases have three fibronectin type 2-like repeats within their catalytic domain, which mediate binding to collagens. MT-MMPs have a single-pass transmembrane domain with a short cytoplasmic C-terminal tail next to their hemopexin-like domains (Sternlicht & Werb, 2001).

1.3.6.2 FUNCTION OF MMP-2 AND MT1-MMP

One of the primary functions of MMP-2 is the degradation of proteins in the ECM. The substrates of MMP-2 are proteins in ECM, pro-MMPs, CSPGs (versican and neurocan), growth factors and cytoskeletal component. Physiologically, MMP-2 in coordination with other MMPs, plays a role in normal tissue remodeling events such as embryonic development, angiogenesis, ovulation, mammary gland involution and wound healing. MMP-2 is also involved in osteoblastic bone formation and inhibits osteoclastic bone resorption. Moreover, MMP-2 has been implicated to contribute to the breakdown of inhibitory molecules in the CNS, clearing the path for axonal regeneration (Nagase *et al*, 2006; Verslegers *et al*, 2013).

Studies performed with MT1-MMP deficient mice have shown the importance of its function during embryogenesis. The lack of MT1-MMP caused craniofacial dysmorphism, arthritis, osteopenia, dwarfism, fibrosis of soft tissues and premature death. It is also required for the wound healing process. The substrates of MT1-MMP are proteins in ECM, pro-MMPs, cell-adhesion molecules, cytokines, growth factors and receptors on the cell membrane. Recent studies have also demonstrated the activation of signal transduction pathways via the cytoplasmic tail of MT1-MMP important for the invasion process of macrophages (Nagase *et al*, 2006; Verslegers *et al*, 2013; Sakamoto & Seiki, 2009).

1.3.6.3 REGULATION OF MMP-2 AND MT1-MMP

As already mentioned, all MMPs are closely regulated at the level of transcription and are activated by cleavage of the cysteine switch by other MMPs, serine proteases or ectopic perturbation. MMP-2 is the exception, as it is often continuously expressed, activated through an unique multistep mechanism at the cell surface (figure 9) and controlled by some degree of post-transcription messenger ribonucleic acid (mRNA) stabilization (Sternlicht & Werb, 2001; Overall *et al*, 2000). The activation pathway of MMP-2 involves a coordinated interplay of MMP-2, TIMP-2 and MT1-MMP. TIMP-2 plays a dual role in MMP-2 regulation, being an inhibitor and an essential component of the MT1-MMP/TIMP-2/MMP-2 activation complex (Deryugina *et al*, 2001; Hernandez-Barrantes *et al*, 2000; Caterina *et al*, 2000). Based on this process, both a deficiency as well as an excess of TIMP-2 may inhibit MMP-2 activation (Strongin *et al*, 1995). The activation of MMP-2 essentially starts with the activation of MT1-MMP. MT1-MMP is activated extracellularly by plasmin, intracellularly by furin or by non-proteolytic disruption of the cysteine switch. Next, the N-terminal inhibitory domain of TIMP-2 binds to the active MT1-MMP at the cell surface (Zucker *et al*, 1998). The resulting MT1-MMP/TIMP-2 complex is crucial for processing and activating pro-MMP-2. Indeed, in a next step, the C-terminal domain of the bound TIMP-2 binds the C-terminal hemopexin-like domain of pro-MMP-2 (68kDa), resulting in the recruitment of pro-MMP-2 from the extracellular milieu to the cell surface. Then, an adjacent uninhibited, active MT1-MMP cleaves the tethered pro-MMP-2 to generate the activation intermediate of MMP-2 (64kDa). Finally, the remaining fragment of the pro-domain is removed by a separate, active MMP-2 at the cell surface, to convert the activation intermediate of MMP-2 into its fully activated form (62kDa) (Sternlicht & Werb, 2001; Gaublomme *et al*, 2014; Visse & Nagase, 2003).

Once active, MMP-2 can be inhibited by interacting with TIMP-2, TIMP-4 and thrombospondin 1 (Overall *et al*, 1991; Bein & Simons, 2000).

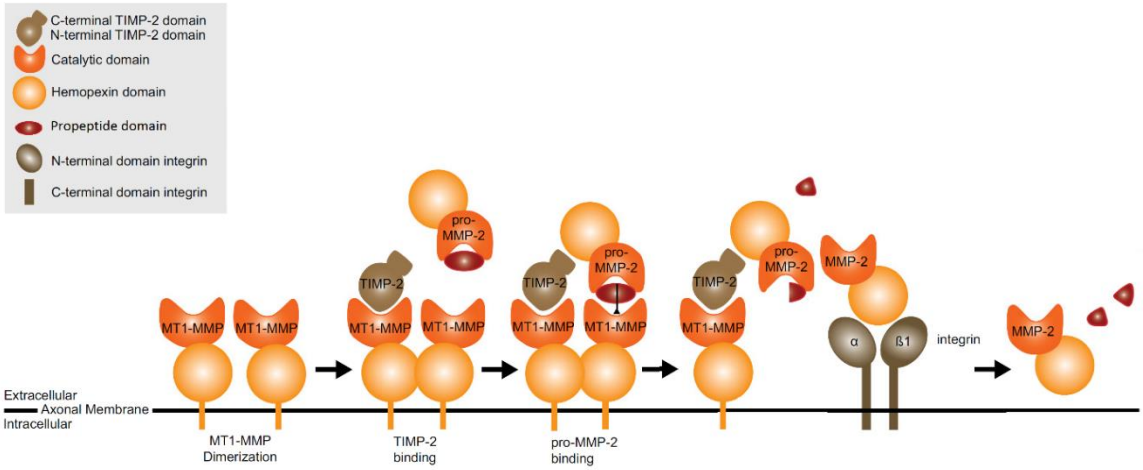

Figure 9: Activation pathway of MMP-2. Pro-MT1-MMP is activated by an intracellular furin during transport to the cell surface, by an extracellular plasmin at the cell surface or by non-proteolytic conformational changes. Active MT-MMP is then inhibited by TIMP-2. This MT1-MMP/TIMP-2 complex recruits extracellular pro-MMP-2 to the cell surface to form a trimolecular complex. Then, an uninhibited MT1-MMP partially activates pro-MMP-2 resulting in the MMP-2 activation intermediate. The remaining part of the propeptide of MMP-2 is removed by another active MMP-2 molecule bound to a cell surface receptor to yield a fully active mature MMP-2. Mature MMP-2 can then be released from the cell surface or bind to another cell surface receptor. Reproduced from (Gaublomme *et al*, 2014).

1.3.6.4 MMP-2 AND MT1-MMP IN AXONAL REGENERATION

MMP-2 has been implicated in axon extension and guidance in the CNS and, in particular also in the retinotectal system (Webber *et al*, 2002; Hehr *et al*, 2005; Verslegers *et al*, 2014). MMP-2 was shown to be expressed in the ON and in retinal Müller glia of developing zebrafish (Janssens *et al*, 2013), in Müller glia of adult mouse retina (De Groef *et al*, 2012) as well as in RGCs, RGC axons, astrocytes and Müller cells in adult human and monkey eyes (Agapova *et al*, 2001, 2003; Limb *et al*, 2002). MT1-MMP was expressed in the RGC axon bundles of the mouse retina. In zebrafish, MT1-MMP was abundantly expressed in RGC axons but was also found in the IPL neurites. MT1-MMP was shown to be upregulated during the injury respons phase and gradually decreased during axonal regeneration (Lemmens *et al*, *submitted*). Expression of MT1-MMP was reported in astrocytes in the ONH and ON of adult humans and monkeys (Agapova *et al*, 2001, 2003). *In vivo* studies in developing *Xenopus* revealed that low concentrations of broad-spectrum MMP inhibitors or a more specific gelatinase inhibitor resulted in RGC axonal navigation defects, while larger doses decreased axonal elongation (Webber *et al*, 2002; Hehr *et al*, 2005). These studies clearly revealed that gelatinases are required for proper development of the optic projection by RGCs and may regulate axon behavior at distinct decision points (Webber *et al*, 2002; Hehr *et al*, 2005; Verslegers *et al*, 2014).

Recent work from the host lab also provided indications for a functional involvement of MMP-2 in the outgrowth of RGC axons towards the optic tectum in developing zebrafish (Janssens *et al*, 2013). Notably, a positive correlation between gelatinase activity and regeneration of RGC axons was found in a rat model of transected ON (Ahmed *et al*, 2005).

Furthermore, using an *in vitro* model of CNS axonal regeneration, the percentage of rat RGCs undergoing axonal regeneration was reported to rise when these RGCs were co-cultured with MMP-2 expressing olfactory glial cells (Pastrana *et al*, 2006). In addition, a recent study performed in the host lab, using an *ex vivo* mouse retinal explant model in combination with broad spectrum and more specific MMP inhibitors, as well as MMP-deficient mice, showed a co-involvement of MMP-2 and MT1-MMP in axonal outgrowth. In this study, it was unveiled that MMP-2, and not MMP-9, is required for optimal axon outgrowth of RGCs. Furthermore, MMP-2 expression was clearly localized in Müller glia and also found in close association with outgrowing axons and their growth cones in the explants (Gaublomme *et al*, 2014). Overall, preliminary data clearly demonstrate that endogenous MMP-2 and MT1-MMP activity are necessary for axonal outgrowth of RGCs in mouse retinal explants. Based on these data, we hypothesized that MMP-2 (and MT1-MMP) may stimulate *in vivo* long-distance axonal outgrowth, elongation and/or guidance in the damaged CNS.

2 OBJECTIVES AND AIMS

As adult mammals lack the capacity to regenerate damaged neurons, dysfunction of the CNS after brain injury or in neurodegenerative diseases increasingly impairs life quality in our aging society. Despite intensive research efforts, induction of regeneration and subsequent functional recovery of the injured mammalian CNS remains a challenge, which makes the search for new regeneration-inducing strategies and interventions essential.

Preliminary *ex vivo* results obtained in the host lab indicate MMP-2 and MT1-MMP as promising neurite outgrowth-promoting molecules (Gaublomme *et al*, 2014) and form the basis for the current *in vivo* study, in which we envisioned to further investigate the possible beneficial role of MMP-2 and MT1-MMP in axonal regeneration.

The overarching goal is to investigate the *in vivo* involvement of MMP-2 and MT1-MMP in axonal regeneration using a recently established mouse regenerative optic nerve crush (RONC) model. Therefore, the first aim was to optimize the implementation of this RONC model in the host lab together with tracing methods for the evaluation of axonal regeneration in the ON. An additional goal in optimizing the methodology to study axonal regeneration in the ON was to overcome the limitations of two-dimensional imaging by implementing optical clearing of ON tissues. The second, and foremost, aim was to evaluate axonal regeneration in wild-type (WT) *versus Mmp-2*$^{-/-}$ mice, and in mice with a conditional Müller glia-specific deletion of *Mt1-mmp.* In addition, it was aimed to determine the spatiotemporal expression pattern of MMP-2 in the retina and ON of mice subjected to the RONC model.

The proposed research project envisions generating novel insights for future regenerative therapeutic approaches towards CNS repair.

3 MATERIAL AND METHODS

The composition of the buffers used in this project can be found in addendum 1.

3.1 *MUS MUSCULUS*

The mouse (*Mus musculus*) is often used as a model organism in very diversified research projects because of many advantages. First of all, a lot of genetically manipulated strains are available. Second, mice are small, have a short generation time, an accelerated lifespan (1 mouse year equals 30 human years) and a high fertility. Also the costs to maintain them, in comparison to other mammals, are low. All of this keeps the space, the time and the expenses required for research manageable. In addition, a lot of research methods have already been described for mice, proving that they form an excellent model organism. The mouse genome shows more than 95% homology with that of humans, which makes research in mice particularly applicable to human diseases. Also in neurobiological research, mice are indispensable.

Mice were obtained from the breeding colony of the University of Leuven (KU Leuven, Belgium). They were housed in temperature, humidity and light controlled rooms with a 12h light/dark cycle and had *ad libitum* access to food and water. All animal experiments were approved by the Institutional Ethical Committee of KU Leuven and were conducted in strict accordance with the European Communities Council Directive of September 22, 2010 (2010/63/EU) and with the Belgian legislation (Koninklijk besluit (KB) of May 29, 2013).

3.1.1 MMP-2 KNOCKOUT MICE

Wild-type (WT) C57Bl/6N mice (*Mmp-2*$^{+/+}$) and *Mmp-2* knockout mice (*Mmp-2*$^{-/-}$) with a 100% C57Bl/6N genetic background (Itoh *et al*, 1997) were used to study MMP-2 expression and its role during axonal regeneration. Both male and female mice were used at the age of 2-4 months. The knockout of the *Mmp-2* gene in the *Mmp-2*$^{-/-}$ mice was achieved by replacement of the exon sequence of the catalytic domain of *Mmp-2* by a selection marker (neomycin resistance gene) via homologous recombination.

3.1.2 MT1-MMP CONDITIONAL KNOCKDOWN MICE

3.1.2.1 CRE-LOXP SYSTEM

The Cre-LoxP system is a tool to generate tissue- and time-specific conditional knockdowns of genes, which cannot be investigated because their ablation induces early lethality in mice with conventional knockout, or when a controllable and tissue- or cell-specific knockdown is needed. Much of the success of the Cre-LoxP system is due to its simplicity. It requires only two components: the Cre recombinase, which is a 38kDa recombinase

enzyme that catalyzes recombination between two LoxP sites, and the LoxP sites themselves, which consist of a 34-base pair (bp) specific sequence.

The orientation and location of the LoxP sites determine whether Cre recombination induces a deletion, an inversion or a chromosomal translocation (figure 10). The *Cre* gene and LoxP sites are not native to the mouse genome, they must be introduced by transgenic technology. Typically, Cre and LoxP strains are developed separately and crossed to produce a Cre-LoxP strain. First, a homozygous LoxP-flanked mouse of interest is mated with a Cre transgenic mouse strain. Approximately 50% of the offspring will be heterozygous for both the LoxP-flanked allele and for the *Cre* transgene. These mice are mated back with the homozygous LoxP-flanked mice. Approximately 25% of the offspring will be homozygous for the LoxP-flanked allele and heterozygous for the *Cre* transgene. These will be the experimental mice, while the mice with the homozygous LoxP-flanked allele and no *Cre* transgene will be the control mice. In this project, a tamoxifen (TXF; Sigma) inducible Cre(ER)T2-LoxP recombination system (figure 11) is used. The method is based on the migration mechanism of nuclear hormone receptors (NHRs) into the nucleus when binding their ligand. NHRs without their ligand are sequestered in the cytoplasm by binding heat shock protein 90 (hsp90). Upon application, the ligands bind to their NHRs and trigger conformational changes. This leads to the release of hsp90 which results in the unmasking of the nuclear localization signal and the DNA-binding domain. The NHRs dimerize and translocate to the nucleus where the NHRs regulate gene expression. In the glutamate aspartate transporter (GLAST)-Cre(ER)T2-LoxP mouse line, the Cre recombinase is fused with a mutated ligand binding domain for the estrogen receptor (ER) T2. The Cre recombinase is non-functional until an inducing agent is administered. Upon administration of TXF, which is an ER agonist, the Cre(ER)T2 construct is able to translocate from the cytoplasm to the nucleus where it will induce recombination between two LoxP sites flanking a floxed gene. ERT2 binds TXF with greater affinity than endogenous estrogens, which allows Cre(ER)T2 to remain in the cytoplasm in animals that are not treated with TXF (Leone *et al*, 2003). The Cre(ER)T2 is under control of a cell-specific GLAST promotor, which results in Cre(ER)T2 expression in the Müller glia of the retina and astrocytes in the brain (Slezak *et al*, 2007).

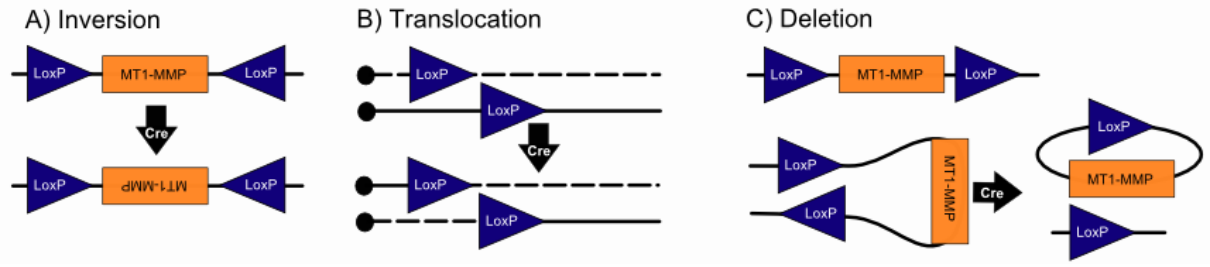

Figure 10: Orientation and location of the LoxP sites determine outcome. (A) If the LoxP sites are positioned in opposite directions, Cre recombinase mediates the inversion of the floxed segment. (B) If the LoxP sites are situated on different chromosomes, Cre recombinase mediates a chromosomal translocation. (C) If the LoxP sites are oriented in the same direction on a chromosome segment, Cre recombinase mediates a deletion of the floxed segment. Reproduced from (Nagy, 2000).

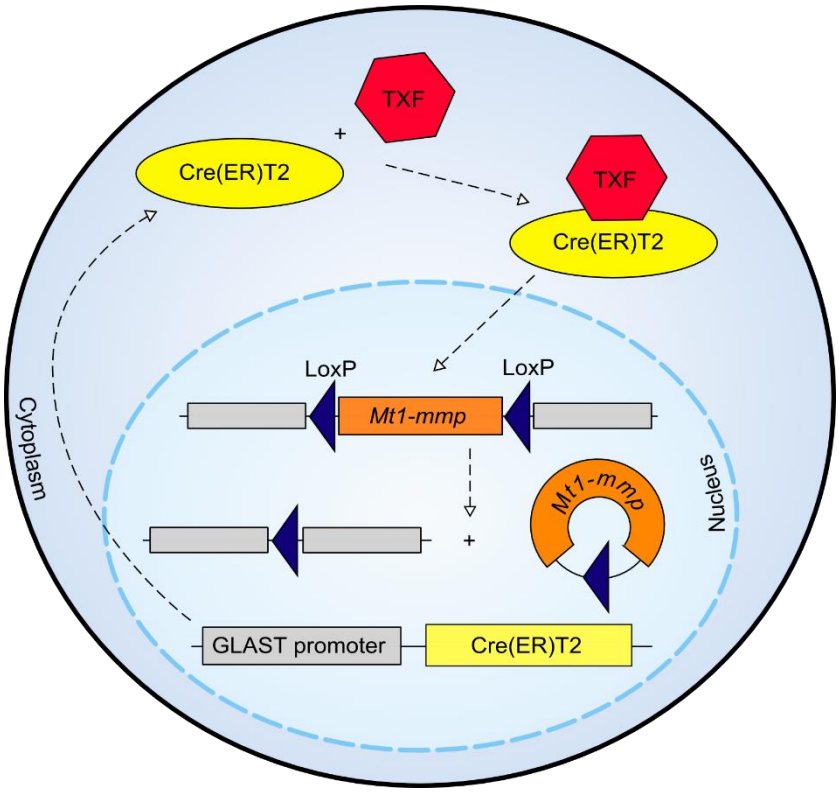

Figure 11: Cre(ER)T2-LoxP recombination system. Cre(ER)T2 is expressed under the control of a GLAST promoter specific for Müller glia cells in the retina and astrocytes in the brain. Cre(ER)T2 is stocked in the cytoplasm. Upon TXF administration, the TXF binds to Cre(ER)T2 and the complex dimerizes and migrates to the nucleus. There, the Cre(ER)T2 functions in the excision of the *Mt1-mmp* gene located between two LoxP sites which leads to the conditional knockout of *Mt1-mmp*. Reproduced from (Imayoshi *et al*, 2011)

3.1.2.2 FLOXED MT1-MMP MICE

Floxed *Mt1-mmp* mice with a mixed genetic background (Jin *et al*, 2011) were used to study the role of MT1-MMP in axonal regeneration. Both male and female mice were used, at the age of 2-4 months. In order to generate a conditional Müller cell-specific knockdown of MT1-MMP, the floxed *Mt1-mmp* mice were crossed with a *GLAST-Cre(ER)T2* mouse line (Mori *et al*, 2006). *Mt1-mmp*$^{flox/flox}$*;GLAST-CreER*$^{+/-}$ mice were used, as well as *Mt1-mmp*$^{flox/flox}$*;GLAST-CreER*$^{-/-}$ mice that served as a negative control group.

3.2 SURGICAL PROCEDURES

3.2.1 ANESTHESIA AND EUTHANASIA

Measures were taken to minimize pain or discomfort during the surgical procedures. All surgical manipulations were done under general anesthesia, induced by intraperitoneal (i.p.) injection of a mixture of ketamine (140mg/kg body weight, ketamine; 1,4mg/kg body weight, medetomidine; 14mg/kg body weight, butorfanol; Nimatek; Eurovet; Heusden-Zolder; Belgium) and xylazine (10mg/kg body weight; XYL-M 2; VMD; Arendonk; Belgium) diluted in autoclaved saline. Before the surgical procedures, a topical anesthetic ointment (Unicaïne; 0,4% oxybuprocaïnehydrochloride, Thea Pharma; Wetteren; Belgium) was applied on the

eye that was treated. While recovering from anesthesia, mice were placed in their cages, and a topical antibiotic ointment (3mg/g body weight; Tobramycine; Tobrex; Alcon; Vilvoorde; Belgium) was applied on both eyes to prevent infection and corneal desiccation. Animals were euthanized with an i.p. injection of an overdose of pentobarbital (0,6 mg/g body weight; Nembutal; Ceva; Libourne; France). A brief overview of the main safety and health regulations employed during this project is given in Addendum 2.

3.2.2 INTRAPERITONEAL INJECTION OF TAMOXIFEN

Translocation of Cre recombinase to the nucleus of *Mt1-mmp*$^{flox/flox}$*;GLAST-CreER*$^{+/-}$ mice was induced by administration of TXF. TXF is stable in the body for approximately 10-12h after administration, therefore 0,75mg TXF (15mg/ml in corn oil; Sigma)) was administered via i.p. injection in awake mice twice a day at 8h and at 20h during 5 days. TXF does not dissolve very well, so it has to be prepared a few hours before use. The solution was freshly prepared the day prior to the first injection and stored at 4°C. Importantly, TXF is sensitive to light and has to be covered with aluminum foil.

3.2.3 OPTIC NERVE CRUSH SURGERY

In order to induce RGC axonal degeneration, ONC was performed as described by Templeton & Geisert, 2012 (figure 12). Briefly, under the guidance of an operating microscope (Leica; Diegem; Belgium), a small incision in the temporal side of the conjunctiva was made using spring scissors (15018-10; fine science tools; Heidelberg; Germany). Care was taken not to cut too deep, as this can result in damage to the underlying musculature or the supplying vasculature. With forceps (11203-23; fine science tools), the conjunctiva was retracted, while rotating the globe nasally. This exposes the posterior aspect of the eye,

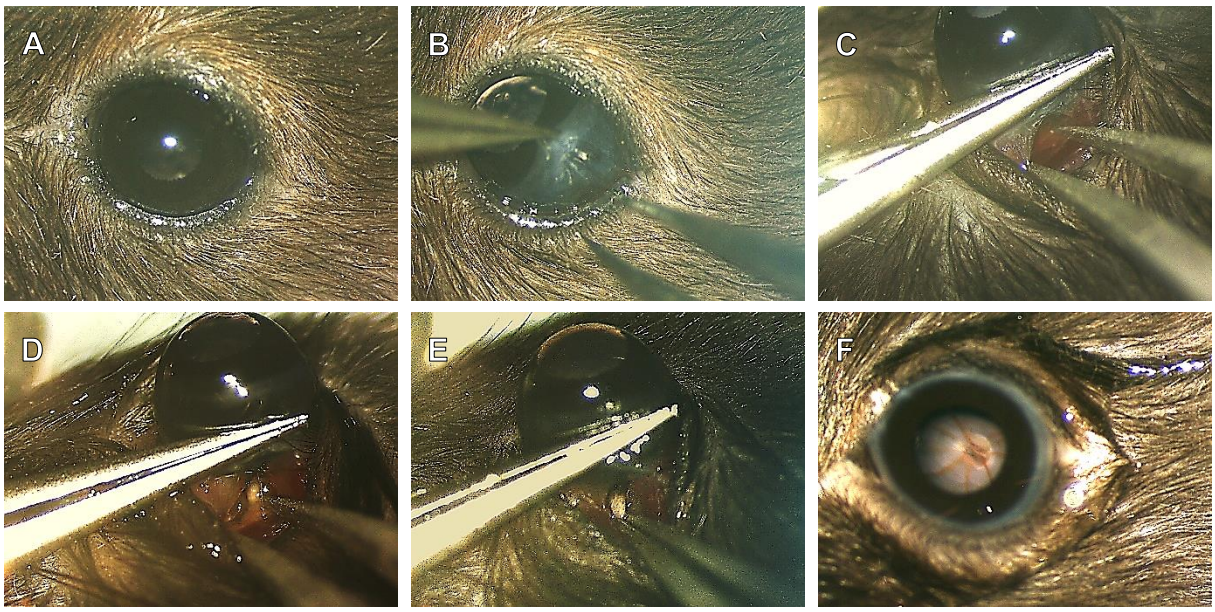

Figure 12: The ONC. A) The eye of a C67Bl/6 mouse. B) The first step was to grasp the conjunctiva and to rotate the eye nasally. C) At this side, a hole was made in the conjunctiva. D) The ON was visualized. E) The ON was grasped 1mm from the ONH with cross-action forceps for 5s. F) The ON was released, the eye rotated back and the fundus of the eye was checked.

allowing to visualize the ON. The exposed ON was grasped approximately 1mm from the ONH with cross-action forceps (11262-30; fine science tools) for 5s, with the only pressure applied being from the self-clamping action of the cross-action forceps. After 5s the ON and the conjunctiva were released, allowing the eye to rotate back into place. After the ONC, ischemia can be a problem. Therefore, the fundus of the eye is checked to confirm that the blood supply to the eye was not restricted.

3.2.4 INTRAVITREAL INJECTION OF ZYMOSAN AND CTB

3.2.4.1 PREPARATION ZYMOSAN AND CTB

Zymosan (Sigma) and Chlorophenylthio-cAMP (CPT-cAMP; cAMP analog; Sigma) were injected at a final concentration of 12,5µg/ml and 50µM respectively. First, zymosan was suspended in sterile saline (Fisher scientific; United Kingdom) at a concentration of 37,5µg/ml. This stock solution was sterilized by heating in the thermomixer (Eppendorf) during 10 minutes at 90°C, and cooled down to room temperature (RT). Second, CPT-cAMP was diluted in sterile saline to a concentration of 150µM. At last, zymosan/CPT-cAMP/saline (1:1:1) were joined just before injection.

Cholera toxin subunit B (CTB; Sigma) was injected at a final concentration of 5µg/ml (0,5%). First, 500µg CTB is diluted in phosphate buffered saline (PBS) containing 1% dimethyl sulfoxide (DMSO) to a 1% stock solution, which was preserved at -20°C. Just before the intravitreal injection, the CTB was diluted in PBS (1:1) so a final CTB concentration of 5% was obtained.

3.2.4.2 INTRAVITREAL INJECTION

Intravitreal injections were performed as described by Chiu *et al*, 2007 (figure 13). Briefly, a microinjector (Micro4 Microsyringe pump controller; World Precision Instruments; Sarasota; USA) equipped with a Hamilton syringe connected to a glass capillary with an outer diameter of 50-70µm was used to inject either 3µl of zymosan and cAMP or 1µl of CTB. Under the guidance of an operation microscope (Leica), the capillary was inserted into the nasal part of the eye, approximately 1mm above the limbus, under a 45° angle. After the intravitreal injection (0,5µl/s), the capillary stayed in the eye for at least 4 minutes before

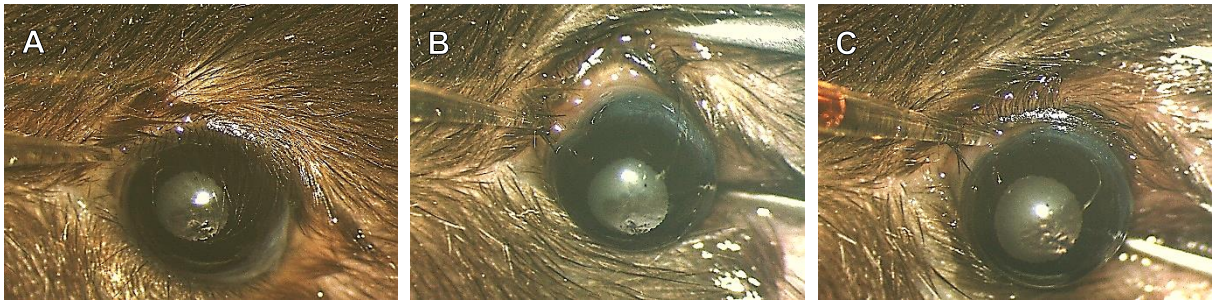

Figure 13: The intravitreal injection. A) The capillary was loaded with the compound that has to be injected and placed in the right place (1mm above the limbus and under 45°). B) The capillary was inserted into the left eye of the mouse. C) The compound is injected in the eye and the capillary stayed in the eye for at least 4 minutes.

retracting, to avoid reflux. Of note, in case intravitreal injection is combined with ONC, the ONC has to be performed first because manipulation of the eye during or just after the intravitreal injection procedure can result in reflux of the injected solution.

3.2.5 SACRIFICE ANIMALS

3.2.5.1 PERFUSION

First, the mice were euthanized (see above). Then, an incision was made in the integument with the help of scissors (91460-11; fine science tools) and forceps and the abdominal wall, the diaphragm and the rib case were removed with scissors and forceps, so the pleural cavity was exposed. A small cut was made in the right atrium of the heart using scissors. First, 12ml of sterile saline was injected into the left ventricle of the heart with a syringe (Henke Sass Wolf; Norm-ject) and a needle (23G; nr.16; BD microlance 3). This was needed to clear most of the blood out of the circulatory system. Red blood cells are autofluorescent and could interfere with fluorescent stainings. Thereafter, with the same syringe and needle, 12ml of phosphate buffered paraformaldehyde (PFA; 4% in PBS) was injected into the left ventricle to fixate the animals. PFA is responsible for creating crosslinks between proteins by linking the NH_2-group at the end of the side chain of lysine to the nitrogen atom of a peptide bond. The fixation was used to inhibit postmortem decay and to preserve a biological sample as close to its original state as possible.

3.2.5.2 DISSECTION OF THE OPTIC NERVE AND THE EYE

After the perfusion, incisions were made around the eye with a scalpel (91003-12; fine science tools) and a small incision in the upper eyelid of the eyes was made so these can be oriented after dissection (figure 14). The integument on top of the head and the bones in the nose and from the skull were removed with scissors and forceps so respectively, the skull and the brain were exposed. The anterior side of the brain was then slowly lifted to expose the ONs, which were cut as close to the brain as possible with the spring scissors. Thereafter, the brain was removed and the two ONs were separated, by cutting the optic chiasm with spring scissors. Carefully, the eye and ON were taken out and were put on a glass slide (VWR). All extra ocular muscles, connective and fatty tissue were removed and the ON was cut as close to the ONH as possible. The ON was cleaned by clamping the ON at the proximal side of the optic chiasm and carefully pulling the ON out of the sheath. The ONs were straightened between two filter papers (Carl Schleicher & Schuell Selecta; Germany). Thereafter, the ONs and the eyes were put in PFA (4% in PBS) during 1h. Overfixation has to be avoided as this increases the autofluorescent background. The ONs and eyes were put in PBS with sodiumazide (0,01%; 65,01M; Merck Schuchardt; Germany) and kept in a 24-well plate. The sodium azide works antibacterial by inhibiting bacterial cytochrome oxidase and has a beneficial effect on preserving the fluorescent signal.

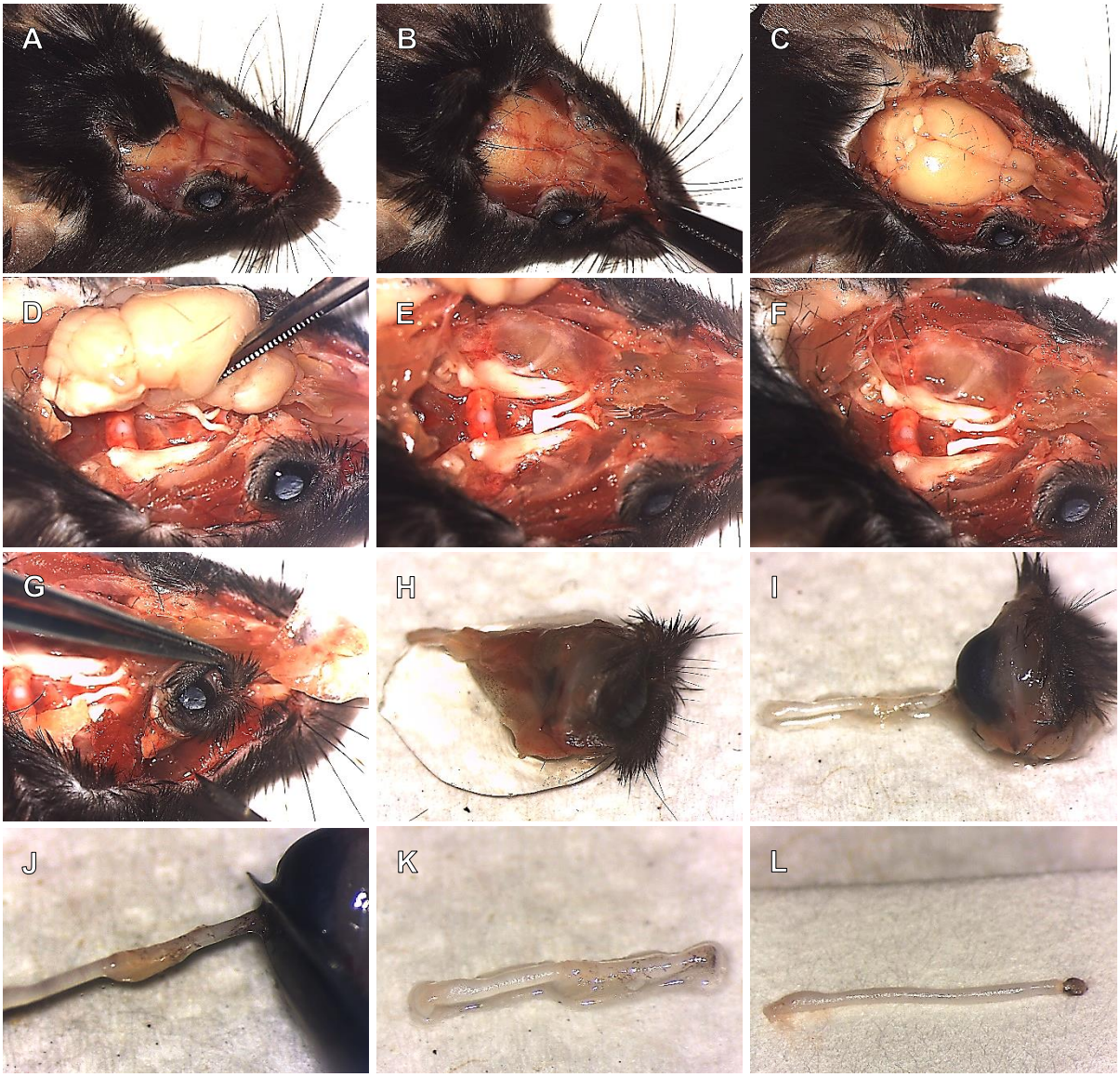

Figure 14: The dissection of the eye and the ON. A) The integument above the skull was removed by making incisions around the eye. B) The bones in the nose were broken. C) The skull was removed so the brain becomes visible. D) The brain was carefully lifted to visualize the ONs and these were cut as close to the brain as possible. E) Then, the brain was removed and the ONs were clearly visible. F) The ONs were separated by cutting the optic chiasm. G) The muscles and connective tissue that attach the eye to the rest of the body were removed. H) The eye with the ON still attached was put on a glass slide. I) The tissue that still surrounds the ON was removed together with the extraocular muscles. J) Then the ON was cut as close to the ONH as possible. K) The ON was cleaned. L) At last, the ON was put in 4% PFA between two filter papers.

3.2.5.3 DISSECTION OF RETINA

A petridish with wax and small needles were used to fixate the eye with the cornea facing up (figure 15). Under the guidance of a binocular microscope (Leica) and with scalpel and scissors, an incision into the limbus was made and the cornea and the iris were removed, as well as the lens. Then, four cuts, one deep cut in the superior part of the retina and three smaller cuts in the other quadrants, were made in the remaining eyecup, resulting in a 4-petaled flower-like structure in which the retina can be oriented. Next, the retina was carefully detached and removed from the underlying tissues with the help of forceps. The retina was cleaned, flattened on filter paper and put in PFA during 1h. Afterwards, the retina was put in PBS with sodiumazide (0,01%) and kept in a 24-well plate.

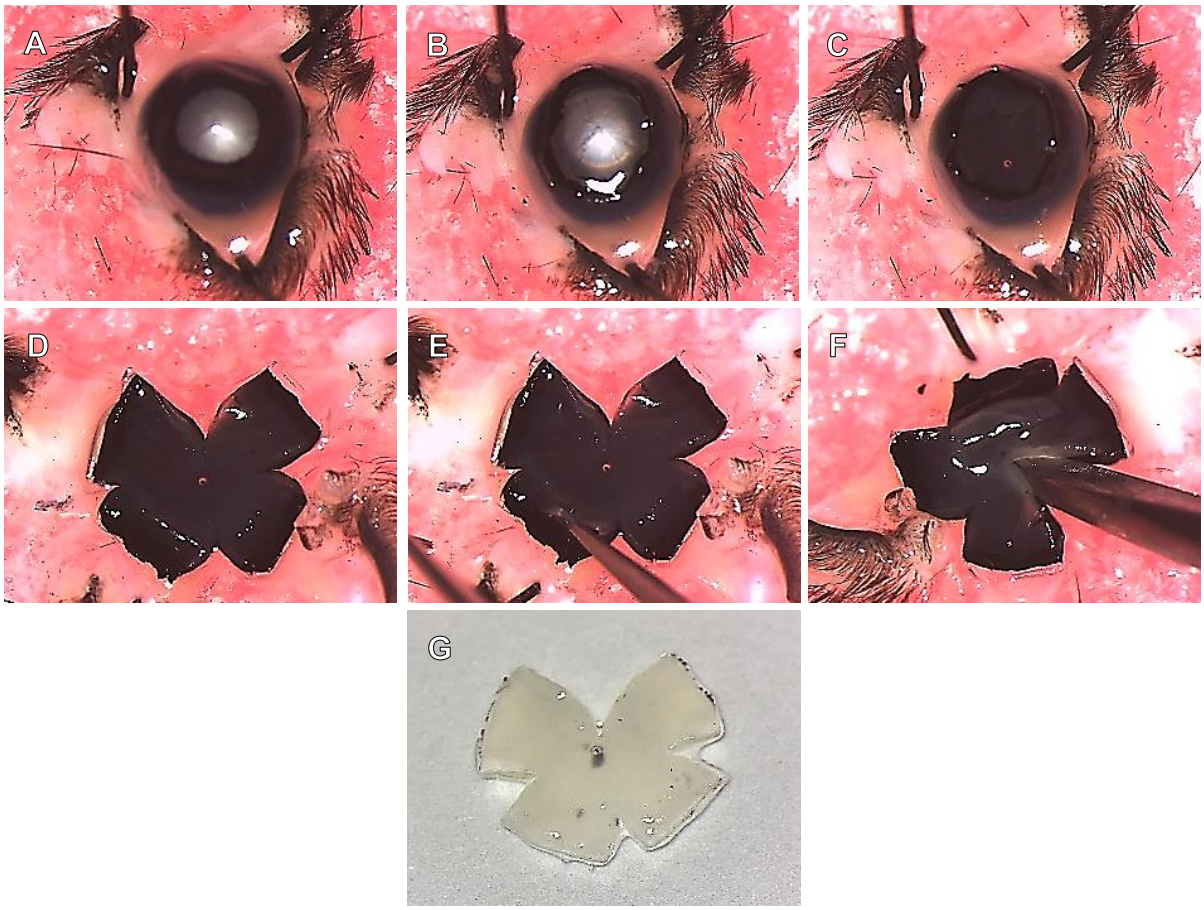

Figure 15: The dissection of the retina. A) The eye was fixed on a petridish filled with pink wax and three needles. B) The cornea was removed together with the iris. C) Also, the lens was removed so only the eye cup is left. The opaque layer that was visible, is the retina. D) Four cuts were made in the eye cup resulting in four petals. E) The retina was separated from the RPE. F) The retina is detached from the rest of the eye by cutting at the height of the ONH. G) The retina was removed from the rest of the eyecup and flattened and cleaned on a glass slide.

3.3 OPTICAL CLEARING

At this moment, deep tissue imaging is not possible for thick tissues as such. This holds especially for dense myelinated tissues, such as the ON. With the multiphoton microscope, the fluorescent signal is not detected beyond 100µm because of light scattering. Thus, to visualize whole mounted ONs, the tissue needs to be made transparent. For this, the optical clearing method, three-dimensional imaging of solvent-cleared organs (3DISCO) was tested (Ertürk *et al*, 2012a). First, the ONs were dehydrated through ascending series of tetrahydrofuran (THF; 50%, 70%, 80% and 2x100%; Sigma) during 20 minutes. This step was followed by an optical clearing step with benzyl alcohol and benzyl benzoate (BABB; 1:2 BA/BB; Sigma/Sigma), which makes the tissue transparent by adjusting the refractive index (RI) of the environment. The ONs were mounted between two coverslips that were 'glued' together with vaseline. The disadvantage is that BABB is a very reactive agent that affects the morphology of the tissue. Optical clearing dissolves the lipid structures in the cell such as the cell membrane and myelin. As such, making sections of cleared tissues results in a bad section morphology. Furthermore, cleared tissues cannot be stored for prolonged periods of time because the clearing solution degrades the fluorescent signal (Pernet *et al*,

2013b). For these reasons, imaging of cleared ONs has to be performed immediately or as soon as possible after the optical clearing step. Rehydration of the tissue disrupts the transparency.

3.4 WESTERN BLOTTING

Western blotting is an analytical technique that uses specific antibodies to identify and relatively quantify proteins that have been separated by gel electrophoresis based on their molecular weight (MW).

3.4.1 SAMPLE PREPARATION

The eye was removed from unfixed anesthetized mice by grasping the eye with a curved forceps and quickly rotating the animals. In this way, the blood vessels were squinted and blood loss was limited. The dissection of the retina was performed on ice, which reduces proteolytic activity and thus degradation of proteins. First, the cornea and the lens were removed and then, the retina was separated by tearing the RPE. Thereafter, the extracted retina was immersed in 100µl lysis buffer on ice, which disrupts the cell membrane and solubilizes the intracellular proteins so they can migrate individually through the gel. Next, the tissue was homogenized by sonicating the sample five times during 10 seconds. The homogenized mixture was heated at 70°C during 5 minutes. Subsequently, the solution was centrifuged at 4°C at 13,000 routs per minute (rpm) during 10 minutes. The supernatant was transferred to a new tube and stored at -80°C.

The protein concentrations of the various samples were determined with the fluorescence-based Qubit protein quantitation assay and the Qubit 2.0 fluorometer (Life Technologies). To be able to determine protein concentration, first, a standard curve was acquired by using three standards (0ng/µl, 200ng/µl and 400ng/µl; Invitrogen). The Qubit working solution was prepared by diluting the Qubit Protein Reagent (1:200; Invitrogen) in Qubit Protein Buffer (Invitrogen). The Qubit Protein Reagent contains advanced molecular probes that become fluorescent upon binding proteins. Of every standard, 10µl was diluted in 190µl of the Qubit working solution. Every sample was diluted 1/800 (first 1/20 in Milli-Q (MQ; Millipore Corporation) and then 1/40 in Qubit working solution). The standards and the samples were vortexed for 2-3 seconds and incubated at RT during 15 minutes to reach the optimal fluorescence. Absorbance values of the standards were plotted in function of the protein concentration and the equation of this standard curve was then used to determine the protein concentration of the samples.

3.4.2 VERTICAL GEL ELECTROPHORESIS AND ELECTRO BLOTTING

Proteins present in the protein mixture need to be separated so specific detection of the target proteins is possible. This was obtained with a lithium dodecyl sulphate-polyacrylamide gel electrophorese (LDS-PAGE) that separates the proteins based on their MW. Briefly,

5-13µl of every protein sample (depending on the concentration) was mixed with 5µl of 4X NuPAGE LDS sample buffer (Novex; Life Technologies; Carlsbad; USA), 2µl 10X NuPAGE sample reducing agent (Novex; Life Technologies) and further diluted with RNase-free water to a total volume of 20µl. LDS sample buffer is an anionic detergent and contains a positively charged lithium group and an apolar side chain. It causes protein denaturation by forming interactions with hydrophobic amino acid residues and applies a negative charge to all proteins. The reducing agent breaks covalent binding between subunits of a protein. This mixture was vortexed shortly and was heated in a heating block at 70°C during 10 minutes. Subsequently, 20µl of the sample mix and 10µl of the standard (Novex Sharp pre-stained Protein Standard; Invitrogen), which contains 12 proteins with a known MW, were loaded onto the gel (NuPAGE 4-12% Bis-Tris gel; Invitrogen). The chambers of the setup were filled with running buffer (Novex NuPAGE MOPS SDS running buffer; Invitrogen). The gel electrophoresis was performed during 55 minutes at 200V whereby the proteins migrated towards the positively charged anode through a polyacrylamide meshwork.

To detect the separated proteins with the help of antibodies, the proteins were transferred by electro blotting the gel onto a polyvinylidene fluoride (PVDF) membrane (0,2µm nitrocellulose; BioRad) using a Trans-Blot Turbo Transfer System apparatus (BioRad) and Trans-blot Turbo Transfer Packs (BioRad). To avoid contamination of the membrane, the blot can only be touched with tweezers.

3.4.3 IMMUNOLOGICAL DETECTION OF PROTEINS OF INTEREST

The membrane was then further processed with antibodies specific for the protein of interest, and these were visualized with secondary antibodies and detection reagents. First, the membrane was incubated with 5% commercial block (ECL blocking agent; GE Healthcare; Diegem; Belgium) dissolved in tris-buffered saline (TBS) during 2h. No milk powder was used since this contains MMPs, which would interfere with the results. The blot was cut into smaller blots and the membrane was incubated overnight in small plastic pockets with the primary antibody (Table 1; Addendum 3) diluted in 5% blocking solution. Subsequently, the membrane was rinsed three times during 10 minutes with TBS. The blot was incubated with horse radish peroxidase (HRP)-conjugated secondary antibody (1/25000 GAR-HRP; DAKO) diluted in 5% blocking solution during 45 minutes and rinsed two times during 10 minutes with TBS and once during 10 minutes with Tris. Then, the membrane was developed with the enhanced chemiluminiscence (ECL) system (Supersignal West Dura Extended Duration, Thermo Scientific). Briefly, the blot was immersed in a mixture of 1,5ml of solution A (luminol) and 1,5ml of solution B (H_2O_2). The HRP that is conjugated to the secondary antibody, catalyzes the oxidation of luminol to 3-aminophthalate, which leads to the emission of low-intensity light at 428nm. The blot was imaged with the BioRad ChemiDoc MP Imaging System (BioRad) that can detect this emission using the Image Lab 4.1 software (BioRad).

3.4.4 STRIPPING OF THE BLOT

After imaging the blot, it was rinsed during at least 30 minutes in TBS at RT followed by stripping during 15 minutes in Restore Western Blot Stripping Buffer (Thermo Scientific) at 37°C in the oven. Subsequently, the blot was rinsed two times during 5 minutes in TBS and 5 minutes in AD. A second protein can be detected on the same blot by repeating the steps from the immunological detection.

3.4.5 TOTAL PROTEIN STAIN

After all the proteins have been detected, a total protein stain was performed. The method is based on the Bradford method, which is a colorimetric protein assay based on the absorption maximum shift of the dye Coomassie Brilliant Blue G-250 (BioRad; Hercules; USA). The red cationic form of the dye with an absorption maximum at 470nm, is converted into its more blue form upon binding to mainly basic and aromatic amino acid residues under acidic conditions. This dye-protein complex results in a maximal absorbance shift to 595nm. The absorbance at 595nm is proportional to the protein concentration. After imaging of the blot, it was rinsed in TBS during at least 30 minutes. Then, the blot was incubated in stripping buffer during 5 minutes and rinsed 2 times during 5 minutes in TBS and 1 time during 5 minutes in MQ. The blot was incubated in Coomassie brilliant blue staining solution during 1 minute and incubated in destaining buffer during 20 minutes. The blot was rinsed in aqua destillata (AD) during 5 minutes and imaged with the BioRad ChemiDoc MP Imaging System.

3.5 EMBEDDING OF TISSUES

3.5.1 OPTIC NERVE

From the ON, cryosections were made. First, the ON was post-fixated in 4% PFA during 1h and then rinsed with PBS. Thereafter, the ON was cryoprotected through ascending series of sucrose (15%, 20% and 30% in PBS; Sigma), which replaces water in the tissue by sucrose. Different methods of embedding have been tested to obtain the best cryosections.

The first method was to embed the ON in 1,5% agarose (in PBS containing 5% sucrose; Life Sciences International). The ON was put on the bottom of a mold as straight as possible and was covered with a thin layer of agarose. After the agarose was solidified, the ON and the agarose were removed and put in a mold on top of a layer of solidified agarose. The mold was then filled with agarose and solidified in the fridge (4°C). Subsequently, the agarose was taken out of the mold and the orientation was marked. The agarose block was incubated in 30% sucrose during at least 2 days at 4°C.

The second approach was to embed the ON in TissueTek (Sakura Finetek; Berchem; Belgium). The mold was first filled with TissueTek and thereafter, the ON was put on the bottom of the mold as straight as possible. The TissueTek was frozen with liquid nitrogen and stored in the mold at -20°C until sectioning.

Another method was embedding the ONs right before cryosectioning. First, an empty TissueTek block was made and mounted on the cryostat (Microm HM650 cryostat; Thermo Scientific). A flat surface was created on the block without changing the angle of the sample stage of the cryostat. The ON was immersed in TissueTek during 15 minutes and then flattened as straight as possible on top of the flat surface of the empty TissueTek block. Thereafter, the ON was covered with TissueTek and frozen inside the cryostat chamber (-16°C). The advantage of the last method when compared to the other two is that this method is much faster and creates longer sections due to the possibility to put the ON more straight. The disadvantage is that sectioning has to happen very carefully because the two layers of TissueTek with the ON between them can separate.

3.5.2 RETINA

The dissected retina was post-fixated in 4% PFA during 1h and then rinsed in PBS. The retina was embedded in 1,5% agarose (in 5% sucrose in PBS). A thin layer of agarose was applied into the mold and solidified. The retina was then cut in half along the dorsal-ventral axis. The first half, the temporal part of the retina, was flattened on top of the first agarose layer with the RGC layer facing upwards. A thin layer of agarose was applied on top of the retina. Then, the second half of the retina, the nasal part, was flattened with the RGC layer upwards, on top of the second agarose layer. A last layer of agarose was applied on top of the retina. Thereafter, the agarose block was removed from the mold and the edges were trimmed in a trapezium-like shape. Sections of the temporal and the nasal retina were made at the same time, in which the latter was always on top. The agarose block was incubated in 30% sucrose during at least 2 days at 4°C.

3.6 PREPARATION OF CRYOSECTIONS

After cryopreserving and embedding, cryosections of 14µm of both ON and retina were made with the cryostat (HM560; Prosan). The specimen temperature was set to -29°C and the knife temperature was set to -27°C when the tissue was embedded in agarose. The agarose block with the ON or the retina was mounted on the cryostat with the help of TissueTek and frozen inside the cryostat chamber. When the tissue was embedded in TissueTek, the specimen temperature was set to -16°C and the knife temperature to -14°C. The sections of the ON and the retina were collected respectively on 5 and 10 glass slides (SuperFrost-plus microsope slides; Thermo Scientific) in series. The sections were stored at -20°C. Of note, sections of the ON that were injected with CTB have to be protected from light.

3.7 HEMOXYLIN AND EOSIN STAINING

To study the morphology of the tissue, hematoxylin and eosin (H&E) staining was performed on cryosections. The sections were rinsed with AD during 5 minutes and then

immersed in hematoxylin (Sigma) during 3 minutes. This stains all the basic structures like ribosomes, nuclei and nucleic acids. Thereafter, the sections were rinsed with running tap water during 10 minutes. Subsequently, they were immersed in eosin (Prosan) during 10 seconds. Eosin stains the acidic structures like the cytoplasm and other eosinophilic structures. Then, the sections were rinsed twice with AD and dehydrated in ascending series of ethanol (50%, 70%, 96%; klinipath) during a few seconds and twice in 100% ethanol (Merck;VWR) during 3 minutes. The sections were immersed in xylene during 2 times 5 minutes and then mounted with depex (DPX; Prosan). They were dried overnight at 37°C.

3.8 IMMUNOHISTOCHEMISTRY

Immunohistochemistry (IHC) is a technique that uses antibodies to visualize certain epitopes of specific proteins in tissue samples and is based on the specific binding of antibodies to epitopes of antigens. The interaction between the antibodies and the epitopes is detected following the indirect method. First, the application of a specific unlabeled primary antibody is responsible for the specificity by binding to the protein of interest. The visualization of this complex can be accomplished with several techniques. A fluorescent labeled secondary antibody can be applied that binds to the constant part (Fc region) of the primary antibody (figure 16A). This method is only possible if the protein of interest is abundant and/or if the primary antibody is sensitive. To improve the sensitivity, the fluorescent signal can be amplified with a tyramide signal amplification (TSA) kit (Perkin Elmer; Waltham; USA) using a short or long amplification procedure. If a short amplification step is needed, the secondary antibody that binds to the primary antibody is labelled with HRP (figure 16B). This catalyzes multiple reactions that convert tyramide together with H_2O_2 to create O_2 and highly reactive free oxygen radicals. Fluorescent labeled tyramide is precipitated and forms covalent bindings in the proximity of the antigen. If a long amplification step is needed, the secondary antibody is biotinylated and streptavidin is labeled with HRP

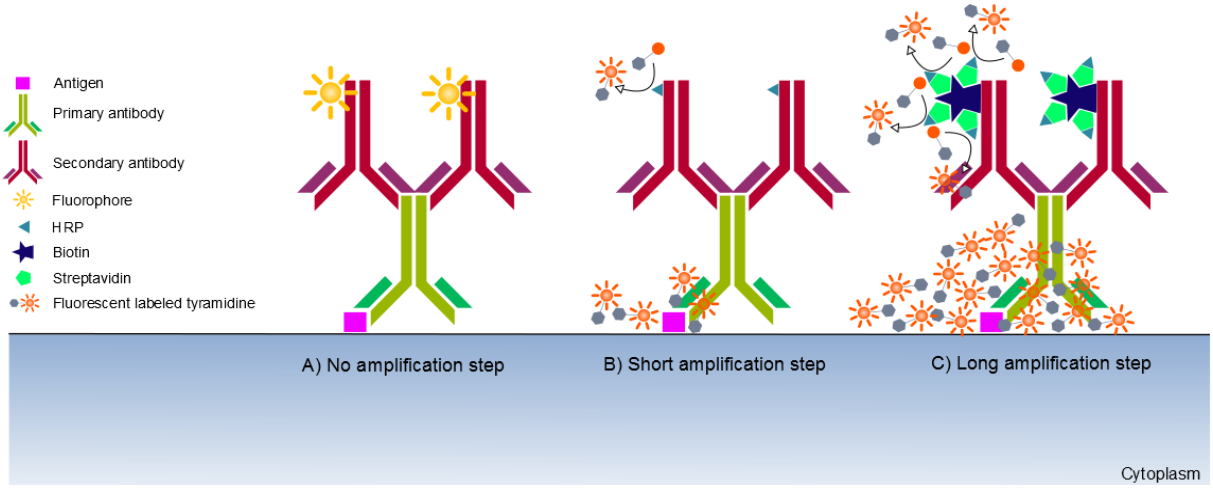

Figure 16: Overview of the indirect method of IHC. A) If no amplification step is needed, the secondary antibody is labeled with a fluorophore. B) During a short amplification step, a primary antibody, a HRP conjugated secondary antibody and fluorescent labeled tyramidine are used to amplify the signal. C) During a long amplification step, a primary antibody, a biotinylated secondary antibody, a HRP conjugated streptavidine and a fluorescent labeled tyramidine are employed to amplify the signal once more. Reproduced from (Boenisch, 2001).

(figure 16C). Biotin is a low molecular vitamin that binds streptavidin with very high affinity. It has multiple binding sites for streptavidin and increases the number of HRP molecules associated with the antigen. Here, the amount of fluorescent labeled tyramide near the protein of interest is even more increased than in the short amplification.

3.8.1 WHOLE MOUNT

First, the retinas were post-fixed in 4% PFA during 1h and then rinsed in PBS during 30 minutes. The retinas were permeabilized during 2 times 10 minutes in PBST and frozen in PBST during 15 minutes at -80°C. The retinas were thawed at RT and rinsed in PBST during 2 times 10 minutes. Then, they were incubated with the primary antibody (1:750 in 2% pre-immune serum and 2% triton X-100 (VWR) in PBS; table 3; Addendum 3) at RT. Thereafter, the retinas were rinsed in PBST during 3 times 10 minutes. The samples were incubated in the dark with the secondary antibody (1:500 in 2% triton X-100 in PBS; table 4; Addendum 3) during 2h. The retinas were rinsed during 3 times 10 minutes with PBST and rinsed with PBS. The retinas were post-fixed in 4% PFA during at least 1h and 30 minutes, rinsed in PBS and flattened on a microscope slide with the RGC layer up, covered with mowiol and mounted with a round coverslip.

3.8.2 CRYOSECTIONS

3.8.2.1 GENERAL PROTOCOL

The sections were rehydrated in AD during 5 minutes and in TBS during 5 minutes. In fixated tissue samples, the chemicals involved in fixation create aldehyde cross-links between proteins which might interfere with the capability of the antibody to recognize its antigen. For epitope retrieval, sections can be placed in citrate buffer, which unmasks the antigens by breaking these cross-links upon heating, using the microwave or oven method. The sections were immersed in citrate buffer and put in the microwave during 2 times 5 minutes at 700W and 5 minutes at 500W. In the oven method, the sections were immersed in preheated citrate buffer and put in the oven during 20 minutes at 95°C. The sections were cooled down during 20 minutes. Then, the slides were rinsed with TBS during 3 times 5 minutes. When an amplification step is needed, blocking the endogenous peroxidases is necessary. The slides were immersed in methanol with 0,3% H_2O_2 during 20 minutes and rinsed with TBS during 3 times 5 minutes. Then, the aspecific binding places were blocked with blocking buffer or pre-immune serum (table 2; Addendum 3) during 45 minutes at RT. The primary antibody (table 3; Addendum 3) was applied and incubated overnight in a humidity chamber. After 3 times 5 minutes rinsing with TBS, the slides were incubated with the secondary antibodies (table 4; Addendum 3) during 2 hours. The slides were rinsed with TBS during 3 times 5 minutes. If the secondary antibody is linked with biotin, the slides were immersed in streptavidin-HRP (1:100 in TNB) during 30 minutes which will bind multiple times to biotin. HRP will convert H_2O_2 in H_2O and oxygen radicals. The slides were rinsed

with TBS during 3 times 5 minutes and the fluorophore, Cy3-Tyr (1:50 in amplification diluent) was applied during 8 minutes, which will precipitate in the vicinity of oxygen radicals. The slides were rinsed with TBS during 3 times 5 minutes. Then, the slides were immersed in 4',6-diamidino-2-phenylindole (DAPI; 1:1000 in PBS) during 30 minutes. All the antibodies were diluted in tris-sodiumchloride blocking buffer (TNB) and the entire protocol is performed at RT. Finally, the slides were mounted with mowiol and a coverslip.

3.8.2.2 GAP-43

The sections were rehydrated in TBS during 5 minutes. Then, the slides were immersed in methanol during 10 minutes and rinsed in TBS during 3 times 5 minutes. The aspecific binding places were blocked with blocking solution (10% pre-immune donkey (PID) in TBS; table 2; Addendum 3) during 1h and the primary antibody (1:200 in solution A; table 3; Addendum 3) was applied overnight. Thereafter, the slides were rinsed in TBS_2T for permeabilization during 1h and blocked in solution A (5% PID; 2% BSA in TBS_2T) during 1h. The slides were rinsed again in TBS_2T during 1h and the secondary antibody 1:500 in solution A; table 4; Addendum 3) was applied during 2h. The slides were rinsed in TBS_2T during 2 times 10 minutes and in TBS during 10 minutes. At last, the sections were mounted with mowiol and a coverslip.

3.9 IMAGING

Imaging of the sections and whole mounts of the ONs and retinas was performed with a multiphoton microscope (BX61WI, Olympus, Aartselaar, Belgium) and a confocal microscope (FV 1000D, Olympus, Aartselaar, Belgium). Unlike conventional fluorescence microscopes, the confocal microscope collects light form a single focal plane by using point illumination and a pinhole in an optically conjugated plane in front of the detector to eliminate out-of-focus signal. It scans the specimen point-by-point and line-by-line and assembles the pixel information into a single image. By moving the focal plane in axial direction, single images can be put together to build up a three-dimensional (3D) stack. A multiphoton microscope uses pulsed long-wavelength light. Where the two long-wavelength photons arrive simultaneously, the electron is excited into a higher energy state, from which it can decay, while emitting a fluorescence signal.

Retinal whole mounts and optical cleared ONs were imaged with the upright FV 1000-M system multiphoton microscope and a MaiTai HP DeepSee laser system (690-1020nm; Spectra Physics) using Fluoview 4.0 software. Serial optical z-sectioning was performed over the entire surface of the retina or ON with a 20x objective (Olympus). The images were taken with dimensions of 512x512 pixels, a step size of 3µm and identical settings for laser intensity, brightness and contrast. The 3D images of the optical cleared ON were created with Imaris (Bitplane; Oxford Instruments company).

Images of the retinal and ON sections were obtained with the inverted IX81 variant confocal scanning microscope FV 1000D equipped with an argon laser (FV5-Lamar-2 with a wavelength of 458, 488 and 514nm), an Neon-Helium laser (FV10-LAHEG2-30-2 with a wavelength of 543nm) and two led diodes (wavelength 405 and 635nm). Images were taken with a 20x objective (Olympus) using the Fluoview 4.0 software. Images were taken with dimensions of 1024x1024 pixels, a step size of 1µm and identical settings for laser intensity, brightness and contrast. The stacks of the images of both microscopes were projected over the z-axis into a single projection and saved as an .oib file or an .tiff file for analysis.

The H&E stained sections were imaged with the Zeiss Imager bright field microscope (Zeiss, Zaventem, Belgium) equipped with an AxioCam (MRc5).

3.10 ANALYSES

3.10.1 RETINAL WHOLE MOUNTS

RGC density (number of RGCs/mm²) was evaluated on entire retinal flatmounts after immunostaining for Brn3a, which is a transcription factor expressed by the RGCs. The number of Brn3a$^+$ cells were automatically computed using Fiji software and an in house made macro (Geerearts et al, *submitted*). Briefly, a rolling ball background subtraction was used and after local tresholding, Brn3a immunopositive RGCs were automatically counted, based on selection criteria for size and shape (circularity). The retinal flatmount was manually outlined and its surface was computed, to yield the total number of RGCs over the total surface of the retina.

3.10.2 OPTIC NERVE SECTIONS

To study axonal regeneration in the ON, the amount of axon growth has to be analyzed. Axon growth is quantified by manually counting the number of CTB or GAP-43$^+$ axons every 300µm (distance d) beyond the crush site, in 2-7 sections per ON with the help of ImageJ and the ZEN software. At each distance, the cross-sectional width of the nerve was measured along with counting the amount of axons. By dividing the amount of axons by the corresponding cross-sectional width of the ON, the number of axons per µm of nerve width can be calculated at each distance and in every section of one ON. For each distance, the amount of axons per µm of nerve width was then averaged over the sections. The average amount of axons per µm of nerve width was then divided by the sectional thickness (t = 14µm), which results in the amount of axons per µm². The total estimated number of axons in the ON extending distance d, measured in a nerve having a radius (r) of 150µm, was then estimated by multiplying the amount of axons per µm² by the surface area of a circle (πr²) (formula 1) (Leon *et al*, 2000).

$$\Sigma a_d = \pi r^2 \, x \, \frac{Average\left(\#\,axons/\mu m\ of\ nerve\ width\right)}{t} \qquad \textbf{Formula 1}$$

3.10.3 WESTERN BLOT

The western blots were analyzed with the Image Lab 4.1 software (BioRad). The total volume of the bands that correspond to the protein of interest was calculated together with the total volume of the total protein staining. These were divided by each other to calculate the relative volume of the protein of interest of each sample.

3.11 STATISTICS

Statistical analysis was performed using GraphPad Prism 5.01 software (GraphPad Software, La Jolla, USA). The values were expressed as mean values ± standard error (SEM). For the RONC experiments, in which statistical differences between two groups with one or more independent variables needed to be analyzed, a repeated measures two-way analysis of variance (ANOVA) was used in combination with a Bonferroni post-test. Differences between groups were considered significant at *p<0,05; **p<0,01 and ***p<0,001.

4 RESULTS

4.1 METHODOLOGY: CHARACTERIZATION AND OPTIMIZATION

4.1.1 RONC AS A MODEL TO STUDY AXONAL REGENERATION

In present study, the role of MMP-2 and MT1-MMP in axonal regeneration is investigated by using the RONC model, which combines an ONC with a controlled intraocular inflammation. In this model, the ON is crushed at 1mm from the ONH during 5 seconds with a self-clamping forceps. Thereafter, the inflammation-inducing agent, zymosan, is injected intravitreally together with CPT-cAMP. The mice are sacrificed 14 days post injury (dpi) and axonal regeneration in the ON is quantified. Although the procedures in the RONC model are standardized, the model suffers from a high inter-animal variability. In most of the ON sections, a glial scar is observed just after the crush site. Most of the axons seem to regenerate around this glial scar, *i.e.* circumvent the glial scar, and only few of them regenerate through the glial scar (figure 17). Also, an accumulation of inflammatory cells is seen in the glial scar (figure 17C). Notably, there is some differential formation of the glial scar in various animals even within the same experiment.

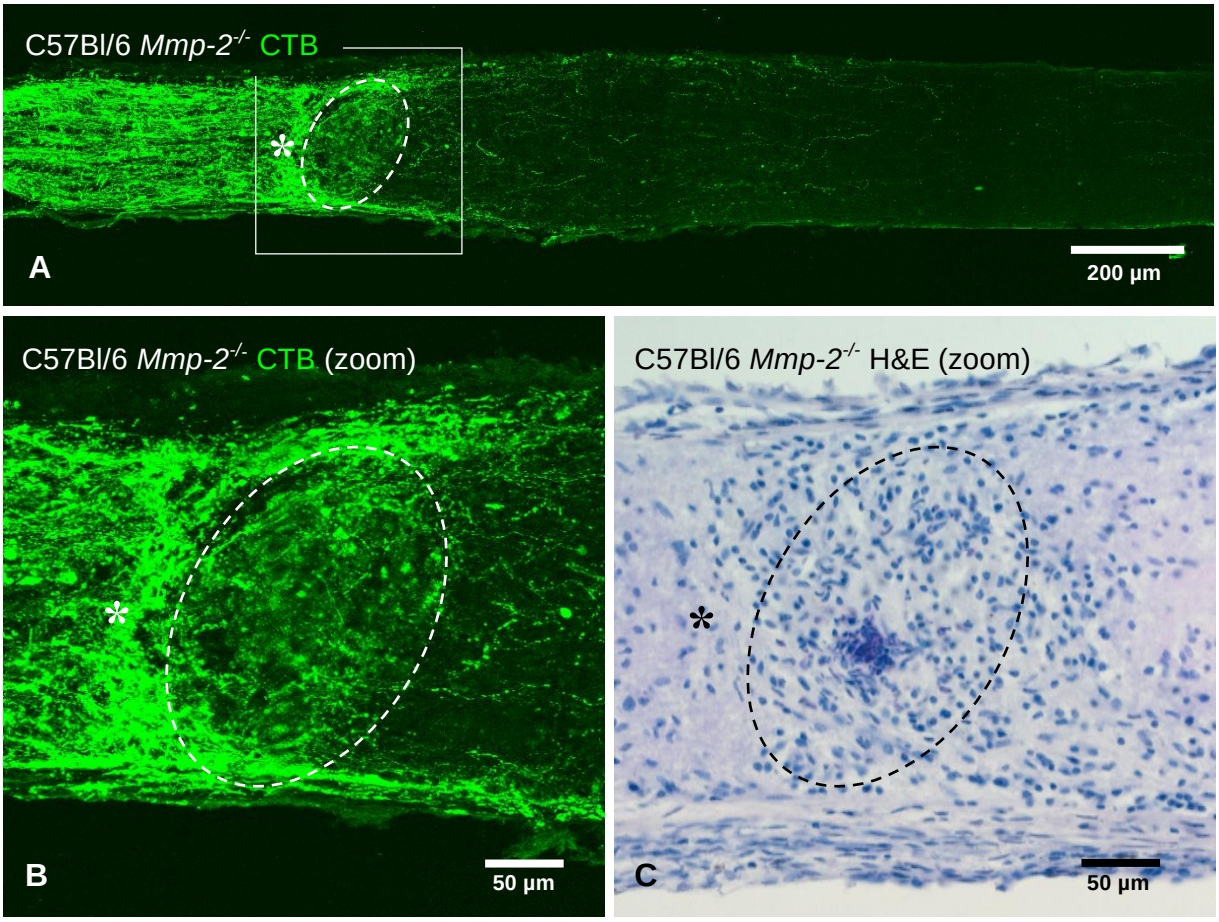

Figure 17: Most of the axons regenerate around the glial scar. A) The behavior of regenerating axons in the presence of a glial scar in the ON at 14 dpi is evaluated. Regenerating axons are traced with CTB in ON sections. B) Enlarged image of figure A showing that the glial scar (circumvented with a dashed line) is formed just after the ONC (indicated with an asterisk). Most of the regenerating axons circumvent the glial scar, while only a few regenerate through the glial scar. C) H&E of the same ON section showing accumulation of nuclei at the glial scar. Scale bar (A): 100µm; Scale bar (B, C): 50µm.

4.1.2 AXONAL TRACING METHOD

To investigate the effect of MMP-2 and MT1-MMP on axonal regeneration, the number of regenerating axons after RONC is determined using two different methods (figure 18). The first tracing method is the intravitreal injection of CTB, which is a powerful tool for labeling neurons and neurites, as this neuronal tracer is anterogradely transported by binding to ganglioside G_{M1} and attaching to living neurons. The other tracing method includes a IHC staining against GAP-43, a growth associated protein, that is specifically expressed in regenerating axons.

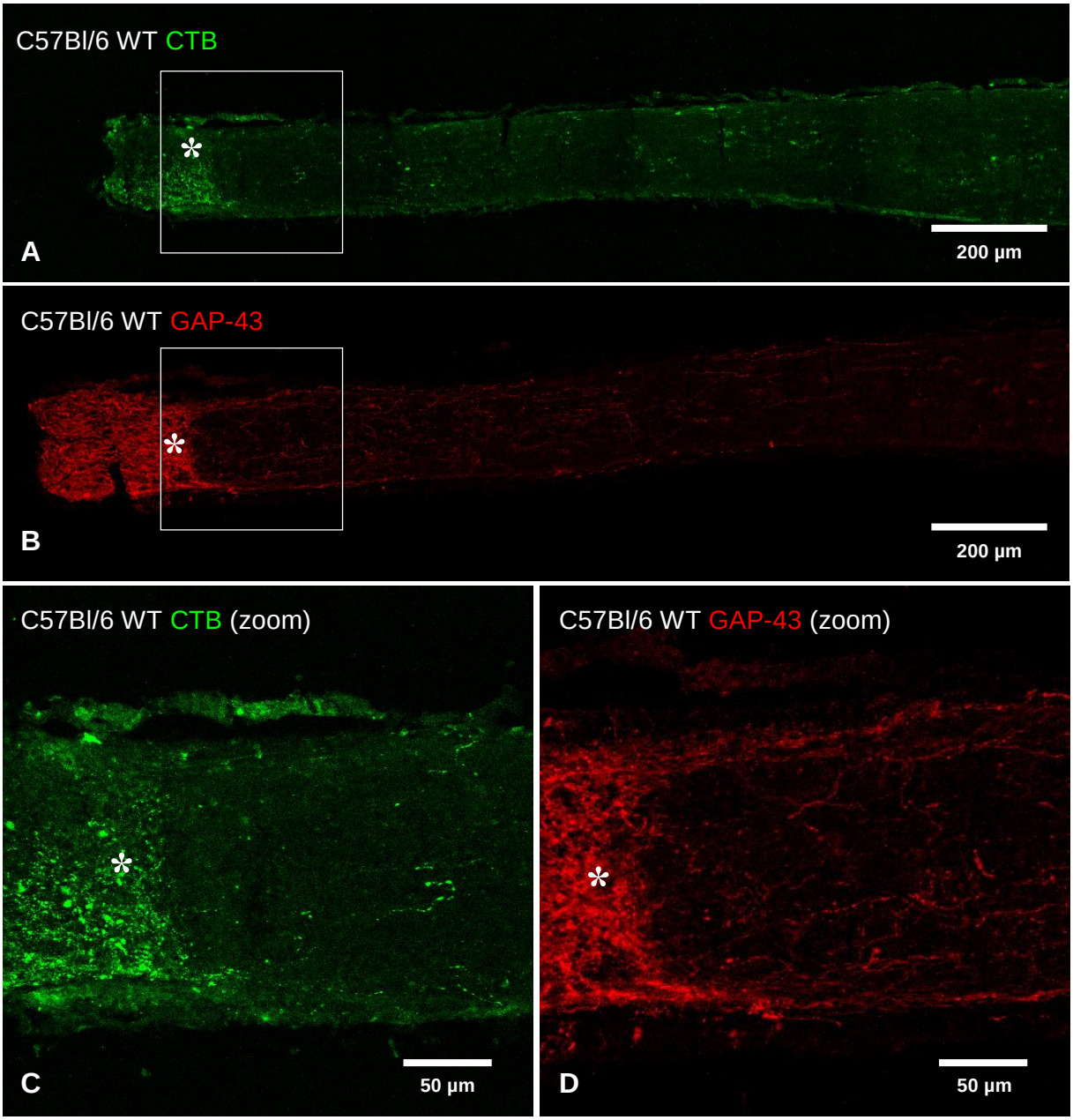

Figure 18: The number of regenerating axons can be visualized with CTB tracing and GAP-43 staining. The two different tracing methods determining the number of regenerating axons per ON at 14 dpi are compared. A) Regenerating axons are anterogradely traced with CTB on ON sections. B) Regenerating axons are stained for GAP-43 on ON sections. C) The number of CTB^+ axons are quantified on ON sections. D) The number of $GAP\text{-}43^+$ axons are quantified on ON sections. The ONC site is denoted with an asterisk. C and D are the enlarged images of respectively A and B indicated by squares. Scale bar (A, B): 200µm; Scale bar (C, D): 50µm

First, sections of the same ON were traced with CTB and then stained for GAP-43. The double stainings of these sections were used to analyse the number of CTB^+ axons and $GAP\text{-}43^+$ axons. However, these sections revealed that the special protocol of the GAP-43 staining probably affects the CTB tracing and that the CTB signal is lost after the staining procedure. As such, a much lower number of CTB^+ axons is counted on sections that were stained with GAP-43 than on unstained sections (data not shown). The IHC protocol for GAP-43 is thus not compatible with the fluorescent tracing, as the latter is quenched. Therefore, no double labeling of RGC axons is possible with the current methods.

To evaluate which method is the better one, the number of CTB^+ axons is compared with the number of $GAP\text{-}43^+$ axons in adjacent sections (14µm) of the same ON (N=3; number of regenerating axons counted every 300µm) (figure 18). There is a trend towards more $GAP\text{-}43^+$ axons (276 ± 48; 158 ± 10; 92 ± 18; 35 ± 8 at 300µm, 600µm, 900µm and 1200µm respectively) than CTB^+ axons (168 ± 57; 85 ± 37; 23 ± 8; 10 ± 3 at 300µm, 600µm, 900µm and 1200µm respectively) (figure 19). However, both methods show a similar axonal regeneration pattern. While the number of axons counted with the CTB methods shows a lower number of axons, differences did not reach significance.

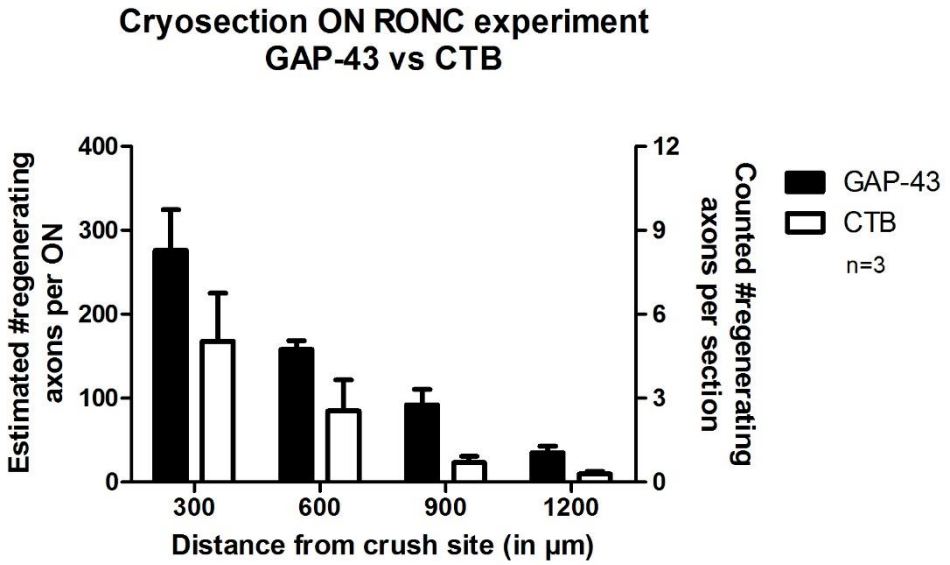

Figure 19: There are more $GAP\text{-}43^+$ regenerating axons in comparison with CTB^+ regenerating axons. Graphic of the estimated number of regenerating axons per ON and the counted number of axons per section in function of the distance from the ONC comparing $GAP\text{-}43^+$ (black) and CTB^+ (white) axons. The number of CTB^+ and $GAP\text{-}43^+$ axons are counted at 300, 600, 900 and 1200µm from the ONC. The number of $GAP\text{-}43^+$ axons is higher than the number of CTB^+ axons at 14 dpi but the data are not statistically significant (Repeated measures two way ANOVA; Mean ± SEM; N=3).

4.1.3 OPTICAL CLEARING TO TRACE AXONAL TRAJECTORIES

3D images come in handy when the navigation and potential misguidance of regenerating axons in the ON post injury is investigated. However, at this moment, it is not possible to image samples as thick as the rodent ON at microscopic resolution because of light scattering in such tissue. This restricts imaging to superficially coursing axons. One potential way to overcome this obstacle is tissue clearing. Therefore, the optical clearing following the

3DISCO method is tested. In the clearing process, the tissue is dehydrated and then immersed in a solution that resembles the RI of lipids in fixated tissue. The ON becomes transparent and light does not scatter, thereby rendering the tissue amenable to deep tissue fluorescence imaging. To investigate whether the 3DISCO works on ON and enables us to visualize the entire ON, uninjured ONs injected with CTB that were cleared were compared with uninjured ONs injected with CTB that were not cleared (figure 20). The optical clearing was also tested on thymocyte antigen 1-yellow fluorescent protein (*Thy1-YFP*) transgenic mice (figure 21). After the final clearing step, the ON was completely transparent (result not shown) and 3D images of the entire ON could be created, whereas in the ON without optical clearing, only the coursing axons near the surface of the ON could be visualized (figure 20,

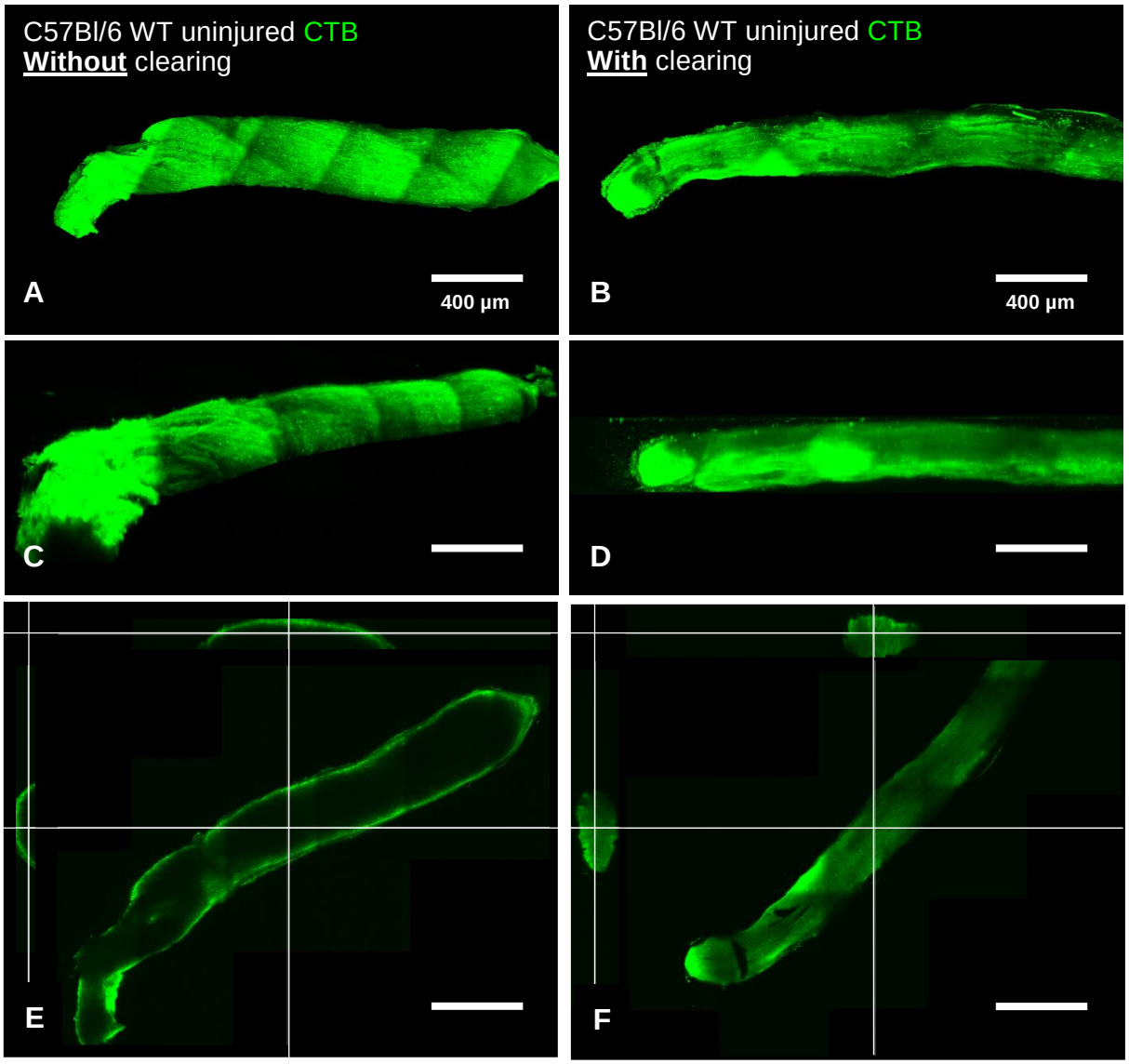

Figure 20: The entire ON can be imaged in 3D using optical clearing. The 3DISCO method was tested comparing cleared and non-cleared uninjured ONs of WT mice of which the axons are traced with CTB. A) The Z-stack of an ON without optical clearing and B) with optical clearing shows the 2D images of ONs. C) 3D image of the ON without optical clearing and D) with optical clearing. E) A single image in the middle of the Z-stack of the ON without optical clearing and F) with optical clearing with the trans sectional images on the left side and above the image. The trans-sectional images show that only the surface of the non-cleared ON is visualized, while the entire ON can be visualized when it is cleared. Scale bar: 400µm.

21). Also, the entire ON of the *Thy1-YFP* transgenic mice can be visualized after tissue clearing (figure 21). Unfortunately, the process to get 3D images with a multiphoton microscope with a resolution that is high enough to be analyzed, is very time consuming.

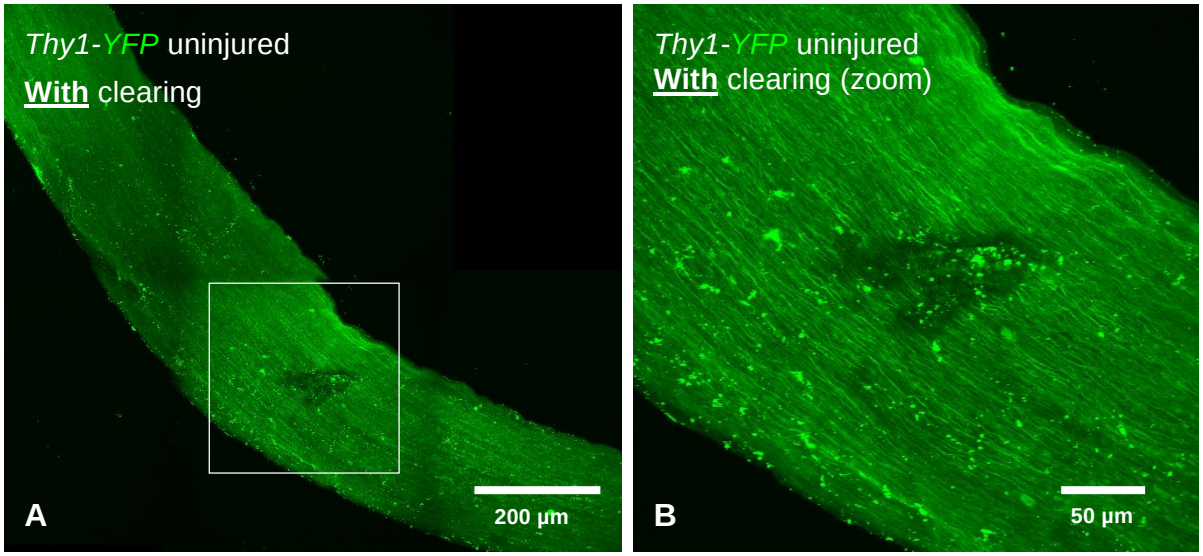

Figure 21: *Thy1-YFP* transgenic mice are compatible with the 3DISCO. A) Uninjured ONs of *Thy1-YFP* transgenic mice are cleared with the 3DISCO method. B) Axons are intrinsically traced since these express YFP under the control of the Thy1 promotor and can be visualized in the entire ON after clearing. Scale bar: 200µm and 50µm.

4.2 THE ROLE OF MMP-2 IN AXONAL REGENERATION

4.2.1 AXONAL REGENERATION IN WT AND *MMP-2*$^{-/-}$ MICE AT 14 DPI

MMP-2 is a gelatinase that has been suggested to contribute to the hydrolysis of molecules that inhibit axonal regeneration in the injured CNS of adult mammals. In that way, it clears the path for axon outgrowth. Since, preliminary *ex vivo* data show that MMP-2 plays a role in neurite outgrowth (Gaublomme *et al*, 2014), *in vivo* experiments are performed in which the RGC axonal regeneration in the ON is examined. The RONC model is applied and the animals are sacrificed at 14 dpi. The day before they are sacrificed, CTB, conjugated to alexa fluor 488, is injected intravitreally. Since the optical clearing protocol is not fully optimized, the number of CTB^{+} axons is quantified with two different approaches. In the first approach, the CTB^{+} axons are visualized in whole mounted ON (figure 22). To lose as little information as possible, both sides of every ON are imaged with a multiphoton microscope and analyzed.

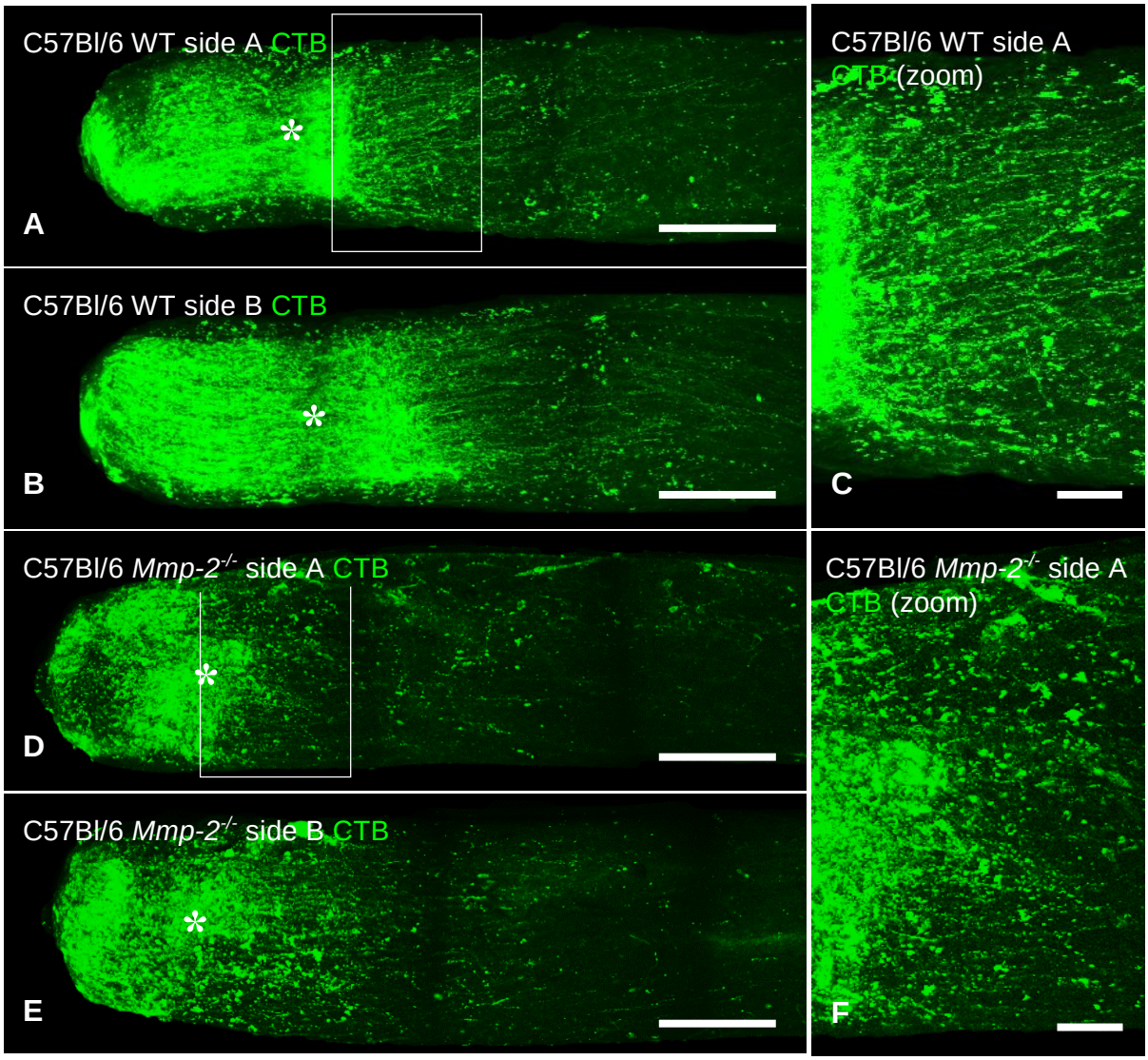

Figure 22: The number of regenerating axons in WT and *Mmp-2*$^{-/-}$ mice can be analyzed on whole mounted ON without clearing. A, B) Axonal regeneration is visualized with CTB tracing in ON of WT mice and D, E) of *Mmp-2*$^{-/-}$ mice at 14 dpi. C) The axons of WT and F) of *Mmp-2*$^{-/-}$ mice are analyzed on both sides of the ON. ONC site is indicated with an asterisk. C and F are the enlarged images of respectively A and D indicated by squares. Scale bar: (A, B, D, E) 200µm and Scale bar: (C, F) 50µm.

In that way, the coursing CTB$^+$ axons near the entire surface of the ON could be visualized. The number of CTB$^+$ axons is quantified in WT (N=5) as well as in *Mmp-2*$^{-/-}$ mice (N=8) every 300µm till 1200µm from the crush site. The resulting number of CTB$^+$ axons post injury in WT mice correspond to the results observed in a previous study where the number of regenerating axons is counted in the same way but using only one side of the ON (Tom Buyens, personal communication; figure 23A). Thereafter, the results of the WT mice are compared to the results of the *Mmp-2*$^{-/-}$ mice. This analysis reveals a trend towards a reduced number of outgrowing axons in *Mmp-2*$^{-/-}$ mice, as compared to WT animals (figure 23B).

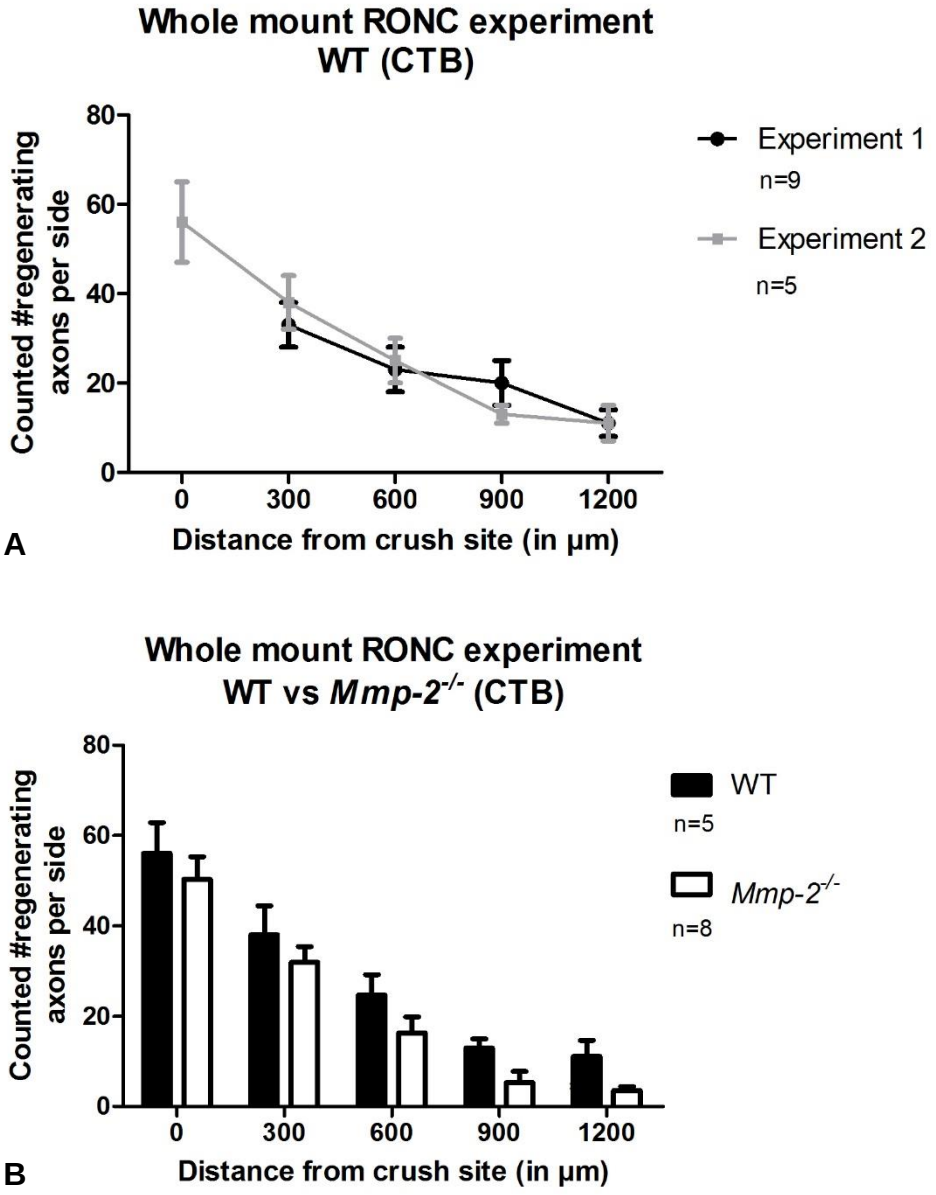

Figure 23: *Mmp-2*$^{-/-}$ mice have a smaller number of regenerating axons compared to WT mice when analyzed on whole mounted ONs without clearing. A) Using this method, the number of regenerating axons of current study, counting on both sides of the ON, corresponds to the number of regenerating axons of previous study, counting on only one side of the ON (performed by Tom Buyens). B) Both sides of the ON of WT and of *Mmp-2*$^{-/-}$ mice are compared. The number of CTB$^+$ axons in WT mice is higher than the number of CTB$^+$ axons in the *Mmp-2*$^{-/-}$ mice. However, the difference is not significant (Repeated measures two way ANOVA; Mean ± SEM; N=5 (WT) and N=8 (*Mmp-2*$^{-/-}$)).

A second approach, that is more used in general, is to make longitudinal, histological, 14µm sections of the ON and determine the number of CTB$^+$ axons on multiple sections (4-6 sections) per ON (figure 24). The total number of CTB$^+$ axons per ON in WT (N=8) and *Mmp-2*$^{-/-}$ (N=15) mice is then estimated every 300µm from the crush site using formula 1. At 300 and 600µm, there is a significant larger number of regenerating axons in the WT mice (respectively, 313 ± 39 and 143 ± 32) than in the *Mmp-2*$^{-/-}$ mice (respectively, 177 ± 16 and 74 ± 39). At 900 and 1200µm, a fewer number of CTB$^+$ axons is observed in the *Mmp-2*$^{-/-}$

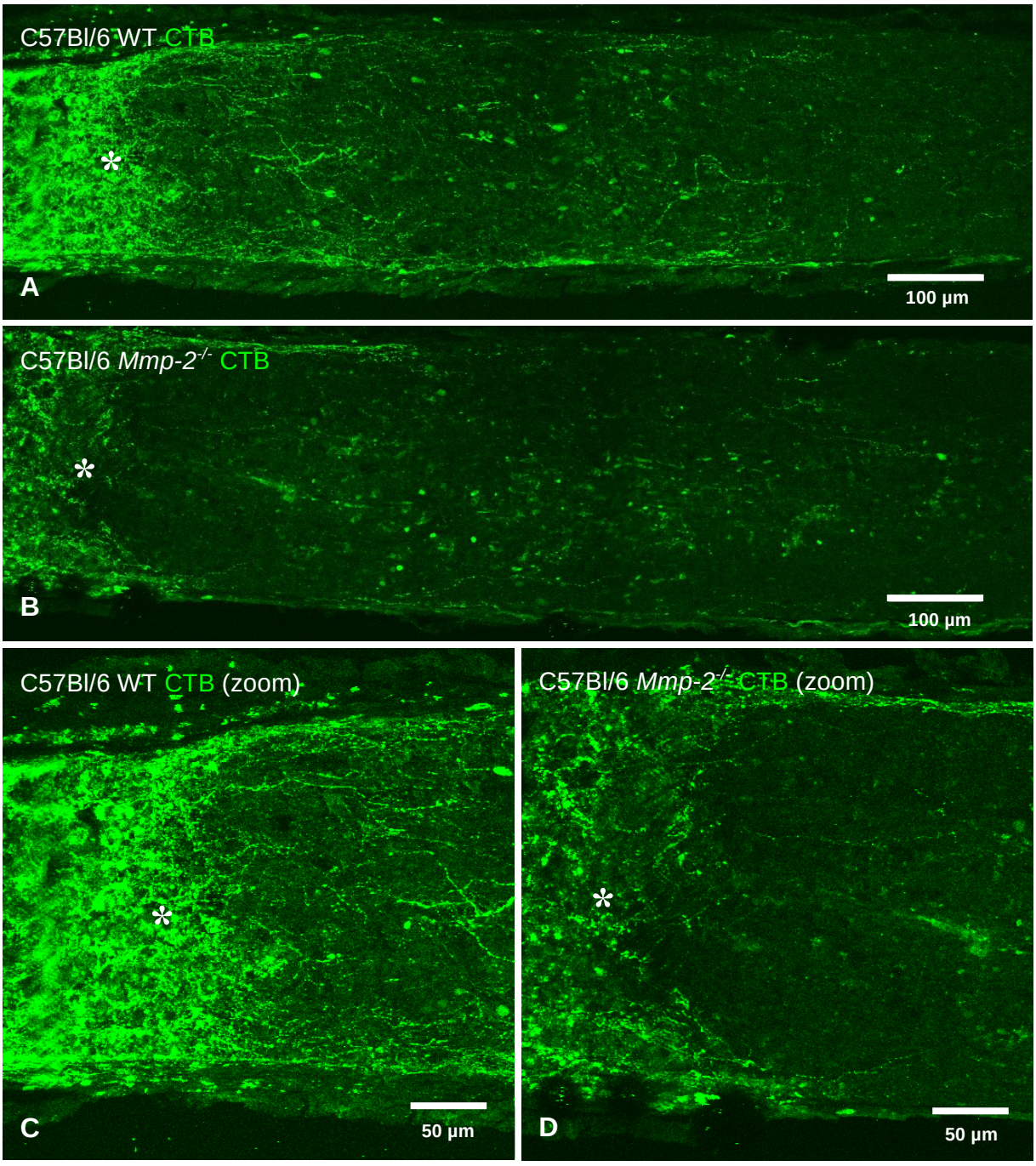

Figure 24: The number of regenerating axons in WT and *Mmp-2*$^{-/-}$ mice can be analyzed on ON sections. A) Axonal regeneration is visualized with CTB tracing in ON sections of WT mice and B) of *Mmp-2*$^{-/-}$ mice at 14 dpi. C) The axons of WT and D) *Mmp-2*$^{-/-}$ mice are analyzed on ON sections. ONC site is indicated with an asterisk. C and D are the enlarged images of respectively A and B. Scale bar (A, B): 100µm; Scale bar (C, D): 50µm.

(respectively 33 ± 7; 25 ± 10) mice than in the WT mice (respectively 58 ± 15; 10 ± 5) but the difference is not statistically significant (figure 25). At all distances, the number of CTB^+ axons in the *Mmp-2*$^{-/-}$ mice is between 40 and 50% lower than the number of CTB^+ axons in the WT ON.

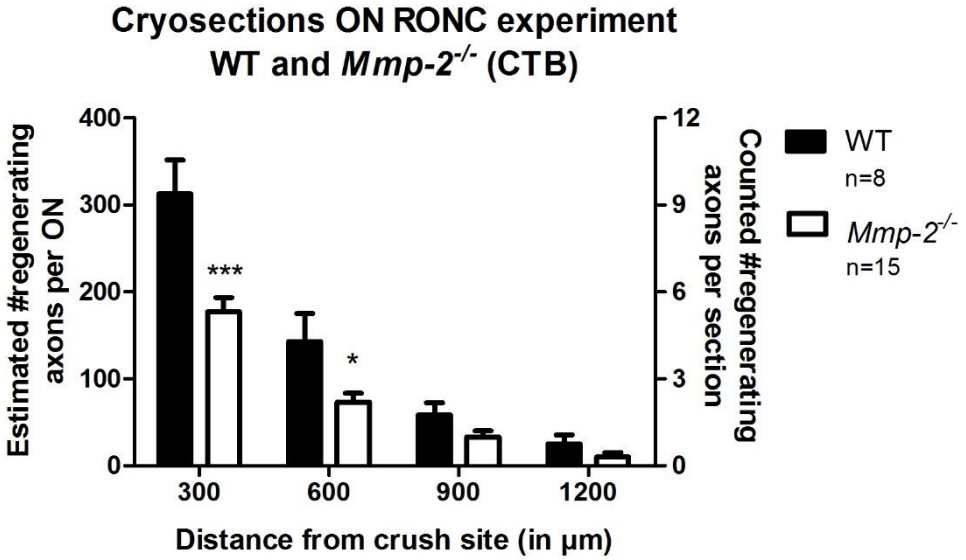

Figure 25: *Mmp-2*$^{-/-}$ mice have a smaller number of regenerating axons compared to WT mice when analyzed on ON sections at 14 dpi. Graphic of the number of CTB^+ axons per ON and counted number of regenerating axons per section in function of the distance from the ONC comparing the number of CTB^+ axons in WT (black) and *Mmp-2*$^{-/-}$ (white) mice at 14 dpi. The number of CTB^+ axons are counted at 300, 600, 900 and 1200µm from the ONC. The number of CTB^+ axons in WT mice is significantly larger at 300 and 600µm from the ONC. The number of CTB^+ axons in WT mice is larger at 900 and 1200µm from the ONC but this is not significant (Repeated measures two way ANOVA; Mean ± SEM; N=8 (WT) and N=15 (*Mmp-2*$^{-/-}$).

4.2.2 AXONAL REGENERATION IN WT AND *MMP-2*$^{-/-}$ MICE AT 42 DPI

To study the axonal regeneration after a longer period of time, a preliminary study is performed by applying the RONC model on a group of WT (N=5) and *Mmp-2*$^{-/-}$ (N=5) mice that are only sacrificed at 6 weeks (42 days) post injury. The CTB is injected one week before sacrificing the animals. The ONs are sectioned and the CTB^+ axons are quantified on multiple sections (2-3 sections) per ON and the total number is estimated with formula 1 every 300µm till 3000µm from the crush site. Again, at 300µm from the crush site, there are significantly more CTB^+ axons in the WT mice (399 ± 56) than in the *Mmp-2*$^{-/-}$ mice (271 ± 29). At the other distances, there is a higher number of CTB^+ axons in WT mice than in *Mmp-2*$^{-/-}$ mice but there is no statistically significant difference (figure 26). At 300, 600, 900, 1200 and 1500µm from the crush site the number of CTB^+ axons in the *Mmp-2*$^{-/-}$ mice is 30-50% lower than in the WT mice. At the other distances, this varies between 10 and 80%.

The number of CTB^+ axons in WT mice and *Mmp-2*$^{-/-}$ mice at 14 and 42 dpi is compared. As expected, the number of CTB^+ axons is higher in the ONs at 42 dpi than in the ONs at 14 dpi in both WT and *Mmp-2*$^{-/-}$ mice. In WT mice, there is a trend towards more CTB^+ axons at 42 dpi but the data are not statistically significant (figure 27). The number of CTB^+ axons in WT mice is 28%, 69%, 176% and 346% higher (for respectively 300, 600, 900 and

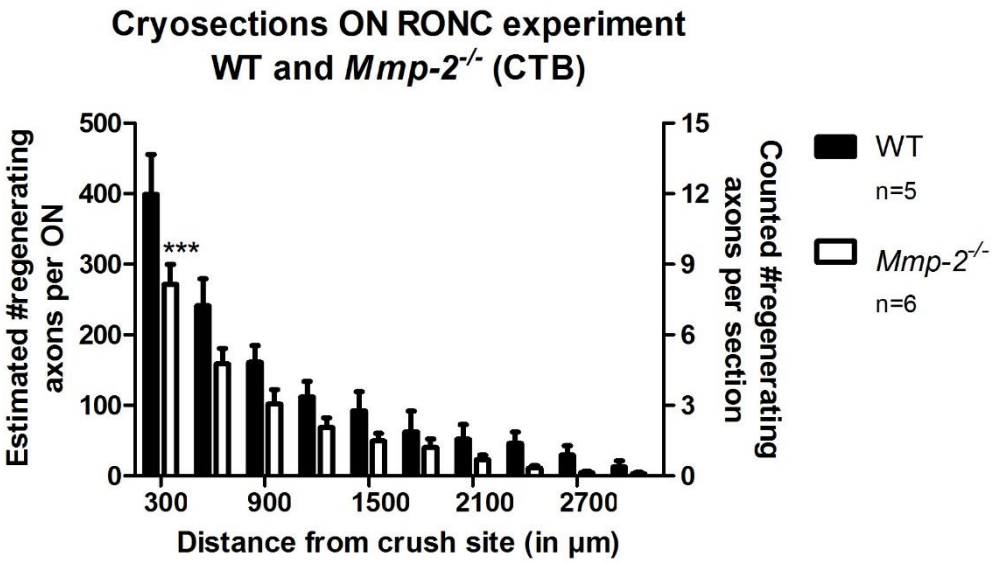

Figure 26: *Mmp-2*$^{-/-}$ mice have a smaller number of regenerating axons compared to WT mice when analyzed on ON sections at 42 dpi. Graphic of the number of CTB^{+} axons per ON and the counted number of regenerating axons per section in function of the distance from the ONC comparing WT (black) and *Mmp-2*$^{-/-}$ (white) mice at 42 dpi. The number of CTB^{+} axons are counted every 300µm till 3mm from the ONC. The number of CTB^{+} axons in WT mice is significantly larger at 300µm from the ONC. The number of CTB^{+} axons in WT mice is larger at every other distance from the ONC but this is not significant (Repeated measures two way ANOVA; Mean ± SEM; N=5 (WT) and N=6 (*Mmp-2*$^{-/-}$)).

1200µm) at 42 dpi than at 14 dpi. In the *Mmp-2*$^{-/-}$ mice, the number of CTB^{+} axons at 42 dpi is also higher than the number of CTB^{+} axons at 14 dpi (figure 28). Here, the results are statistically significant at every distance from the crush site measured. The number of CTB^{+} axons in *Mmp-2*$^{-/-}$ mice is 53%, 116%, 209% and 576% higher (for respectively 300, 600, 900, 1200µm) at 42 dpi than at 14 dpi.

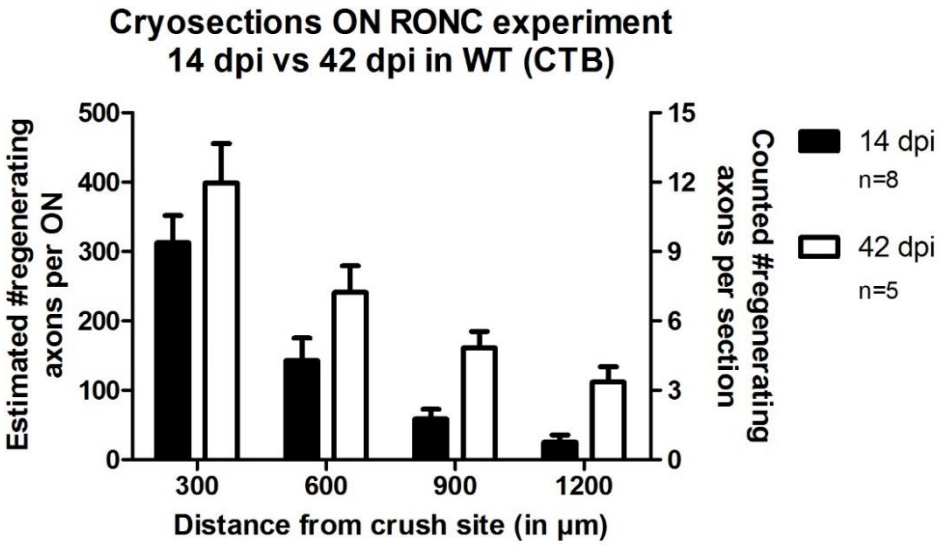

Figure 27: WT mice have a smaller number of regenerating axons at 14 dpi compared to 42 dpi when analyzed on ON sections. Graphic of the number of CTB^{+} axons per ON and counted number of regenerating axons per section in function of the distance from the ONC comparing the number of CTB^{+} axons at 14 (black) and at 42 (white) dpi. The number of CTB^{+} axons are counted at 300, 600, 900 and 1200µm from the ONC. In WT mice, the number of CTB^{+} axons at 42 dpi is larger than at 14 dpi but this is not significant (Repeated measures two way ANOVA; Mean ± SEM; N=8 (14dpi) and N=5 (42dpi)).

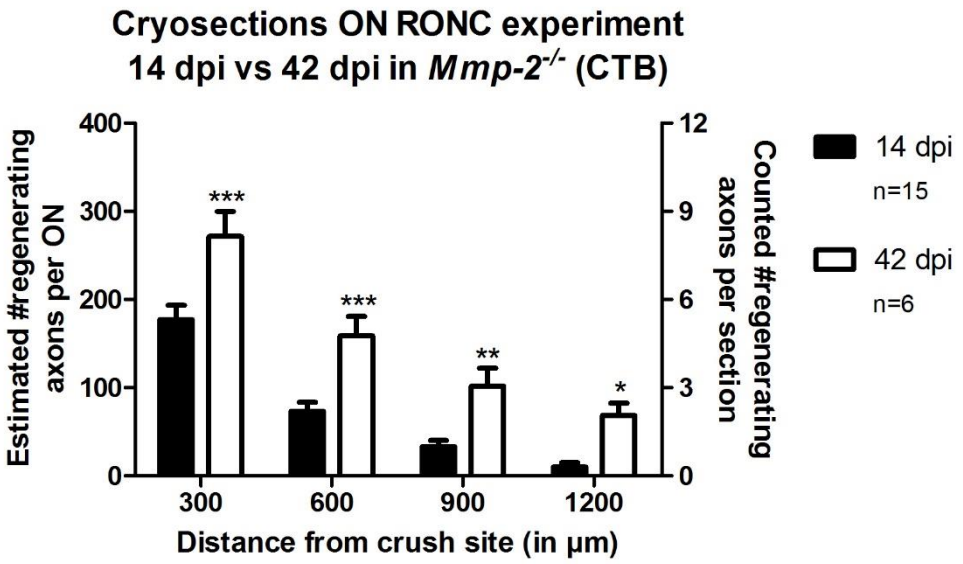

Figure 28: *Mmp-2*$^{-/-}$ mice have a smaller number of regenerating axons at 14 dpi compared to 42 dpi when analyzed on ON sections. Graphic showing the number of CTB^{+} axons per ON and counted number of regenerating axons per section in function of the distance from the ONC comparing the number of CTB^{+} axons at 14 (black) and at 42 (white) dpi The number of CTB^{+} axons are counted at 300, 600, 900 and 1200µm from the ONC. In *Mmp-2*$^{-/-}$ mice, the number of CTB^{+} axons at 42 dpi is significantly higher than at 14 dpi at all distances measured (Repeated measures two way ANOVA; Mean ± SEM; N=15 (14 dpi) and N=6 (42 dpi)).

4.2.3 MMP-2 EXPRESSION IN THE REGENERATING OPTIC NERVE AND RETINA.

To investigate the expression pattern of MMP-2 in the healthy and regenerating ON and retina, an IHC study is done on tissues of WT mice (N=4). The mice are sacrificed at 2, 7 and 14 dpi. Both the retina and the ON are sectioned and stained for MMP-2, followed by a DAPI counterstaining. The MMP-2 staining in the ONs does not show a specific signal at first sight and needs further optimization (figure 29).

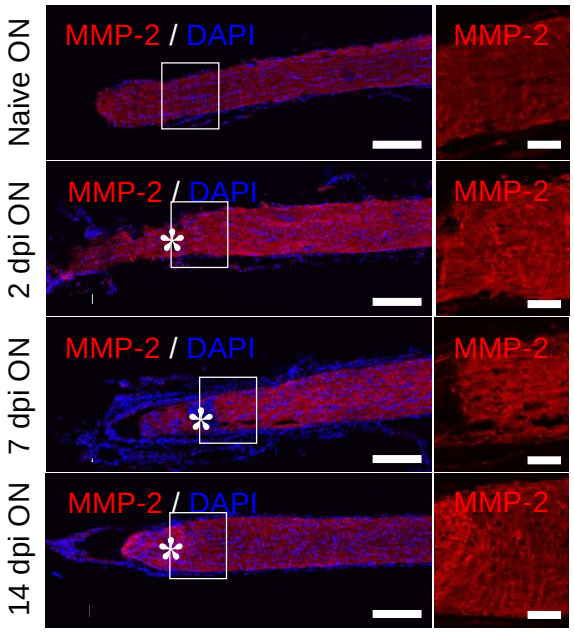

Figure 29: Expression pattern of MMP-2 in the ON. ON dissected at 2, 7 and 14 dpi together with naive ON that serve as control. The ONs are stained with MMP-2 (red) and counterstained with DAPI (blue). The asterisks show the ONC. The right column are the enlarged images of the left column indicated by the square. Scale bar left column: 150µm; Scale bar right column: 50µm.

MMP-2 in the healthy and injured adult retina is expressed in the Müller glia. MMP-2 expression in the retina at 7 dpi seems to be upregulated (figure 30A-D). In most of the retinas at 2 dpi (N=3/4) but also in some of the retinas at 7 and 14 dpi (N=2/4), MMP-2^{+} cells accumulate in the vitreous of the eye of zymosan injected WT animals (figure 31I-L).

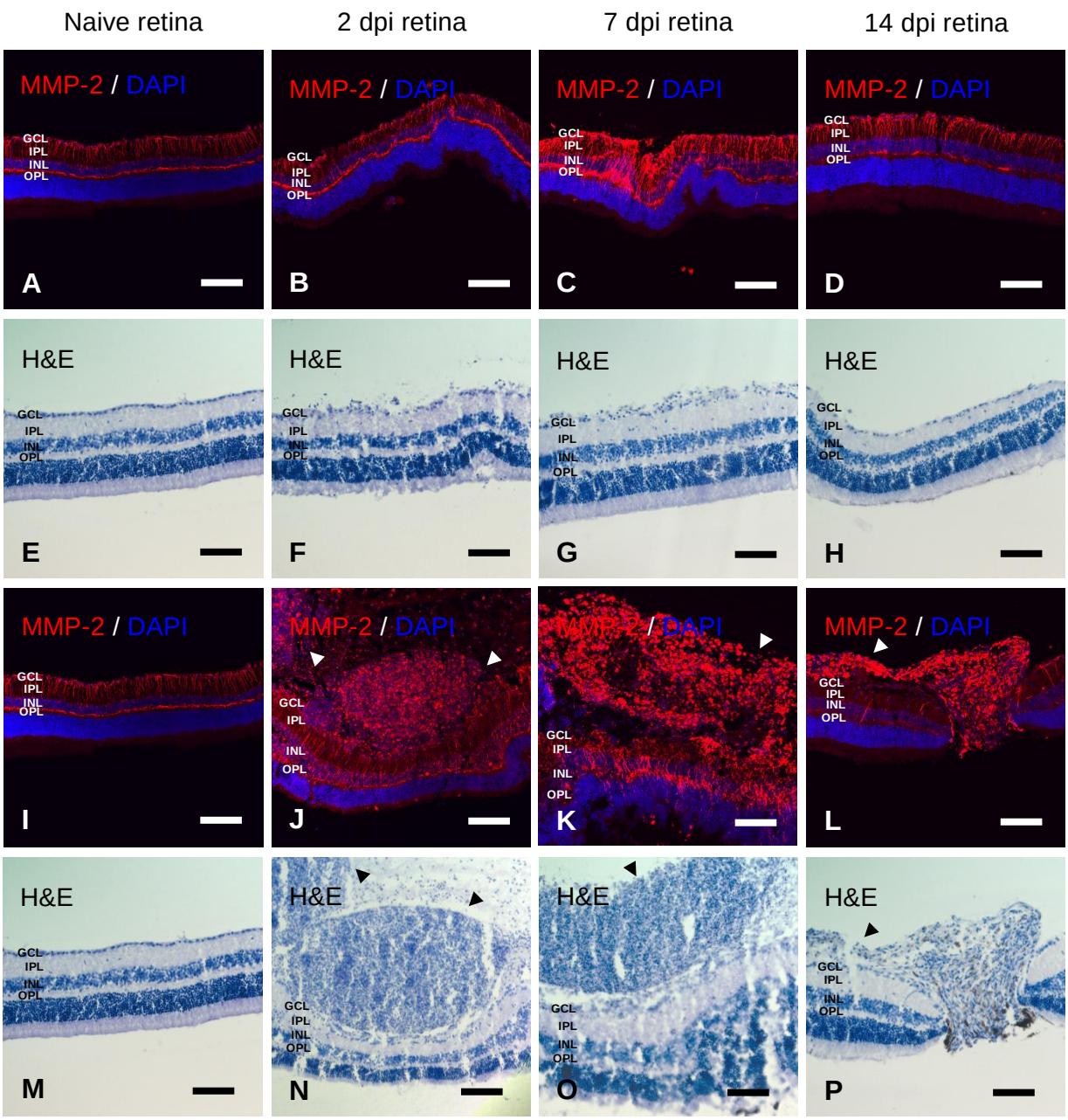

Figure 30: Expression pattern of MMP-2 in the retina. Retinas are dissected at 2, 7 and 14 dpi together with naive retinas that serve as control. A-H) Retinal sections without infiltrating cells are stained for MMP-2 (red) and counterstained with DAPI (blue) (A-D) and a H&E staining (E-H). I-P) Retina with infiltrating cells (except for the naïve retina), which are indicated by arrowheads, are stained for MMP-2 (red) and counterstained with DAPI (blue) (I-L) and a H&E staining (M-P). There seems to be an upregulation of MMP-2 expression at 7 dpi. Scale bar: 100µm.

4.2.4 RGC SURVIVAL IN WT AND *MMP-2*$^{-/-}$ MICE AT 14 DPI

To study the effect of *Mmp-2* deficiency on RGC survival, the retinas of the WT and *Mmp-2*$^{-/-}$ mice, harvested at 14 dpi, are used to quantify the RGC density. Hereto, retinal flat mount retinas are stained with Brn3a, which is a transcription factor expressed by the RGCs. The RGC density of the right eyes (uninjured eye, oculus dexter; OD) is set to 100%. The percentages of RGC density in the left eyes are calculated. No significant difference in the number of Brn3a^{+} RGCs is observed in the left eyes (injured eye; oculus sinister; OS) of WT (N=4) and the *Mmp-2*$^{-/-}$ (N=7) mice (figure 31).

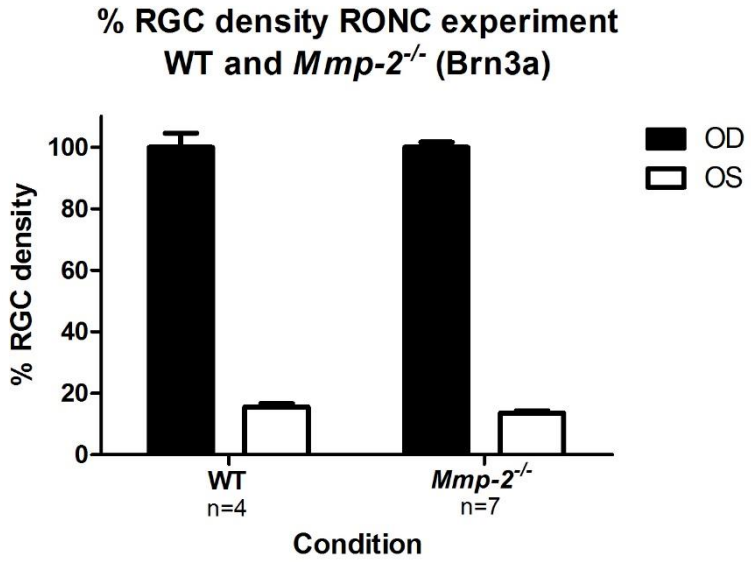

Figure 31: There is no difference observed in the percentage of RGC density in WT and *Mmp-2*$^{-/-}$ mice at 14 dpi. Graphic with the percentage of RGC density in function of the different conditions comparing WT and *Mmp-2*$^{-/-}$ mice. The number of Brn3a^{+} RGCs in the OD (black) is set to 100%. There is no significant difference in the percentage of RGC survival in the OS (white) of the WT and *Mmp-2*$^{-/-}$ mice after ONC (Repeated measures two way ANOVA; Mean ± SEM; N=4 (WT) and N=7 (*Mmp-2*$^{-/-}$)).

4.3 THE ROLE OF MT1-MMP IN AXONAL REGENERATION

MT1-MMP is a membrane anchored MMP, which has been shown to be essential in the degradation of connective tissue and is the endogenous activator of pro-MMP-2. To study the role of MT1-MMP in axonal regeneration, the expression of the *Mt1-mmp* gene has to be disrupted. However, due to the inadequate collagen turnover, MT1-MMP deficient mice develop dwarfism, osteopenia, arthritis and connective tissue disease which results in postnatal mortality due to wasting (Holmbeck *et al*, 1999). Therefore, a *Mt1-mmp*$^{flox/flox}$ transgenic mouse line was generated to enable conditional, cell-specific deletion of *Mt1-mmp*. The *Mt1-mmp*$^{flox/flox}$ mouse line was mated with inducible *GLAST-Cre(ER)T2* mice. In that way, a Müller glia-specific knockdown of *Mt1-mmp* is created. The knockdown of the *Mt1-mmp* gene is obtained via the systemic administration of TXF, which induces the relocation of Cre recombinase from the cytoplasm to the nucleus where it cleaves at the LoxP sites and as such removes the *Mt1-mmp* gene from the genome. To ensure efficient Cre recombinase-mediated *Mt1-mmp* ablation, RONC was applied 14 days after the last TXF injection.

4.3.1 EFFICIENCY OF THE *MT1-MMP* KNOCKDOWN

The efficiency of the knockdown of *Mt1-mmp* is evaluated with a western blot for MT1-MMP using the retina of the eyes with an uninjured ON. Two different polyclonal rabbit anti-MT1-MMP antibodies were used; antibody Ab53712 recognizes the hemopexin domain of MT1-MMP, while RP3 recognizes the catalytic domain of MT1-MMP. Both antibodies recognize soluble, active MT1-MMP (50-53kDa) but only RP3 recognizes membrane-bound, active MT1-MMP (57kDa). Some variation in MT1-MMP expression was present even in the control mice. The amount of soluble and membrane-bound MT1-MMP expression in the control mice is set to 100%. A lower amount of membrane-bound, active MT1-MMP (100,0 ± 8,9% *versus* 12,1 ± 7,2%), soluble, active MT1-MMP (100,0 ± 19,3% *versus* 14,6 ± 10,7%) as well as MT1-MMP degradation products (data not shown) was observed in the *Mt1-mmp*$^{flox/flox}$*;GLAST-CreER*$^{+/-}$ mice as compared to the control mice (figure 32).

With the same samples, a western blot for MMP-2 is performed to check whether the downregulation of MT1-MMP has an effect on the levels of active MMP-2. A polyclonal rabbit anti-MMP-2 antibody is used, that recognizes the hemopexin domain of MMP-2. This antibody recognizes active MMP-2 better than pro-MMP-2. There is no significant difference between the amount of active MMP-2 in the *Mt1-mmp*$^{flox/flox}$*;GLAST-CreER*$^{+/-}$ mice (96,6 ± 6,2%) and the respective control mice (100,0 ± 6,8%) (data not shown).

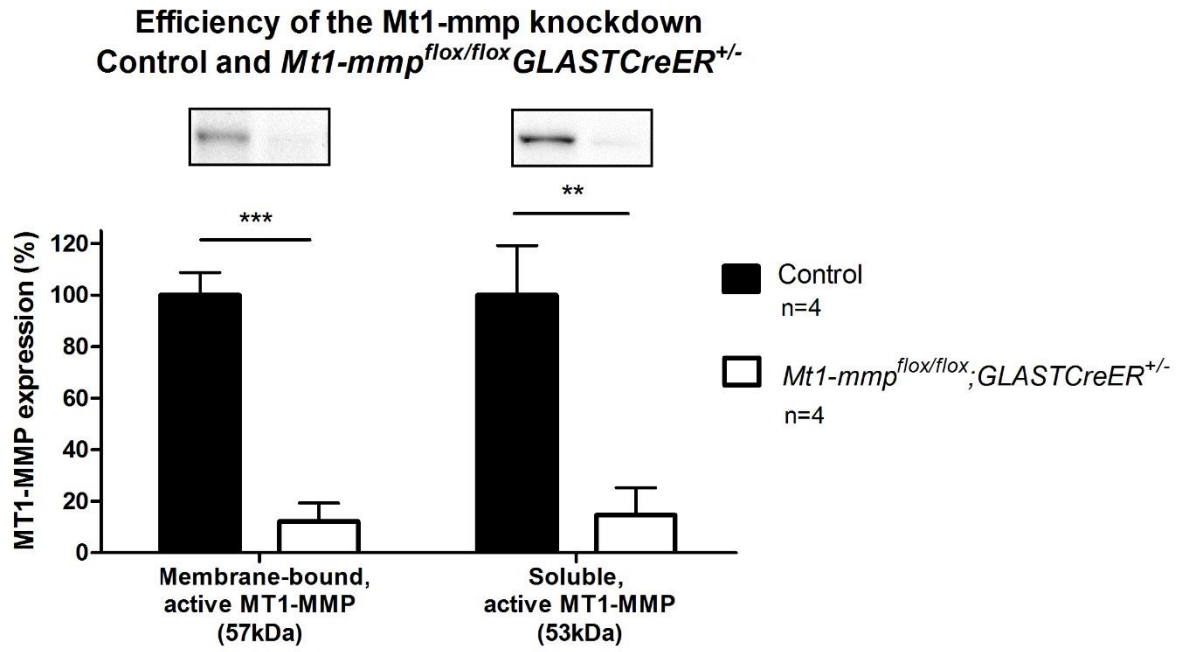

Figure 32: Expression of MT1-MMP in the healthy adult mouse retina *Mt1-mmp$^{flox/flox}$;GLAST-CreER$^{+/-}$* is decreased upon Cre recombinase activation. Graphic showing the percentage of membrane-bound, active MT1-MMP and soluble, active MT1-MMP expression comparing control and *Mt1-mmp$^{flox/flox}$;GLAST-CreER$^{+/-}$* mice. Western blot reveals less soluble, active MT1-MMP and membrane-bound, active MT1-MMP in the *Mt1-mmp$^{flox/flox}$;GLAST-CreER$^{+/-}$* mice (Repeated measures two way ANOVA; Mean ± SEM; N=4).

4.3.2 AXONAL REGENERATION IN CONTROL AND *MT1-MMP$^{FLOX/FLOX}$;GLAST-CREER$^{+/-}$* MICE AT 14 DPI

Another 14 days after injury, axonal regeneration is quantified in control and *Mt1-mmp$^{flox/flox}$;GLAST-CreER$^{+/-}$* mice. The number of GAP-43^{+} axons regenerating beyond the ONC is counted on multiple cryosections (2-4 sections) per ON every 300µm from the crush site (figure 33). Then, the total number of GAP-43^{+} axons per ON is estimated with formula 1, which reveals that at every distance measured, the number of GAP-43^{+} axons is lower in mice with *Mt1-mmp* knockdown (423 ± 88; 278 ± 81; 154 ± 48 and 76 ± 33 for respectively 300, 600, 900 and 1200µm) as compared to the control mice (557 ± 90; 342 ± 65; 188 ± 34 and 77 ± 21 for respectively 300, 600, 900 and 1200µm) (figure 34). The number of GAP-43^{+} axons in the *Mt1-mmp$^{flox/flox}$;GLAST-CreER$^{+/-}$* mice is 25%, 10%, 9% and 1% lower than in the control mice for respectively 300, 600, 900 and 1200µm from the crush site.

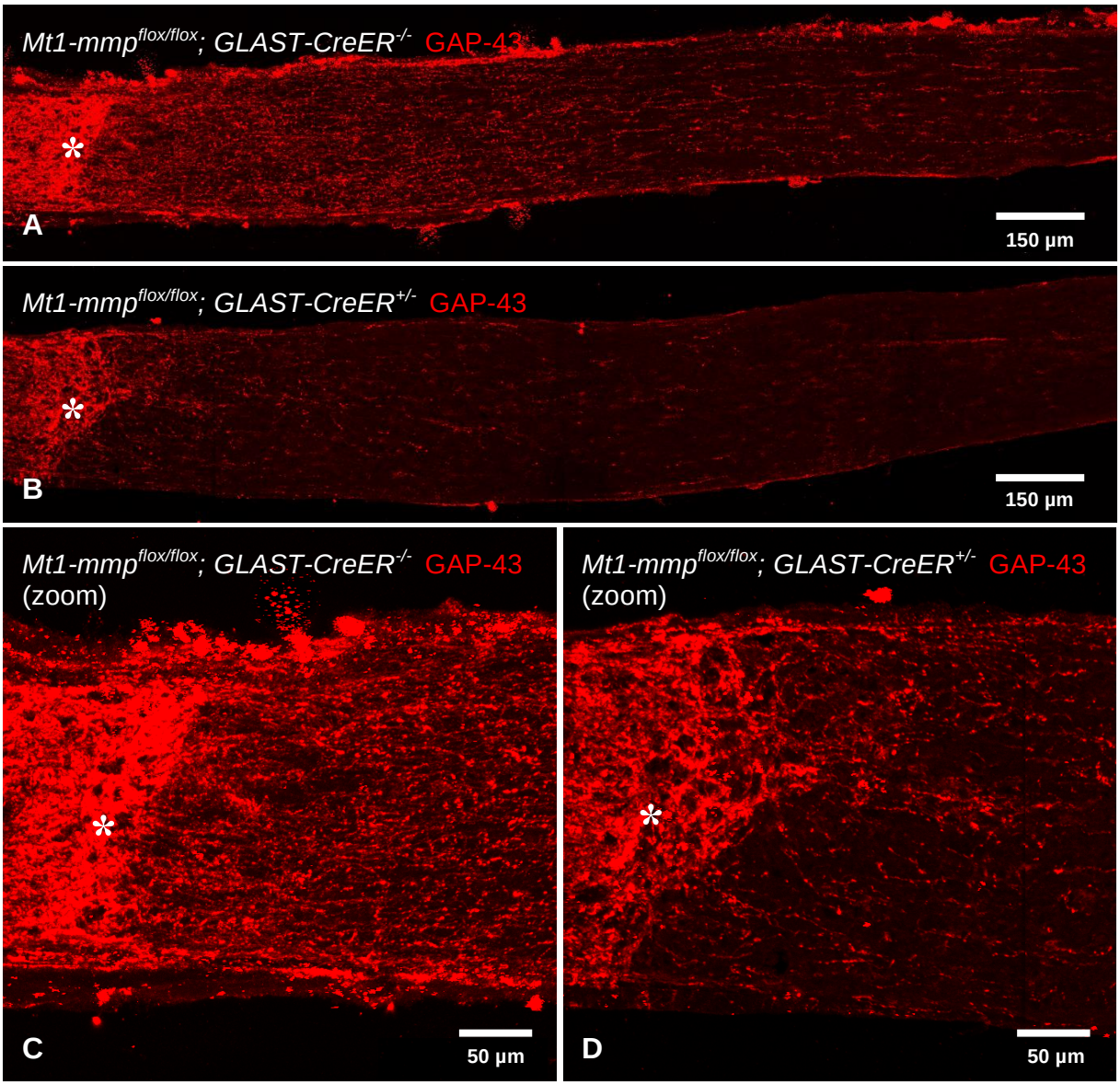

Figure 33: The number of regenerating axons in control and *Mt1-mmp$^{flox/flox}$;GLAST-CreER$^{+/-}$* mice can be analyzed on ON sections at 14 dpi. A) Axonal regeneration is visualized with a GAP-43 immunostaining on ON sections in control mice and B) in *Mt1-mmp$^{flox/flox}$;GLAST-CreER$^{+/-}$* mice. C) The axons of the control and D) *Mt1-mmp$^{flox/flox}$;GLAST-CreER$^{+/-}$* mice are analyzed on ON sections. ONC is indicated with an asterisk. C and D are the enlarged images of respectively A and B. Scale bar (A, B): 150µm; Scale bar (C, D): 50µm.

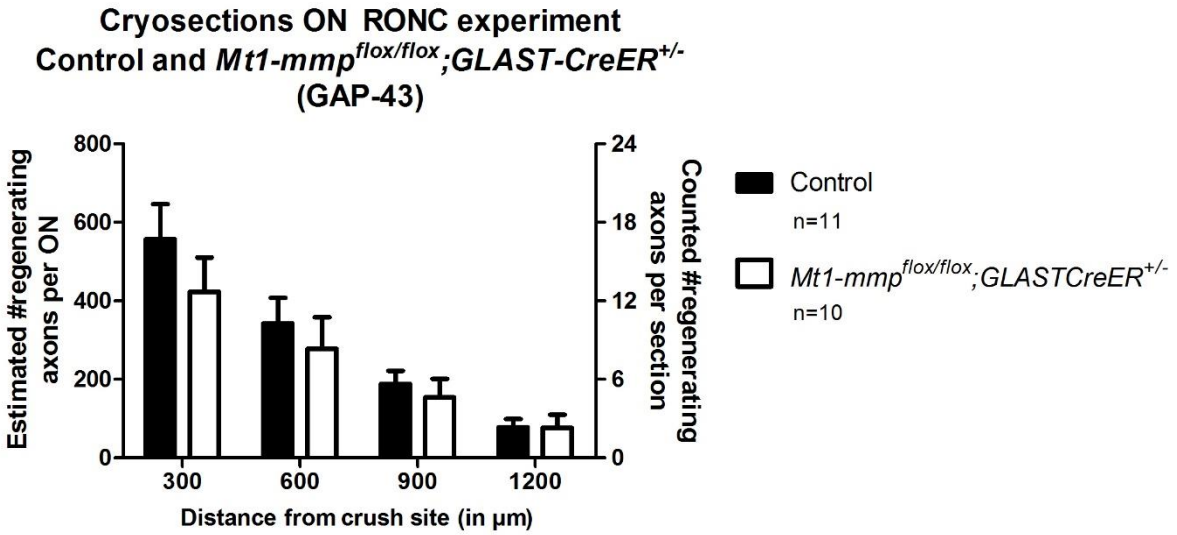

Figure 34: *Mt1-mmp*$^{flox/flox}$*;GLAST-CreER*$^{+/-}$ have a smaller number of regenerating axons compared to WT mice when analyzed on ON sections at 14 dpi. Graphic of the number of GAP-43^{+} axons per ON and counted number of regenerating axons per section in function of the distance from the ONC comparing the number of GAP-43^{+} axons in WT (black) and *Mt1-mmp*$^{flox/flox}$*;GLAST-CreER*$^{+/-}$ (white) mice at 14 dpi. The number of GAP-43^{+} axons are counted at 300, 600, 900 and 1200µm from the ONC. The number of GAP-43^{+} axons in control mice is larger at every distance from the ONC. However, the difference is not statistically significant at any distance (Repeated measures two way ANOVA; Mean ± SEM; N=11 (control) and N=10 (*Mt1-mmp*$^{flox/flox}$*;GLAST-CreER*$^{+/-}$)).

5 DISCUSSION AND FUTURE PERSPECTIVES

5.1 METHODOLOGY: CHARACTERIZATION AND OPTIMIZATION

5.1.1 RONC MODEL AS MODEL TO STUDY AXONAL REGENERATION

The working hypothesis of the current study is that MMP-2 and MT1-MMP have a beneficial effect on RGC axonal regeneration. This hypothesis is derived from previously performed *ex vivo* studies executed in the host lab (Gaublomme *et al*, 2014), which conclude that MMP-2 and MT1-MMP are essential for the successful outgrowth of neurites from retinal explants. These data need to be confirmed with further *in vivo* experiments. If MMP-2 and MT1-MMP are essential for axonal outgrowth, the knockout of *Mmp-2* or the knockdown of *Mt1-mmp* would result in reduced RGC axonal regeneration in comparison to the respective control mice. However to detect a lower number of regenerating axons, a minimum amount of axonal regeneration in the control mice is necessary. The problem is that the adult CNS of mammals lacks the robust capacity to regenerate damaged axons. Thus, after injury alone, there is almost no axonal regeneration. Consequently, axonal outgrowth has to be induced to study the *in vivo* role of MMP-2 and MT1-MMP in mammalian axonal regeneration. In present study, this is accomplished by using a regenerative ONC or RONC model, in which regeneration is induced by an inflammatory stimulus.

Although the various manipulations within the ONC injury model are as standardized as possible, a high inter-animal variability is still present, which makes it difficult to obtain statistically significant data and necessitates an increased number of animals (increased sample size). This variability can be explained by many different factors: (1) variation in the amount of inflammation and/or axonal regeneration induced in the RONC model; (2) differential formation of a glial scar and (3) diverging sensitivity of the methods used for the quantification of axonal regeneration.

First, some of the animals can intrinsically induce more or less inflammation than others, which makes the variation in axonal regeneration only higher (Jiang *et al*, 2013). Moreover, less regeneration is observed in present experiments when compared to the number of regenerating axons reported in literature (Kurimoto *et al*, 2010). This could either mean that the RONC model in this study induces less regeneration or that the detection (sectioning, tracing, imaging and analysis) methods used in this study do not detect all regenerating axons present (see below). However, more importantly, most of the published RONC models in mice combine (multiple) zymosan and cAMP injections with *Pten* and/or *Socs3* deletion (Kurimoto *et al*, 2010; Sun *et al*, 2011; Luo *et al*, 2013; de Lima *et al*, 2012), which are known to induce increased axonal regeneration. Consequently, our model has intrinsically lower numbers of regenerating axons. On the one hand, this means that possible effects of MMP-2 or MT1-MMP can be less clear than in models that induce more axonal regeneration. On the

other hand, the models that induce more regeneration cause more robust axonal outgrowth, so possibly less variation in the number of regenerating axons.

Second, another possible reason for the variability in the amount of regeneration is the differential formation of the glial scar in different animals (even within the same experiment). The ONC results in injury to and transection of the axons and damages the ON tissue. In response to this CNS injury, ON astrocytes become reactive, inflammatory cells are recruited to the site of injury and a glial scar is formed by the activated astrocytes. This process goes together with the increased deposition of glial scar-derived inhibitory molecules, like CSPGs, in the glial scar, which further limit axonal regrowth. Indeed, the glial scar forms a hostile environment for axonal regeneration. It is very difficult for the axons to grow through the glial scar because of all these extrinsic inhibitors (Silver & Miller, 2004). This is probably the reason why most of the axonal regeneration is seen at the surface of the ON, circumventing the glial scar, and only a few axons regenerate through the glial scar.

Third, there is also the possibility that not all the regenerating axons are detected. Two commonly used tracing methods have been tested. The first method is CTB tracing (Pernet *et al*, 2013a, 2013b). The cholera toxin is derived from *Vibrio cholerae* and comprises two subunits, α and β. The α subunit is an adenine diphosphate (ADP)-ribosyltransferase, which disrupts the proper signaling of G proteins and eventually leads to dehydration of the cell. The nontoxic β subunit is important to the protein complex as it allows the protein to bind to cellular surfaces. The recombinant version of the β subunit is conjugated with a fluorophore (alexa fluor 488) and is commonly used as an anterograde neuronal tracer. In this tracing method, no distinction is made between regenerating axons and spared axons. The second method is IHC staining for GAP-43 (Kurimoto *et al*, 2010, 2013). GAP-43 is a growth protein since it is expressed at high levels in neuronal growth cones during development and during axonal regeneration. This protein is considered to be a crucial component of an effective regenerative response in the nervous system. The GAP-43 staining only visualizes the regenerating axons. Therefore, it is expected that the number of CTB^+ axons is larger than the number of $GAP\text{-}43^+$ axons in ON after injury. However, when different sections of the same ON are used (instead of the double stainings) to determine the number of CTB^+ axons and $GAP\text{-}43^+$ axons, a lower number of CTB^+ axons than $GAP\text{-}43^+$ axons is observed. Though, the difference is not statistically significant. It can be concluded that CTB tracing as well as GAP-43 staining are good approaches to trace axons in the ON. GAP-43 is preferred because, by using CTB, there is still a possibility that the number of regenerating axons is underestimated. In addition, CTB tracing is very expensive and not specific for regenerating axons. Another method of axon tracing is by using *Thy1-YFP* transgenic mice that express YFP in neuronal processes. However, YFP expression in *Thy1-YFP* transgenic mice is rapidly downregulated upon injury. Further experiments as to whether the YFP expression is restarted upon axonal regeneration in the *Thy1-YFP* transgenic mice after ONC need to be performed. If YFP expression fails during axonal regeneration after injury, the *Thy1-YFP*

transgenic mice are no option for tracing axonal regeneration in sections or after optical clearing (see below).

Taken together, inducing and quantifying RGC axonal regeneration is a complex, multi-step procedure and during every step, a lot of variability can be induced. In addition, several experimental approaches to induce axonal regeneration in the RONC model exist and might have diverging success rates. All these factors are apparent in the rather high inter-animal variability observed in current studies.

5.1.2 OPTICAL CLEARING TO TRACE AXONAL TRAJECTORIES

Diverse studies related to axonal regeneration, rely on histological sectioning. However, this method yields inadequate spatial information and is, therefore, prone to misinterpretation. One main reason for inconsistencies is that cryosections provide a two-dimensional (2D) picture of the regenerating axons, showing only fragments. Hence, it is often unclear where a specific regenerating axon originates and where it ends. Thereby, spared axons can be mistaken for regenerating axons in histological sections. If the ONs are sectioned, information about the behavior of the regenerating axons like axon pathfinding, navigation and synaptogenesis and the anomalies of the regenerating axons such as axonal branching, U-turns and misguidance are easy to misinterpret. In order to trace axonal trajectories and evaluate regenerating axons without any doubt, it would be preferable to image axons in whole CNS tissues, like the ON. 3D imaging of the trajectories of the regenerating axons would come in handy when investigating the above. However, at this moment, it is not possible to image samples as thick as the rodent ON at microscopic resolution. If whole mounted ONs are visualized as such, the fluorescent signal cannot be detected beyond 100µm (Ertürk *et al*, 2012b). The aberrant RI of the lipids present in the CNS tissue is responsible for light scattering, which causes the limited detection range of the signal and results in the loss of information. Light is scattered at the boundary between materials with different RIs. So, the removal of lipids and/or the adjustment of the RI difference between lipids and the surrounding areas are potential approaches for increasing tissue transparency and detection range of the fluorescent signal (Susaki *et al*, 2014). An approach to overcome this obstacle is tissue clearing. Therefore, optical clearing following the 3DISCO method is tested on uninjured ON in which the axons are traced with CTB and images are taken with a multiphoton microscope. In the clearing process, the tissue is dehydrated with THF and cleared with BABB. BABB has a RI close to the RI of lipids in fixated tissue, which renders the ON transparent and makes the tissue amenable to deep tissue fluorescence imaging. With the 3DISCO method, the ON is completely transparent after the protocol and the whole ON can be visualized by virtual coronal sections. However, the process to get 3D images with a multiphoton microscope with a resolution that is high enough to allow analysis of axon trajectories, is very time consuming. Indeed, the successful implementation of 3D imaging is primarily hampered by the lack of access to a thin light sheet

microscope that would reduce the time needed to make 3D images. The major advantage of thin light sheet microscopy is that this technique scans the sample, using a plane of light instead of a point illumination (confocal microscope or multiphoton microscope). As such, it can acquire images at speeds of 100-1000 times faster than those taken by point scanning microscopes (Santi, 2011; Ertürk *et al*, 2012b).

As a part of our efforts to optimize 3D imaging of axonal trajectories, the 3DISCO optical clearing is tested on ON of uninjured YFP transgenic mice. The images are taken with a multiphoton microscope and results were similar to the ON with CTB tracing. Of note, the 3DISCO method is less compatible with slow high-resolution imaging and the instability of native fluorescence in BABB constrains imaging of fine neuronal projections because of rapid quenching of the fluorescent signal (Chung *et al*, 2013). Therefore, alternative clearing methods like FocusClear (Diekmann *et al*, 2015; Moy *et al*, 2013; Fu *et al*, 2010; Chiu *et al*, 2012; Fu *et al*, 2013; Tang *et al*, 2013), Sca/eA2 (Hama *et al*, 2011), SeeDB (Ke *et al*, 2013), CLARITY (Chung *et al*, 2013) and CUBIC (Susaki *et al*, 2014), should be tested. The first method is very fast and simple, compatible with light sheet microscopy, but very expensive for large samples and not possible to optimize for different biological samples because the contents are proprietary. The tissue is immersed in the clearing solution 'FocusClear' overnight to render the tissue transparent, and is mounted in MountClear, ready to be imaged. A trial in the host lab is currently ongoing. The other methods for tissue clearing mentioned above are more complicated and take much more time (up to several weeks).

5.2 THE ROLE OF MMP-2 IN AXONAL REGENERATION

5.2.1 AXONAL REGENERATION

Is there a beneficial role for MMP-2 in RGC axonal regeneration?

Quantification of the CTB^+ axons in WT and *Mmp-2*$^{-/-}$ mice reveals that less RGC axonal regeneration is observed upon *Mmp-2* deletion at 14 as well as at 42 dpi. This confirms the hypothesis that MMP-2 might be required for the successful regeneration of the RGC axons post injury.

First, the axonal outgrowth was quantified 14 dpi, a time point that is generally used in experiments investigating axonal regeneration and at which growth past the crush site is clear-cut but before the effect of a single injection of zymosan and cAMP might have subsided (Leon *et al*, 2000). The number of CTB^+ axons in *Mmp-2*$^{-/-}$ mice is between 40-50% lower than in the WT mice at all distances from the crush site at 14 dpi. At 300 and 600µm, the difference in the number of CTB^+ axons is statistically significant. Also, although not significant, at 900 and 1200µm from the ONC, there is a lower number of CTB^+ axons. The variability in the RONC model can be the reason that no significant difference is observed at longer distances. Another explanation can be that MMP-2 has a primary effect on the initiation of axonal regeneration and less on the elongation of regenerating axons. A follow-up experiment to confirm this data is ongoing, including more animals and quantifying $GAP\text{-}43^+$ regenerating axons instead of the CTB^+ axons.

In addition to quantifying the number of CTB^+ axons on cryosections of 14µm, the number of CTB^+ axons in WT *versus* *Mmp-2*$^{-/-}$ mice is also quantified on whole mount ON without clearing. The results indicate a trend towards a reduced number of CTB^+ axons in the *Mmp-2*$^{-/-}$ mice as compared to WT animals. With this approach, only the coursing axons on the surface of the ON could be visualized due to light scattering in the latter. Thus, in this approach, the central part of the ON is left out of the analysis. This would be no problem if the number of regenerating axons is evenly dispersed across the entire volume of every ON. However, as already discussed, a glial scar in the center of the ON causes more regenerating axons going around the glial scar than through the glial scar, which results in a larger number of axons that regenerate at the surface of the ON than in the center of the ON. Consequently, this experiment, which is performed to confirm the data found with the cryosections, is less reliable and this could explain why a trend, yet no statistically significant difference, in the number of regenerating axons in WT *versus* *Mmp-2*$^{-/-}$ mice is seen. So, as long as it is not possible to visualize the entire ON as a whole mount, the approach using cryosections is preferred, rather than the approach using whole mount ONs that are not cleared, to quantify the regenerating axons and investigate the role of MMP-2 in RGC axonal regeneration.

Second, the axonal regeneration was quantified at a later time point. The number of CTB^+ axons is determined at 42 dpi. The animals are injected with zymosan and cAMP and CTB is injected one week before sacrificing the animals to be sure the regenerating axons are

traced till their distal tip (personal communications; Eline Dekeyster). Of note, as the CTB tracer is transported all the way to the axonal terminals by this time, this allows clear visualization of the growing tips of the axons, yet their trajectories in the ON are less clear. Therefore, in next experiments, injection of CTB 3-5 days before sacrificing the animals is preferred over one week. Of note, GAP-43 staining is rejected in experiments studying axonal regeneration over longer periods of time because the expression in the axons is not that prominent anymore. As expected, longer axons are detected, extending beyond 3mm from the crush site. At 300µm, the *Mmp-2*$^{-/-}$ animals have a significantly lower number of CTB^{+} axons than the WT mice at 42 dpi. The results at the other distances from the crush site are not statistically significant but suggest that there is more regeneration in the WT mice than in the *Mmp-2*$^{-/-}$ mice. The number of CTB^{+} axons at 42 dpi is compared to the number of CTB^{+} axons at 14 dpi in both WT and *Mmp-2*$^{-/-}$ mice. In both WT and *Mmp-2*$^{-/-}$, the number of CTB^{+} axons is higher at 42 dpi, only in the *Mmp-2*$^{-/-}$ mice these differences are statistically significant at all distances. The number of CTB^{+} axons in WT mice is 28%, 69%, 176% and 346% higher (for respectively 300, 600, 900 and 1200µm) at 42 dpi than at 14 dpi. The number of CTB^{+} axons in *Mmp-2*$^{-/-}$ mice is 53%, 116%, 209% and 576% higher (for respectively 300, 600, 900, 1200µm) at 42 dpi than at 14 dpi. The further the distance from the crush site, the higher the increase in the number of CTB^{+} axons at 42 dpi. This indicates that not only the number of CTB^{+} axons increases but also the length of the axons. As such the axons regenerate over a longer distance. The data suggest that the axons could eventually reach the SCN or even the SC (de Lima *et al*, 2012). However, this would take a long time in mice without *Pten* deletion and only treated with a single injection of zymosan and cAMP. Generally, it can be demonstrated that MMP-2 has a beneficial role in RGC axonal regeneration.

Axonal regeneration in the absence of MMP-2 is reduced in the CNS and the PNS

In vivo studies in rats report a correlation between MMP-2 expression and RGC axonal regeneration (Ahmed *et al*, 2005). Also, the percentage of rat RGCs with axonal regeneration is reported to rise when the RGCs are co-cultured with MMP-2 expressing olfactory glial cells (Pastrana *et al*, 2006). Other *in vivo* studies in *Xenopus* show that low concentrations of broad-spectrum MMP inhibitors or more specific gelatinase inhibitors result in RGC axonal navigation defects, while larger doses of these inhibitors result in decreased axonal elongation (Webber *et al*, 2002; Hehr *et al*, 2005). Previous *in vivo* studies from the host lab in developing zebrafish show that the combined knockdown of *zMt1-mmp* and *zMmp-2* significantly reduces the innervation of the optic tectum as compared to single *zMt1-mmp* knockdown, which indicates that both proteinases have an effect on RGC axonal outgrowth (Janssens *et al*, 2013).

In addition, the reduced regeneration in the ON upon *Mmp-2* deletion in current *in vivo* study is consistent with the data obtained by *ex vivo* studies using retinal explants from MMP deficient pups (Gaublomme *et al*, 2014). The need for MMP-2 activity during RGC axonal

outgrowth is demonstrated by administering broad-spectrum inhibitors or more specific gelatinase inhibitors and by a rescue experiment in which purified MMP-2 is administered. The present *in vivo* experiments, in which the RONC model is applied in *Mmp-2*$^{-/-}$ mice reveals a similar reduction in axonal regeneration in *Mmp-2*$^{-/-}$ mice as compared to WT mice. Taken together, it can be concluded that MMP-2 is an essential factor during axonal regeneration.

However, the way in which MMP-2 influences axonal regeneration is still unclear. The *ex vivo* studies on retinal explants propose that MMP-2 might either cleave the molecules interacting with β-integrin (e.g., cell adhesion molecule L1 and laminin) or directly shed β1-integrin, stimulating axonal regeneration via a process closely resembling β1-integrin-mediated cell migration (Gaublomme *et al*, 2014). Alternatively, in a study where axonal regeneration in rats is induced by transplantation of neural tube-derived chicken embryonic stem cells at the site of injury together with the intravitreal transplantation of a PNG, there has been reported that MMP-2 can also perform a path-clearing function and as such degrades inhibitory molecules such as CSPGs (Charalambous *et al*, 2008; Ahmed *et al*, 2005). Likewise, neurite outgrowth-promoting activity associated with the subretinal transplantation of CNS progenitor cells and mediated by induction of MMP-2 expression by activated glial cells (Müller cells) is reported. This increased MMP-2 activity causes proteolysis of neurite growth inhibitory neurocan and CD44, resulting in enhanced neurite outgrowth across the host transplant border (Zhang *et al*, 2007). Also in the PNS, MMP-2 inhibition results in reduced neurogenesis and neurite elongation from *ex vivo* inner ear spiral ganglion explants (Ali *et al*, 2014; Sung *et al*, 2014). Thus, both data from the PNS and the CNS suggest that MMP-2 is a beneficial factor during axonal regeneration.

Alternative strategies to investigate the role of MMP-2 in axonal regeneration

The current study makes use of the genetic knockout of *Mmp-2*, which offers the opportunity to identify essential functions of MMP-2 by comparing them to control animals. However, in the present study, using mice that never expressed MMP-2, compensatory mechanisms can develop. First, enzymatic redundancy can take place in which enzymes expressed at the same time and in the same place as MMP-2 can substitute for its essential functions. Second, enzymatic compensation can arise in which a certain enzyme is upregulated to substitute for MMP-2 that lost its function. Third, adaptive development can occur in which the organism compensates for the loss of the *Mmp-2* gene by performing the essential functions of that gene in another way. A good indication for this theory is that, in spite of the fact that MMP-2 has some essential functions in embryonic development of mice, *Mmp-2*$^{-/-}$ mice have a surprisingly subtle phenotype (Page-McCaw *et al*, 2007). Thus, if compensatory mechanisms develop, the effect of MMP-2 and its deficiency on axonal regeneration is masked and will appear smaller. So, using *Mmp-2*$^{-/-}$ mice is a good starting point for further experiments. A first solution for these compensatory mechanisms would be to make floxed *Mmp-2* mice, in which a conditional knockdown can be induced such as in

the *Mt1-mmp*$^{flox/flox}$*;GLAST-CreER*$^{+/-}$ mouse line (see below). However, currently, a *Mmp-2*$^{flox/flox}$ mouse line is not available. A second approach could be to work with broad-spectrum inhibitors (GM6001; Santa Cruz Biotechnology; Dallas; Texas; USA) or more specific gelatinase inhibitors (ABT-518 and ABT-770; Abbott Laboratories; Abbott Park; Illinois; USA) in WT mice (Gaublomme *et al*, 2014). A third method is RNA interference (RNAi) using small interfering RNAs (short interfering; silencing; siRNAs) to target MMP-2. Here, the specific siRNA that is complementary to the MMP-2 mRNA forms double-stranded RNA and degrades it with the help of a RNA induced silencing complex (RISC).

In addition, the data found in present study can be confirmed by overexpression and rescue experiments through delivery of recombinant MMP-2 via viral vectors or via intravitreal injections in WT and *Mmp-2*$^{-/-}$ mice, respectively. An *ex vivo* experiment performed in the host lab with retinal explants shows that administration of purified MMP-2 to retinal explants from *Mmp-2*$^{-/-}$ mice rescues the reduced axonal outgrowth (Gaublomme *et al*, 2014).

Finally, it would be interesting to study the role of MMP-2 in a RONC model with more axonal regeneration, i.e. with more robust or longer axons. This could be performed by studying axonal regeneration at later time points (10-12 weeks), using multiple injections of zymosan and cAMP (de Lima *et al*, 2012). Moreover, *Pten* and/or *Socs3* deletion in combination with multiple injections of zymosan and CPT-cAMP treatment can induce even more and faster regeneration (Kurimoto *et al*, 2010). The *Pten* deletion is created with *Pten*$^{flox/flox}$ mice, which either can be crossed with mice that express Cre recombinase, or can be injected with Cre recombinase-expressing AAV2/2 vectors.

In the future, next to the axonal outgrowth, the function of MMP-2 in axonal navigation and in the behavior of regenerating RGC axons needs to be investigated. As mentioned above, these kind of studies require 3D imaging to trace the trajectories of the regenerating axons. The implementation of whole mount ON imaging and deep tissue imaging was initiated but was hampered primarily by the lack of access to a thin light sheet microscope.

5.2.2 EXPRESSION PATTERN OF MMP-2 IN THE INJURED, ADULT MOUSE RETINA

Is the MMP-2 expression in the injured, adult mouse retina upregulated?

In order to gain more insight into the role of MMP-2 during axonal regeneration, an IHC study to investigate the spatiotemporal expression pattern of MMP-2 is performed. IHC with a polyclonal rabbit anti-MMP-2 antibody is executed on retinal and ON sections, at different time points post RONC injury. The specificity and sensitivity of this antibody are validated by performing western blot with retinal tissue lysates and recombinant MMPs (De Groef *et al; submitted*).

The expression pattern of MMP-2 in the ON of healthy adult mice and in injured adult mice at 2, 7 and 14 dpi is investigated. However, staining the ON seems difficult and likely requires adjustment of standard protocols (e.g., special protocol for GAP-43 staining of ON). Indeed,

no clear specific signal seems to be observed upon IHC with the protocol for the retinal sections.

In addition to the ON, MMP-2 expression in the healthy adult retina is compared with injured adult retina of mice that are sacrificed at 2, 7 and 14 days after RONC injury. Similar expression patterns are observed, revealing MMP-2 expression in the Müller glia, however, there seems to be an upregulation of MMP-2 expression at 7 dpi.

In some of the retinas at 2, 7 and 14 dpi, foci of cells are observed in the vitreous cavity adjacent to the retina. These foci probably consist of inflammatory cells that accumulate in the vitreous due to zymosan-induced ocular inflammation.

Of note, at 7 and 14 dpi, a lot of $DAPI^+$ cells are observed in the vicinity of the crush site and dispersed along the length of the ON as well. As already described, after injury, numerous macrophages are seen in the crush site and dispersed along the length of the ON between 7 and 21 dpi (Leon *et al*, 2000).

MMP-2 expression in the healthy adult retina and in inflammatory cells

The current IHC results confirm previous studies describing MMP-2 expression in the Müller glia, in the astrocytes and in the RGCs in the healthy mouse retina (Zhang, 2004; De Groef *et al, submitted*). In primates, MMP-2 is expressed in the RGC somata and their axons in the NFL but no glial expression was detected (Agapova *et al*, 2001, 2003). Moreover, several studies report that MMP-2 expression in healthy *versus* glaucomatous retina remains unchanged (De Groef *et al*, 2014; Zhang, 2004; Agapova *et al*, 2001), while others reveal an upregulation in MMP-2 expression in the first hours post injury (Zhang, 2004). Of note, in the models mentioned above no axonal regeneration is present in contrast to the RONC model used in present study.

Furthermore, the foci of cells in the vitreous in the present study are also described in other reports (Baldwin *et al*, 2015). Intriguingly, our preliminary immunostainings suggest that these cells are MMP-2 immunopositive. Indeed, it has been shown that neutrophils and macrophages express MMP-2 (Ishida *et al*, 2015; Kvanta *et al*, 2000; Esparza *et al*, 2015). This could suggest that part of the observed increase in MMP-2 in the retina at 7 dpi, reflects the infiltration of inflammatory cells that constitutively express MMP-2 rather than an actual upregulation of MMP-2 expression in the Müller glia. Future experiments are needed to clarify the findings.

Alternative approaches to investigate MMP-2 activity in injured CNS tissue

The protocol for MMP-2 immunostaining for ON will be refined, based on the experience with the GAP-43 staining. Then, IHC stainings for MMP-2 as well as double stainings to identify $MMP\text{-}2^+$ cells in the ON and in the retina can be performed. Also, a first objective of future experiments would be to study the accumulation of inflammatory cells in the vitreous after RONC, to investigate which cell types express MMP-2 in these foci and whether this MMP-2 is activated.

First, IHC stainings for infiltrating macrophages, resident microglia, neutrophils ($CD45^+$, Iba1, Mac3) and Müller glia (glutamin synthetase) should be performed. With IHC stainings, it is difficult to differentiate between macrophages and microglia. However, there is a big difference in operating mechanism, microglia are resident in the retina, while macrophages migrate from the blood vessels into the retina upon injury. A possible approach to make a distinction between invading cells and resident cells is bone marrow transplantation (Luttun *et al*, 2004). The bone marrow of the host is destroyed with irradiation and bone marrow of another strain of mice (e.g., expressing green fluorescent protein (GFP)) is transplanted in the host mice. In this case GFP^+ cells invading the retina represent infiltrating macrophages that originate from the bone marrow, while the GFP^- cells are the resident microglia.

In addition, sections of the entire eye should be made to confirm that the infiltrating cells accumulate in the vitreous.

Next to IHC studies, optical coherence tomography (OCT) can be used to investigate the spatiotemporal pattern of the infiltration of inflammatory cells. OCT is an *in vivo* imaging technique that allows making high resolution images of the entire eye, and can be used to longitudinally follow intraocular inflammation after RONC.

Other approaches to study the spatiotemporal expression of MMP-2 in retina such as western blot or *in situ* gelatinase zymography are necessary to confirm the temporal expression data found in the IHC study. In contrast to the latter, it is possible with western blot and gel gelatinase zymography to quantify the difference between MMP-2 expression in healthy and injured adult retinas and to distinguish the active form of MMP-2 from the other forms such as pro-MMP-2 and the degradation products. The disadvantage of western blot is that different antibodies for MMP-2 have a different specificity and sensitivity for the pro-MMP-2 and the active MMP-2. This can be resolved by a technique called gel gelatinase zymography (Toth *et al*, 2012; Zhang *et al*, 2007), which makes it possible to distinguish between gelatinolytic activity of MMP-2 and MMP-9 by separating the two MMPs based on their molecular weight.

5.2.3 RGC SURVIVAL

Is there a role for MMP-2 in RGC survival?

The general approach to investigate RGC density, survival and protection, is to stain whole mounted retinas with Brn3a. RGC survival is quantified with a homemade macro in ImageJ that automatically counts the $Brn3a^+$ cells. However, this is not the optimal way to analyze RGC survival in retinas after RONC. First, due to the inflammation induced by zymosan, the dissection of the retinas is difficult and retinal whole mounts are often damaged. Second, due to the inflammation, the vitreous becomes more gelatinous and forms a network of fibers on top of the RGC layer, these are autofluorescent, which makes it very challenging for the macro to distinguish the RGCs from the unspecific signal.

The present data show no difference between the RGC density of WT mice and *Mmp-2*$^{-/-}$ mice, which would indicate that MMP-2 has no effect on RGC survival or neuroprotection. However because of the problems dissecting and analyzing the retinas of mice subjected to the RONC model, only 4 and 7 retinas of respectively WT and *Mmp-2*$^{-/-}$ mice are suitable to be analyzed by the macro in ImageJ.

Brn3a as marker for RGCs to study RGC survival and protection

Another problem that recently appeared is the current discussion whether Brn3a is a good marker for RGCs in the RONC model. It has been reported that Brn3a can be used as a reliable, efficient marker to identify and quantify RGCs in control as well as ON-injured retinas (Nadal-Nicolás *et al*, 2009). In this study, fluorogold (FG) is applied before ONC and will be present in the RGCs until they die. Brn3a immunostaining is shown to be maintained in injured RGCs, but the Brn3a^{+} RGCs loss was detected earlier than the FG^{+} RGCs loss, which means that the Brn3a expression after ONC decreases before the RGCs die (Nadal-Nicolás *et al*, 2009, 2015). However, the lab of Prof. Dr. Fischer (Heinrich-Heine-University of Düsseldorf; Düsseldorf; Germany) now shows that RGCs in zebrafish lose their Brn3a expression upon injury or when dying (personal communications). These RGCs are still present but are not detected anymore with the Brn3a staining. This could also explain why Brn3a stainings do not work on explants or on cells in culture.

In the literature, little is known about the role of MMP-2 in neuroprotection. *Mmp-2* deficiency does not protect from RGC death after ischemia-reperfusion injury (Chintala *et al*, 2002). However, the expression of MMP-2 in the healthy and glaucomatous retina suggests that MMP-2 might be important in retinal health. In contrast to MMP-9 that has a clear negative impact on RGC survival, the role of MMP-2 remains obscure (Chintala *et al*, 2002; De Groef *et al*, 2014; Verslegers *et al*, 2013).

Alternative approaches to study the effect of MMP-2 on RGC survival

Further experiments are needed to confirm that MMP-2 has no effect on RGC survival, by increasing the number of animals, preferably by making cryosections of the entire eye and staining those for Brn3a or an alternative marker such as RNA-binding protein with multiple splicing (RPBMS) (Rodriguez *et al*, 2014). The latter will most likely resolve the issues related to retinal whole mount dissection.

5.3 THE ROLE OF MT1-MMP IN AXONAL REGENERATION

Is there a beneficial role for MT1-MMP in RGC axonal regeneration?

Conventional knockout of the *Mt1-mmp* gene generates the only lethal MMP knockout mouse line. *Mt1-mmp* deficient mice are normal at birth but develop multiple abnormalities and die by 3-12 weeks. Of note, also the *Mmp-2/Mt1-mmp* double knockouts die at birth (Page-McCaw *et al*, 2007). Thus, to investigate the role of MT1-MMP in axonal regeneration, *Mt1-mmp*$^{flox/flox}$ transgenic mice are mated with inducible *GLAST-Cre(ER)T2* mice. In that way, a conditional Müller glia-specific knockdown of MT1-MMP is generated. The knockdown of the *Mt1-mmp* gene is obtained via the systemic administration of TXF.

Quantification of the number of GAP-43^{+} axons post injury in *Mt1-mmp*$^{flox/flox}$*;GLAST-CreER*$^{+/-}$ and *Mt1-mmp*$^{flox/flox}$*;GLAST-CreER*$^{-/-}$ (control) mice shows that there is less axonal regeneration when the *Mt1-mmp* gene is deleted in Müller glia. Although a lot of variation is present, not only within the same experiment, but also between experiments, the data obtained indicate that MT1-MMP might have an effect on RGC axonal regeneration after ON injury and might be necessary for proper axonal outgrowth or elongation. However, the results of this experiment are not statistically significant, yet the number of GAP-43^{+} axons is 25%, 10%, 9% and 1% lower (at respectively 300, 600, 900 and 1200µm from the crush site) in *Mt1-mmp*$^{flox/flox}$*;GLAST-CreER*$^{+/-}$ mice than in control animals. The further away from the crush site, the smaller the difference between the control mice and the *Mt1-mmp*$^{flox/flox}$*;GLAST-CreER*$^{+/-}$ mice, which indicates that the direct or indirect (via MMP-2) effect of MT1-MMP on axonal regeneration is primarily during initiation of axonal outgrowth.

This is a good indication to initiate follow-up experiments in which the number of animals should be increased and the variability of the RONC model should be reduced, to increase the statistical power of the experiment. Here, next to the experimental setup, the variability in axonal regeneration can be explained by biological factors. Several aspects might contribute to this variation: intrinsic variability in the RONC model and quantification of axon outgrowth (see above), as well as a different degree of *Mt1-mmp* knockdown. The latter could be targeted by reducing the inter-animal variation with more exact TXF dosing. Indeed, all animals receive a similar amount of TXF and although littermates are used, the body weight of the animals varied (30,2 ± 1,3g). Therefore, the animals receive a different amount of TXF per body weight, potentially resulting in differential relocation of the Cre recombinase and in variability of *Mt1-mmp* knockdown efficiency. Taken together, the current study suggests a beneficial role for MT1-MMP by activating MMP-2, but further studies are needed to confirm these results.

Efficiency of *Mt1-mmp* deletion and its effect on active MMP-2

The western blot with the polyclonal rabbit anti-MT1-MMP RP3 antibody reveals bands at 57kDa representing the mature MT1-MMP (active, membrane bound) and at 50-53kDa

representing the soluble MT1-MMP (active), while the polyclonal rabbit anti-MT1-MMP Ab53712 antibody reveals only the soluble MT1-MMP. In addition, a series of bands could be detected representing subspecies of MT1-MMP resulting from autocatalytic (44kDa, 40kDa and 18kDa) and non-autocatalytic (32kDa and 27kDa) processing and shedding of the 57kDa MT1-MMP (Toth *et al*, 2005).

In the *Mt1-mmp*$^{flox/flox}$*;GLAST-CreER*$^{+/-}$ mouse line, the amount of membrane-bound MT1-MMP and soluble MT1-MMP, determined with western blot, is decreased in *Mt1-mmp*$^{flox/flox}$*;GLAST-CreER*$^{+/-}$ mice. Indeed, the efficiency of the *Mt1-mmp* knockdown in present study revealed an average decrease of ~80% of the soluble and membrane-bound MT1-MMP in the retina of *Mt1-mmp*$^{flox/flox}$*;GLAST-CreER*$^{+/-}$. The use of the *GLAST-Cre(ER)T* mouse line to induce conditional gene ablation in astroglia throughout the mouse brain has already been described and reveals targetting efficiencies between 30 and 80% (Slezak *et al*, 2007; Mori *et al*, 2006). In the retina, the *GLAST-Cre(ER)T* mouse line has been reported as an effective method to create a conditional knockdown in Müller glia, however no specific percentage of the efficiency is mentioned (Haenold *et al*, 2014). The fact that different antibodies for MT1-MMP have different sensitivity and specificity for different forms of the MT1-MMP must be taken into account. A more accurate technique to find out if the *Mt1-mmp* gene ablation is effective in the *Mt1-mmp*$^{flox/flox}$*;GLAST-CreER*$^{+/-}$ mouse line is by quantitative polymerase chain reaction (qPCR) using TaqMan probes and specific primers for the *Mt1-mmp* gene.

Furthermore, the western blot for MMP-2 using a polyclonal rabbit anti-MMP-2 antibody, reveals no differences in the optical density of bands at 72kDa (representing the pro-MMP-2) and at 62kDa (representing the active MMP-2), indicating that there is no clear effect of *Mt1-mmp* deletion on MMP-2 activity.

The effect of MT1-MMP on axonal regeneration is milder than the effect of MMP-2

The reduced number of GAP-43^{+} axons in the ON of the *Mt1-mmp*$^{flox/flox}$*;GLAST-CreER*$^{+/-}$ mice in this *in vivo* experiment corresponds to the reduced neurite outgrowth observed in the retinal explants from mouse pups treated with function-blocking antibodies or from *Mt1-mmp*$^{-/-}$ mouse pups (Gaublomme *et al*, 2014). In addition, similar beneficial effects of MT1-MMP on neurite outgrowth in cultured cerebellar granule cells have been described (Loers *et al*, 2012). In the *ex vivo* study performed in the host lab, the effect of MT1-MMP on MMP-2 activation is investigated as described in 1.3.6.3 (Gaublomme *et al*, 2014). It reveals that in the retinal explant models, MT1-MMP promotes axonal regeneration via the activation of pro-MMP-2. However, the effects of MT1-MMP inhibition are milder than the effects of MMP-2 inhibition. This could be explained by the remaining MMP-2 activity in retinal explants in which the MT1-MMP was inhibited. Indeed, MMP-2 can also be activated by other molecules like thrombin, MT2-MMP or activated protein C (Gaublomme *et al*, 2014; Galis *et al*, 1997; Morrison *et al*, 2001; Nguyen, 2000). These data also suggest that activating MMP-2 would be the primary role of MT1-MMP on axonal regeneration. Similarly, in these *in*

vivo experiments using the RONC model, the effects of the *Mt1-mmp* deletion on axonal regeneration are less drastic than the effects of *Mmp-2* deletion (see above).

Moreover, the fact that the effect of *Mt1-mmp* deletion on the MMP-2 activity is unclear at 14 dpi would suggest that either other activators take over the role of MT1-MMP in activating MMP-2, or that there is still enough MT1-MMP present to activate MMP-2. Indeed, western blot quantification of MT1-MMP levels in *Mt1-mmp$^{flox/flox}$;GLAST-CreER$^{+/-}$* mice suggest that there is still some MT1-MMP present in the Müller glia. Another potential reason for the milder effect of *Mt1-mmp* deletion is the possibility of MT1-MMP expression by cells other than Müller glia e.g., the inflammatory cells that infiltrate the vitreous upon zymosan injection, since the *Mt1-mmp* deletion in the *Mt1-mmp$^{flox/flox}$;GLAST-CreER$^{+/-}$* mice is only achieved in the Müller glia. In this case, MT1-MMP expressed by other cells could have a rescue effect in the *Mt1-mmp$^{flox/flox}$;GLAST-CreER$^{+/-}$* mice and result in the activation of MMP-2.

Alternative strategies to investigate the role of MT1-MMP in axonal regeneration

Immunostainings indicate that MT1-MMP expression is not only seen in Müller glia, but also in RGC axons (De Groef *et al; submitted*). There are Cre recombinase-expressing mouse lines available, which target other cell populations in the retina, like the *Thy1-Cre* mouse line that targets the RGCs (Young *et al*, 2008). Mating this line with the *Mt1-mmp$^{flox/flox}$* mice could induce *Mt1-mmp* gene ablation specific for the RGCs and their axons. An alternative approach is, instead of mating the floxed animals with a Cre recombinase-expressing mouse line, injecting them with Cre recombinase-expressing AAV vectors. This would be an alternative approach to induce *Mt1-mmp* gene ablation in RGC (axons) or Müller glia using AAV2/2 (Kurimoto *et al*, 2010; Luo *et al*, 2013) or ShH10 vector (Pernet *et al*, 2013a; Klimczak *et al*, 2009), respectively.

Further experiments, studying the axonal regeneration in mice with co-deletion of the *Mt1-mmp* gene and the *Mmp-2* gene could expand the knowledge of their interaction and co-involvement in axonal regeneration. In addition, rescue experiments and overexpression studies by administration of recombinant MMP-2 and MT1-MMP via viral vector delivery or intravitreal injections, in WT, *Mmp-2$^{-/-}$* or *Mt1-mmp$^{flox/flox}$;GLAST-CreER$^{+/-}$* mice, and experiments investigating the spatiotemporal expression patterns of both MMP-2 and MT1-MMP in the ON after RONC might improve the understanding of the role of these molecules in axonal regeneration post injury. Of note, potential rescue experiments for membrane-bound MT1-MMP are difficult. Recombinant, soluble MT1-MMP can be administered but it is not known, and rather unlikely, whether this soluble MT1-MMP will exert the same actions as membrane-bound MT1-MMP.

Other approaches to study the role of MT1-MMP in axonal regeneration are with the MT1-MMP blocking antibody DX-2400 or with siRNA (see above) (Gaublomme *et al*, 2014). The question whether MT1-MMP only has a role in axonal regeneration by activating MMP-2 or also has an effect independent of MMP-2 can be solved by using the recently developed anti-MT1-MMP antibody that specifically blocks the MMP-2 activating function of MT1-MMP

without targeting its overall proteinase activity (Ingvarsen *et al*, 2013). In the *ex vivo* experiments, the latter antibody reduces the neurite outgrowth to a similar extent as DX-2400, which suggests that the main substrate through which MT1-MMP affects axonal regeneration is MMP-2 (Gaublomme *et al*, 2014).

5.4 CONCLUSIONS AND PERSPECTIVES

Taken together, the current study provided evidence for the involvement of MMP-2 and MT1-MMP in RGC axonal regeneration. The present experiments, using an *in vivo* model for ON axonal regeneration (RONC), revealed that RGC axonal regeneration is decreased upon general *Mmp-2* deletion and cell-specific *Mt1-mmp* gene ablation in the Müller glia, although the effect of the latter is less pronounced. These data correspond to previous *ex vivo* studies of the host lab describing a decreased neurite growth in retinal explants of *Mmp-2*$^{-/-}$ and *Mt1-mmp*$^{-/-}$ mice, and upon administration of MMP-2 and MT1-MMP inhibitors to retinal explants of WT mice. Furthermore, the expression pattern of MMP-2 in the healthy and injured adult retina was investigated and showed an upregulation of MMP-2 by the Müller glia, within the first week after RONC. Also, preliminary evidence for invading inflammatory cells in the vitreous humor that express MMP-2 was gathered.

Follow-up experiments such as rescue experiments, overexpression studies and alternative approaches to induce MMP-2 or MT1-MMP knockout/knockdown (floxed mice, MMP inhibitors, siRNA, *etc.*) are needed to confirm the data found in the current study. On the long run, these might lead to the identification of novel, MMP-based approaches to induce axonal regeneration and, more in general, CNS recovery.

REFERENCES

Agapova O a, Kaufman PL, Lucarelli MJ, Gabelt BT & Hernandez MR (2003) Differential expression of matrix metalloproteinases in monkey eyes with experimental glaucoma or optic nerve transection. *Brain Res.* **967:** 132–43

Agapova O a, Ricard CS, Salvador-Silva M & Hernandez MR (2001) Expression of matrix metalloproteinases and tissue inhibitors of metalloproteinases in human optic nerve head astrocytes. *Glia* **33:** 205–16

Agrawal SM, Lau L & Yong VW (2008) MMPs in the central nervous system: where the good guys go bad. *Semin. Cell Dev. Biol.* **19:** 42–51

Ahmed Z, Aslam M, Lorber B, Suggate EL, Berry M & Logan A (2010) Optic nerve and vitreal inflammation are both RGC neuroprotective but only the latter is RGC axogenic. *Neurobiol. Dis.* **37:** 441–54

Ahmed Z, Dent RG, Leadbeater WE, Smith C, Berry M & Logan A (2005) Matrix metalloproteases: degradation of the inhibitory environment of the transected optic nerve and the scar by regenerating axons. *Mol. Cell. Neurosci.* **28:** 64–78

Ali S, Driscoll HE, Newton VL & Gardiner NJ (2014) Matrix metalloproteinase-2 is downregulated in sciatic nerve by streptozotocin induced diabetes and/or treatment with minocycline: Implications for nerve regeneration. *Exp. Neurol.* **261:** 654–65

Bähr M (2000) Live or let die – retinal ganglion cell death and survival during development and in the lesioned adult CNS. *Trends Neurosci.* **23:** 483–90

Baker AH, Edwards DR & Murphy G (2002) Metalloproteinase inhibitors: biological actions and therapeutic opportunities. *J. Cell Sci.* **115:** 3719–27

Baldwin KT, Carbajal KS, Segal BM & Giger RJ (2015) Neuroinflammation triggered by β-glucan/dectin-1 signaling enables CNS axon regeneration. *Proc. Natl. Acad. Sci. U. S. A.* **112:** 2581–6

Bear MF, Connors BW & Paradiso MA (2006) Neuroscience, Exploring the Brain

Bein K & Simons M (2000) Thrombospondin type 1 repeats interact with matrix metalloproteinase 2. Regulation of metalloproteinase activity. *J. Biol. Chem.* **275:** 32167–73

Benowitz L & Yin Y (2007) Combinatorial Treatments for Promoting Axon Regeneration in the CNS: Strategies for Overcoming Inhibitory Signals and Activating Neurons' Intrinsic Growth State. *Dev. Neurobiol.***:** 1148–1165

Benowitz L & Yin Y (2008) Rewiring the injured CNS: lessons from the optic nerve. *Exp. Neurol.* **209:** 389–98

Benowitz L & Yin Y (2010) Optic Nerve Regeneration. *Arch. Ophtalmol.* **128:** 1059–1064

Benowitz LI & Popovich PG (2011) Inflammation and axon regeneration. *Curr. Opin. Neurol.* **24:** 577–83

Berry M, Ahmed Z, Lorber B, Douglas M & Logan A (2008) Regeneration of axons in the visual system. *Restor. Neurol. Neurosci.* **26:** 147–74

Boenisch T (2001) Immunochemical Staining Methods

Cai D, Qiu J, Cao Z, McAtee M, Bregman BS & Filbin MT (2001) Neuronal cyclic AMP controls the developmental loss in ability of axons to regenerate. *J. Neurosci.* **21:** 4731–9

Caterina JJ, Yamada S, Caterina NC, Longenecker G, Holmbäck K, Shi J, Yermovsky a E, Engler J a & Birkedal-Hansen H (2000) Inactivating mutation of the mouse tissue inhibitor of metalloproteinases-2(Timp-2) gene alters proMMP-2 activation. *J. Biol. Chem.* **275:** 26416–22

Charalambous P, Hurst LA & Thanos S (2008) Engrafted chicken neural tube-derived stem cells support the innate propensity for axonal regeneration within the rat optic nerve. *Invest. Ophthalmol. Vis. Sci.* **49:** 3513–24

Chen MS, Huber AB, Van der Haar ME, Frank M, Schnell L, Spillmann AA, Christ F & Schwab ME (2000) Nogo-A is a myelin-associated neurite outgrowth inhibitor and an antigen for monoclonal antibody IN-1. *Lett. to Nat.* **403:** 434–9

Chilton JK (2006) Molecular mechanisms of axon guidance. *Dev. Biol.* **292:** 13–24

Chintala SK, Zhang X, Austin JS & Fini ME (2002) Deficiency in matrix metalloproteinase gelatinase B (MMP-9) protects against retinal ganglion cell death after optic nerve ligation. *J. Biol. Chem.* **277:** 47461–8

Chiu K, Chang RC-C & So K-F (2007) Intravitreous injection for establishing ocular diseases model. *J. Vis. Exp.* **41:** 313

Chiu Y-C, Hua T-E, Fu Y-Y, Pasricha PJ & Tang S-C (2012) 3-D imaging and illustration of the perfusive mouse islet sympathetic innervation and its remodelling in injury. *Diabetologia* **55:** 3252–3261

Chung K, Wallace J, Kim S, Kalyanasundaram S, Andalman AS, Davidson TJ, Mirzabekov JJ, Zalocusky KA, Mattis J, Denisin AK, Pak S, Bernstein H, Ramakrishnan C, Grosenick L, Gradinaru V & Deisseroth K (2013) Structural and molecular interrogation of intact biological systems. *Nature* **497:** 332–337

Cui Q, Yin Y & Benowitz LI (2009) The role of macrophages in optic nerve regeneration. *Neuroscience* **158:** 1039–48

Curcio C & Allen KA (1990) Topography of Ganglion Cells in Human Retina. *J. Comp. Neurol.* **300:** 5–25

Czaja K, Fornaro M & Geuna S (2012) Neurogenesis in the adult peripheral nervous system. *Neural Regen. Res.* **7:** 1047–54

Dallimore EJ, Cui Q, Beazley LD & Harvey AR (2002) Postnatal innervation of the rat superior colliculus by axons of late-born retinal ganglion cells. *Eur. J. Neurosci.* **16:** 1295–1304

Deister C & Schmidt CE (2006) Optimizing neurotrophic factor combinations for neurite outgrowth. *J. Neural Eng.* **3:** 172–9

Dent EW & Gertler FB (2003) Cytoskeletal dynamics and transport in growth cone motility and axon guidance. *Neuron* **40:** 209–27

Deryugina EI, Ratnikov B, Monosov E, Postnova TI, DiScipio R, Smith JW & Strongin a Y (2001) MT1-MMP initiates activation of pro-MMP-2 and integrin alphavbeta3 promotes maturation of MMP-2 in breast carcinoma cells. *Exp. Cell Res.* **263:** 209–23

Dickson BJ (2002) Molecular mechanisms of axon guidance. *Science* **298:** 1959–64

Diekmann H, Kalbhen P & Fischer D (2015) Characterization of optic nerve regeneration using transgenic zebrafish. *Front. Cell. Neurosci.* **9:** 1–11

Dittrich F, Theonen H & Sendtner M (1994) Ciliary neurotrophic factor: pharmacokinetics and acute-phase response in rat. *Ann. Neurol.* **35:** 151–63

Domeniconi M, Cao Z, Spencer T, Sivasankaran R, Wang KC, Nikulina E, Kimura N, Cai H, Deng K, Gao Y, He Z, Filbin MT, Avenue P & York N (2002) Myelin-Associated Glycoprotein Interacts with the Nogo66 Receptor to Inhibit Neurite Outgrowth. *Neuron* **35:** 283–290

Duchossoy Y, Horvat JC & Stettler O (2001) MMP-related gelatinase activity is strongly induced in scar tissue of injured adult spinal cord and forms pathways for ingrowing neurites. *Mol. Cell. Neurosci.* **17:** 945–56

Erskine L & Herrera E (2007) The retinal ganglion cell axon's journey: insights into molecular mechanisms of axon guidance. *Dev. Biol.* **308:** 1–14

Ertürk A, Becker K, Jährling N, Mauch CP, Hojer CD, Egen JG, Hellal F, Bradke F, Sheng M & Dodt H (2012a) Three-dimensional imaging of solvent-cleared organs using 3DISCO. *Nat. Protoc.* **7:** 1983–1995

Ertürk A, Mauch CP, Hellal F, Förstner F, Keck T, Becker K, Jährling N, Steffens H, Richter M, Hübener M, Kramer E, Kirchhoff F, Dodt HU & Bradke F (2012b) Three-dimensional imaging of the unsectioned adult spinal cord to assess axon regeneration and glial responses after injury. *Nat. Med.* **18:** 166–71

Esparza BJ, Vilardell C, Calvo J, Juan M, Vives J, Yagu J & Cid MC (2015) Fibronectin Upregulates Gelatinase B (MMP-9) and Induces Coordinated Expression of Gelatinase A (MMP-2) and Its Activator MT1-MMP (MMP-14) by Human T Lymphocyte Cell Lines. A Process Repressed Through RAS/MAP Kinase Signaling Pathways. *Blood* **94:** 2754–66

Ethell IM & Ethell DW (2007) Review Matrix Metalloproteinases in Brain Development and Remodeling : Synaptic Functions and Targets. *J. Neurosci. Res.* **85:** 2813–23

Filbin MT (2003) Myelin-associated inhibitors of axonal regeneration in the adult mammalian CNS. *Nat. Rev. Neurosci.* **4:** 703–13

Fischer D, He Z & Benowitz LI (2004a) Counteracting the Nogo receptor enhances optic nerve regeneration if retinal ganglion cells are in an active growth state. *J. Neurosci.* **24:** 1646–51

Fischer D, Petkova V, Thanos S & Benowitz LI (2004b) Switching mature retinal ganglion cells to a robust growth state in vivo: gene expression and synergy with RhoA inactivation. *J. Neurosci.* **24:** 8726–40

Fitch MT & Silver J (2008) CNS injury, glial scars, and inflammation: Inhibitory extracellular matrices and regeneration failure. *Exp. Neurol.* **209:** 294–301

Fournier AE, Grandpre T & Strittmatter SM (2001) Identification of a receptor mediating Nogo-66 inhibition of axonal regeneration. *Nature* **409:** 341–6

Fu Y-Y, Lu C-H, Lin C-W, Juang J-H, Enikolopov G, Sibley E, Chiang A-S & Tang S-C (2010) Three-dimensional optical method for integrated visualization of mouse islet microstructure and vascular network with subcellular-level resolution. *J. Biomed. Opt.* **15:** 046018

Fu Y-Y, Peng S-J, Lin H-Y, Pasricha PJ & Tang S-C (2013) 3-D imaging and illustration of mouse intestinal neurovascular complex. *Am. J. Physiol. Gastrointest. Liver Physiol.* **304:** G1–11

Galis ZS, Kranzhofer R, Fenton JW & Libby P (1997) Thrombin Promotes Activation of Matrix Metalloproteinase-2 Produced by Cultured Vascular Smooth Muscle Cells. *Arterioscler. Thromb. Vasc. Biol.* **17:** 483–489

Gaublomme D, Buyens T, De Groef L, Stakenborg M, Janssens E, Ingvarsen S, Porse A, Behrendt N & Moons L (2014) Matrix metalloproteinase 2 and membrane type 1 matrix metalloproteinase co-regulate axonal outgrowth of mouse retinal ganglion cells. *J. Neurochem.* **129:** 966–79

Geerearts E, Dekeyster E & Moons L Automated neuronal counting in retinal whole mounts: ImageJ as a free-to-use tool for retinal ganglion cell quantification.

Goldberg JL, Klassen MP, Hua Y & Barres B a (2002) Amacrine-signaled loss of intrinsic axon growth ability by retinal ganglion cells. *Science* **296:** 1860–4

Grandpré T, Nakamura F, Vartanian T & Strittmatter SM (2000) Identification of the Nogo inhibitor of axon regeneration as a Reticulon protein. *Lett. to Nat.* **403:** 439–44

De Groef L, Gaublomme D, Janssens E, Dekeyster E & Moons L (2012) Retinal MMP expression is upregulated in an excitotoxic mouse model of glaucoma. *Acta Ophthalmol.* **11:** 4657 x

De Groef L, Van Hove I, Dekeyster E, Stalmans I & Moons L (2014) MMPs in the neuroretina and optic nerve: modulators of glaucoma pathogenesis and repair? *Invest. Ophthalmol. Vis. Sci.* **55:** 1953–64

De Groef L, Lemmens K, Van Hove I & Moons L Matrix metalloproteinases in the mouse retina: a comparative study of expression patterns and MMP-2 antibodies. *J. Histochem. Cytochem.*

Gross J & Lapiere CM (1962) brane model in which such a phenomenon might be observed , and that thus far the binding energies agree satisfactorily with those calculated from in vivo experiments only when the model contains lipid . In so far as we understand the behavior of the tial. *Proc. Natl. Acad. Sci. U. S. A.* **48:** 1014–1022

Haenold R, Weih F, Herrmann K-H, Schmidt K-F, Krempler K, Engelmann C, Nave K-A, Reichenbach JR, Löwel S, Löwel S, Witte OW & Kretz A (2014) NF-κB controls axonal regeneration and degeneration through cell-specific balance of RelA and p50 in the adult CNS. *J. Cell Sci.* **127:** 3052–65

Hama H, Kurokawa H, Kawano H, Ando R, Shimogori T, Noda H, Fukami K, Sakaue-Sawano A & Miyawaki A (2011) Scale: a chemical approach for fluorescence imaging and reconstruction of transparent mouse brain. *Nat. Neurosci.* **14:** 1481–8

Haupt C & Huber AB (2008) How axons see their way-axonal guidance in the visual system. *Front. Biosci.* **13:** 3136–3149

Hehr CL, Hocking JC & McFarlane S (2005) Matrix metalloproteinases are required for retinal ganglion cell axon guidance at select decision points. *Development* **132:** 3371–9

Hernandez-Barrantes S, Toth M, Bernardo M, Yurkova M, Gervasi DC, Raz Y, Sang QA & Fridman R (2000) Binding of Active (57 kDa) Membrane Type 1-Matrix Metalloproteinase (MT1-MMP) to Tissue Inhibitor of Metalloproteinase (TIMP)-2 Regulates MT1-MMP Processing and Pro-MMP-2 Activation. *J. Biol. Chem.* **275:** 12080–9

Herrera E, Brown L, Aruga J, Rachel R a, Dolen G, Mikoshiba K, Brown S & Mason C a (2003) Zic2 patterns binocular vision by specifying the uncrossed retinal projection. *Cell* **114:** 545–57

Hildebrand GD & Fielder AR (2011) Anatomy and Physiology of the Retina. In *Pediatric Retina*, Reynolds J & Olitsky S (eds) pp 39–65. Berlin, Heidelberg: Springer Berlin Heidelberg

Holmbeck K, Bianco P, Caterina J, Yamada S, Kromer M, Kuznetsov SA, Mankani M, Robey PG, Poole AR, Pidoux I, Ward JM, Birkedal-hansen H, Sapienza U La, Aquila U & Aquila L (1999) MT1-MMP-Deficient Mice Develop Dwarfism , Osteopenia , Arthritis , and Connective Tissue Disease due to Inadequate Collagen Turnover. *Cell* **99:** 81–92

Hübener M (2003) Mouse visual cortex. *Curr. Opin. Neurobiol.* **13:** 413–420

Huber AB, Kolodkin AL, Ginty DD & Cloutier J-F (2003) Signaling at the growth cone: ligand-receptor complexes and the control of axon growth and guidance. *Annu. Rev. Neurosci.* **26:** 509–63

Huber AB, Weinmann O, Bro C, Oertle T & Schwab ME (2002) Patterns of Nogo mRNA and Protein Expression in the Developing and Adult Rat and After CNS Lesions. *J. fo Neurosci.* **22:** 3553–67

Imayoshi I, Sakamoto M & Kageyama R (2011) Genetic methods to identify and manipulate newly born neurons in the adult brain. *Front. Neurosci.* **5:** 64

Ingvarsen S, Porse A, Erpicum C, Maertens L, Jürgensen HJ, Madsen DH, Melander MC, Gårdsvoll H, Høyer-Hansen G, Noel A, Holmbeck K, Engelholm LH & Behrendt N (2013) Targeting a single function of the multifunctional matrix metalloprotease MT1-MMP: impact on lymphangiogenesis. *J. Biol. Chem.* **288:** 10195–204

Ishida Y, Kuninaka Y, Nosaka M, Kimura A, Kawaguchi T, Hama M, Sakamoto S, Shinozaki K, Eisenmenger W & Kondo T (2015) Immunohistochemical analysis on MMP-2 and MMP-9 for wound age determination. *Int. J. Legal Med.* **March:** 1–6

Itoh T, Ikeda T, Gomi H, Nakao S, Suzuki T & Itohara S (1997) Unaltered Secretion of -Amyloid Precursor Protein in Gelatinase A (Matrix Metalloproteinase 2)-deficient Mice. *J. Biol. Chem.* **272:** 22389–22392

Janssens E, Gaublomme D, De Groef L, Darras VM, Arckens L, Delorme N, Claes F, Van Hove I & Moons L (2013) Matrix metalloproteinase 14 in the zebrafish: an eye on retinal and retinotectal development. *PLoS One* **8:** e52915

Jeon C, Strettoi E & Masland RH (1998) The Major Cell Populations of the Mouse Retina. *Jounal Neurosci.* **18:** 8936–46

Jiang LI, Sternweis PC & Wang JE (2013) Zymosan activates protein kinase A via adenylyl cyclase VII to modulate innate immune responses during inflammation. *Mol. Immunol.* **54:** 14–22

Jin G, Zhang F, Chan KM, Xavier Wong HL, Liu B, Cheah KSE, Liu X, Mauch C, Liu D & Zhou Z (2011) MT1-MMP cleaves Dll1 to negatively regulate Notch signalling to maintain normal B-cell development. *EMBO J.* **30:** 2281–93

Ke M, Fujimoto S & Imai T (2013) SeeDB : a simple and morphology-preserving optical clearing agent for neuronal circuit reconstruction. *Nat. Neurosci.***:** 1–9

Klimczak RR, Koerber JT, Dalkara D, Flannery JG & Schaffer D V (2009) A novel adeno-associated viral variant for efficient and selective intravitreal transduction of rat Müller cells. *PLoS One* **4:** e7467

Kurimoto T, Yin Y, Habboub G, Gilbert H-Y, Li Y, Nakao S, Hafezi-Moghadam A & Benowitz LI (2013) Neutrophils express oncomodulin and promote optic nerve regeneration. *J. Neurosci.* **33:** 14816–24

Kurimoto T, Yin Y, Omura K, Gilbert H, Kim D, Cen L-P, Moko L, Kügler S & Benowitz LI (2010) Long-distance axon regeneration in the mature optic nerve: contributions of oncomodulin, cAMP, and pten gene deletion. *J. Neurosci.* **30:** 15654–63

Kvanta A, Sarman S, Fagerholm P, Seregard S & Steen B (2000) Expression of Matrix Metalloproteinase-2 (MMP-2) and Vascular Endothelial Growth Factor (VEGF) in Inflammation-associated. *Exp. Eye Res.* **70:** 419–428

Lambot M-A, Depasse F, Noel J-C & Vanderhaeghen P (2005) Mapping labels in the human developing visual system and the evolution of binocular vision. *J. Neurosci.* **25:** 7232–7

Leaver SG, Cui Q, Plant GW, Arulpragasam A, Hisheh S, Verhaagen J & Harvey a R (2006) AAV-mediated expression of CNTF promotes long-term survival and regeneration of adult rat retinal ganglion cells. *Gene Ther.* **13:** 1328–41

Leibinger M, Müller A, Andreadaki A, Hauk TG, Kirsch M & Fischer D (2009) Neuroprotective and axon growth-promoting effects following inflammatory stimulation on mature retinal ganglion cells in mice depend on ciliary neurotrophic factor and leukemia inhibitory factor. *J. Neurosci.* **29:** 14334–41

Lemmens K, De Groef L, Van Hove I, Dekeyster E & Moons L (2015) Biphasic expression pattern of MMP-14 in the zebrafish retina during optic nerve regeneration. *Prep.*

Leon S, Yin Y, Nguyen J, Irwin N & Benowitz LI (2000) Lens injury stimulates axon regeneration in the mature rat optic nerve. *J. Neurosci.* **20:** 4615–26

Leone DP, Genoud S téphan., Atanasoski S, Grausenburger R, Berger P, Metzger D, Macklin WB, Chambon P & Suter U (2003) Tamoxifen-inducible glia-specific Cre mice for somatic mutagenesis in oligodendrocytes and Schwann cells. *Mol. Cell. Neurosci.* **22:** 430–440

Levkovitch-Verbin H (2004) Animal models of optic nerve diseases. *Eye (Lond).* **18:** 1066–74

De Lima S, Habboub G & Benowitz LI (2012) Combinatorial therapy stimulates long-distance regeneration, target reinnervation, and partial recovery of vision after optic nerve injury in mice. *Int. Rev. Neurobiol.* **106:** 153–72

Limb GA, Daniels JT, Pleass R, Charteris DG, Luthert PJ & Khaw PT (2002) Differential Expression of Matrix Metalloproteinases 2 and 9 by Glial Müller Cells. *Am. J. Pathol.* **160:** 1847–1855

Liu BP, Fournier A, GrandPré T & Strittmatter SM (2002) Myelin-associated glycoprotein as a functional ligand for the Nogo-66 receptor. *Science* **297:** 1190–3

Loers G, Makhina T, Bork U, Dörner A, Schachner M & Kleene R (2012) The interaction between cell adhesion molecule L1, matrix metalloproteinase 14, and adenine nucleotide translocator at the plasma membrane regulates L1-mediated neurite outgrowth of murine cerebellar neurons. *J. Neurosci.* **32:** 3917–30

Lorber B, Berry M, Douglas MR, Nakazawa T & Logan A (2009) Activated retinal glia promote neurite outgrowth of retinal ganglion cells via apolipoprotein E. *J. Neurosci. Res.* **87:** 2645–52

Lorber B, Berry M & Logan A (2005) Lens injury stimulates adult mouse retinal ganglion cell axon regeneration via both macrophage- and lens-derived factors. *Eur. J. Neurosci.* **21:** 2029–34

Lorber B, Guidi A, Fawcett JW & Martin KR (2012) Activated retinal glia mediated axon regeneration in experimental glaucoma. *Neurobiol. Dis.* **45:** 243–52

Lowery LA & Van Vactor D (2009) The trip of the tip: understanding the growth cone machinery. *Nat. Rev. Mol. Cell Biol.* **10:** 332–43

Luo X, Salgueiro Y, Beckerman SR, Lemmon VP, Tsoulfas P & Park KK (2013) Three-dimensional evaluation of retinal ganglion cell axon regeneration and pathfinding in whole mouse tissue after injury. *Exp. Neurol.* **247:** 653–62

Luttun A, Lutgens E, Manderveld A, Maris K, Collen D, Carmeliet P & Moons L (2004) Loss of matrix metalloproteinase-9 or matrix metalloproteinase-12 protects apolipoprotein E-deficient mice against atherosclerotic media destruction but differentially affects plaque growth. *Circulation* **109:** 1408–14

Martini FH, Nath JL & Bartholomew EF (2014) Fundamentals of Anatomy and Physiology Tenth. Pearson

Mccurley AT & Callard G V (2010) Time Course Analysis of Gene Expression Patterns in Zebrafish Eye During Optic Nerve Regeneration. *J. Exp. Neurosci.* **2010:** 17–33

Mori T, Tanaka K, Buffo A & Wurst W (2006) Inducible Gene Deletion in Astroglia and Radial Glia — A Valuable Tool for Functional and Lineage Analysis Generation of Mice. *Glia* **54:** 21–34

Morrison CJ, Butler GS, Bigg HF, Roberts CR, Soloway PD & Overall CM (2001) Cellular activation of MMP-2 (gelatinase A) by MT2-MMP occurs via a TIMP-2-independent pathway. *J. Biol. Chem.* **276:** 47402–10

Moy AJ, Wiersma MP & Choi B (2013) Optical histology: a method to visualize microvasculature in thick tissue sections of mouse brain. *PLoS One* **8:** e53753

Nadal-Nicolás FM, Jiménez-López M, Sobrado-Calvo P, Nieto-López L, Cánovas-Martínez I, Salinas-Navarro M, Vidal-Sanz M & Agudo M (2009) Brn3a as a marker of retinal ganglion cells: qualitative and quantitative time course studies in naive and optic nerve-injured retinas. *Invest. Ophthalmol. Vis. Sci.* **50:** 3860–8

Nadal-Nicolás FM, Salinas-Navarro M, Vidal-Sanz M & Agudo-Barriuso M (2015) Two methods to trace retinal ganglion cells with fluorogold: from the intact optic nerve or by stereotactic injection into the optic tract. *Exp. Eye Res.* **131:** 12–9

Nagase H, Visse R & Murphy G (2006) Structure and function of matrix metalloproteinases and TIMPs. *Cardiovasc. Res.* **69:** 562–73

Nagy A (2000) Cre recombinase: the universal reagent for genome tailoring. *Genesis* **26:** 99–109

Nakagawa S, Brennan C, Johnson KG, Shewan D, Harris W a & Holt CE (2000) Ephrin-B regulates the Ipsilateral routing of retinal axons at the optic chiasm. *Neuron* **25:** 599–610

Nguyen M (2000) Activated Protein C Directly Activates Human Endothelial Gelatinase A. *J. Biol. Chem.* **275:** 9095–9098

Okada T, Ichikawa M, Tokita Y, Horie H, Saito K, Yoshida J & Watanabe M (2005) Intravitreal macrophage activation enables cat retinal ganglion cells to regenerate injured axons into the mature optic nerve. *Exp. Neurol.* **196:** 153–63

Overall CM, Tam E, McQuibban G a, Morrison C, Wallon UM, Bigg HF, King a E & Roberts CR (2000) Domain interactions in the gelatinase A.TIMP-2.MT1-MMP activation complex. The ectodomain of the 44-kDa form of membrane type-1 matrix metalloproteinase does not modulate gelatinase A activation. *J. Biol. Chem.* **275:** 39497–506

Overall CM, Wranag L & Sodek J (1991) Transcriptional and Post-transcriptional Regulation of 72-kDa Gelatinase / Type IV Collagenase by Transforming Growth Factor-beta1 in Human Fibroblasts. *J. Biol. Chem.* **266:** 14064–71

Page-McCaw A, Ewald AJ & Werb Z (2007) Matrix metalloproteinases and the regulation of tissue remodelling. *Nat. Rev. Mol. Cell Biol.* **8:** 221–33

Park K, Liu K, Hu Y, Smith P, Wang C, Cai B, Xu B, Connolly L, Kramvis I, Sahin M & He Z (2008) Promoting Axon Regeneration in the Adult CNS by Modulation of the PTEN/mTOR Pathway. *Science (80-.).* **322:** 963–66

Park KK, Liu K, Hu Y, Kanter JL & He Z (2010) PTEN/mTOR and axon regeneration. *Exp. Neurol.* **223:** 45–50

Pastrana E, Moreno-Flores MT, Gurzov EN, Avila J, Wandosell F & Diaz-Nido J (2006) Genes associated with adult axon regeneration promoted by olfactory ensheathing cells: a new role for matrix metalloproteinase 2. *J. Neurosci.* **26:** 5347–59

Pernet V, Joly S, Dalkara D, Jordi N, Schwarz O, Christ F, Schaffer D V, Flannery JG & Schwab ME (2013a) Long-distance axonal regeneration induced by CNTF gene transfer is impaired by axonal misguidance in the injured adult optic nerve. *Neurobiol. Dis.* **51:** 202–13

Pernet V, Joly S, Jordi N, Dalkara D, Guzik-Kornacka A, Flannery JG & Schwab ME (2013b) Misguidance and modulation of axonal regeneration by Stat3 and Rho/ROCK signaling in the transparent optic nerve. *Cell Death Dis.* **4:** e734

Pernet V & Polo A Di (2006) Synergistic action of brain-derived neurotrophic factor and lens injury promotes retinal ganglion cell survival , but leads to optic nerve dystrophy in vivo. *Brain* **129:** 1014–26

Perry VH (1981) Evidence for an Amacrine Cell System in the Ganglion Cell Layer of the Rat Retina. *Neuroscience* **6:** 931–44

Prinjha R, Moore S, Vinson M, Blake S, Morrow R, Christie G & Michalovich D (2000) Inhibitor of neurite outgrowth in humans. *Nature* **403:** 383–384

Purves D, Augustine GJ, Fitzpatrick D, Hall WC, LaMantia A-S, McNamara JO & Williams SM (2004) Neuroscience

Remington LA (2011) Clinical Anatomy of the Visual System

Rivera S, Khrestchatisky M, Kaczmarek L, Rosenberg G a & Jaworski DM (2010) Metzincin proteases and their inhibitors: foes or friends in nervous system physiology? *J. Neurosci.* **30:** 15337–57

Rodriguez AR, Müller LP & Brecha NC (2014) The RNA binding protein RBPMS is a selective marker of ganglion cells in the mammalian retina. *J. Comp. Neurol.* **522:** 1411–43

Sakamoto T & Seiki M (2009) Cytoplasmic tail of MT1-MMP regulates macrophage motility independently from its protease activity. *Genes Cells* **14:** 617–26

Salinas-Navarro M, Jiménez-López M, Valiente-Soriano FJ, Alarcón-Martínez L, Avilés-Trigueros M, Mayor S, Holmes T, Lund RD, Villegas-Pérez MP & Vidal-Sanz M (2009) Retinal ganglion cell population in adult albino and pigmented mice: a computerized analysis of the entire population and its spatial distribution. *Vision Res.* **49:** 637–47

Santi PA (2011) Light sheet fluorescence microscopy: a review. *J. Histochem. Cytochem.* **59:** 129–38

Schwab ME (2010) Functions of Nogo proteins and their receptors in the nervous system. *Nat. Rev. Neurosci.* **11:** 799–811

Schwob JE (2002) Neural regeneration and the peripheral olfactory system. *Anat. Rec.* **269:** 33–49

Sernagor E, Eglen SJ & Wong RO. (2001) Development of Retinal Ganglion Cell Structure and Function. *Prog. Retin. Eye Res.* **20:** 139–174

Silver J & Miller JH (2004) Regeneration beyond the glial scar. *Nat. Rev. Neurosci.* **5:** 146–56

Slezak M, Oritz CG, Niemiec A, En JF, Chambon P, Metzger D & Pfrieger FW (2007) Transgenic Mice for Conditional Gene Manipulation in Astroglial Cells. *Glia* **55:** 1565–76

Smith PD, Sun F, Park KK, Cai B, Wang C, Kuwako K, Martinez-Carrasco I, Connolly L & He Z (2009) SOCS3 deletion promotes optic nerve regeneration in vivo. *Neuron* **64:** 617–23

Sperry RW (1963) Chemoaffinity in the Orderly Growth of Nerve Fiver Patterns and Connections. *Proc. Natl. Acad. Sci.* **50:** 703–10

Standring S (2008) Gray 's Anatomy

Sternlicht MD & Werb Z (2001) How Matrix Metalloproteinases Regulate Cell Behaviour. *Annu. Rev. Cell Dev. Biol.* **17:** 463–516

Strongin AY, Collier I, Bannikov G, Marmer BL, Grant GA & Goldberg GI (1995) Mechanism of Cell Surface Activation of 72-kDa Type IV Collagenase. *J. Biol. Chem.* **270:** 5331–8

Sun F, Park KK, Belin S, Wang D, Lu T, Chen G, Zhang K, Yeung C, Feng G, Yankner B a & He Z (2011) Sustained axon regeneration induced by co-deletion of PTEN and SOCS3. *Nature* **480:** 372–5

Sung M, Wei E, Chavez E, Jain N, Levano S, Binkert L, Ramseier A, Setz C, Bodmer D, Ryan AF & Brand Y (2014) Inhibition of MMP-2 but not MMP-9 influences inner ear spiral ganglion neurons in vitro. *Cell. Mol. Neurobiol.* **34:** 1011–21

Susaki EA, Tainaka K, Perrin D, Kishino F & Tawara T (2014) Resource Whole-Brain Imaging with Single-Cell Resolution Using Chemical Cocktails and Computational Analysis. *Cell* **157:** 726–739

Tang S-C, Chiu Y-C, Hsu C-T, Peng S-J & Fu Y-Y (2013) Plasticity of Schwann cells and pericytes in response to islet injury in mice. *Diabetologia* **56:** 2424–2434

Templeton JP & Geisert EE (2012) A practical approach to optic nerve crush in the mouse. *Mol. Vis.* **18:** 2147–52

Teng FYH & Tang BL (2006) Axonal regeneration in adult CNS neurons--signaling molecules and pathways. *J. Neurochem.* **96:** 1501–8

Thanos S, Böhm MRR, Schallenberg M & Oellers P (2012) Traumatology of the optic nerve and contribution of crystallins to axonal regeneration. *Cell Tissue Res.* **349:** 49–69

Tkatchenko T V, Shen Y & Tkatchenko A V (2010) Analysis of postnatal eye development in the mouse with high-resolution small animal magnetic resonance imaging. *Invest. Ophthalmol. Vis. Sci.* **51:** 21–7

Toth M, Osenkowski P, Hesek D, Brown S, Meroueh S, Sakr W, Mobashery S & Fridman, R (2005) Cleavage at the stem region releases an active ectodomain of the membrane type 1 matrix metalloproteinase. *Biochem. J.* **387:** 497–506

Toth M, Sohail A & Fridman R (2012) Assessment of Gelatinases (MMP-2 and MMP-9) by gelatin zymography. In *Metastasis Research Protocols*, Dwek M Brooks SA & Schumacher U (eds) pp 121–135. Totowa, NJ: Humana Press

Venkatesh K, Chivatakarn O, Lee H, Joshi PS, Kantor DB, Newman B a, Mage R, Rader C & Giger RJ (2005) The Nogo-66 receptor homolog NgR2 is a sialic acid-dependent receptor selective for myelin-associated glycoprotein. *J. Neurosci.* **25:** 808–22

Verslegers M, Van Hove I, Dekeyster E, Gantois I, Hu T-T, D'Hooge R, Arckens L & Moons L (2014) MMP-2 mediates Purkinje cell morphogenesis and spine development in the mouse cerebellum. *Brain Struct. Funct.*

Verslegers M, Lemmens K, Van Hove I & Moons L (2013) Matrix metalloproteinase-2 and -9 as promising benefactors in development, plasticity and repair of the nervous system. *Prog. Neurobiol.* **105:** 60–78

Visse R & Nagase H (2003) Matrix metalloproteinases and tissue inhibitors of metalloproteinases: structure, function, and biochemistry. *Circ. Res.* **92:** 827–39

Wang KC, Kim JA & Sivasankaran R (2002) p75 interacts with the Nogo receptor as a co-receptor for Nogo , MAG and OMgp. *Nature* **420:** 97–101

Waterston RH, Lindblad-Toh K, Birney E, Rogers J, Abril JF, Agarwal P, Agarwala R, Ainscough R, Alexandersson M, An P, Antonarakis SE, Attwood J, Baertsch R, Bailey J, Barlow K, Beck S, Berry E, Birren B, Bloom T, Bork P, et al (2002) Initial sequencing and comparative analysis of the mouse genome. *Nature* **420:** 520–62

Webber C a, Hocking JC, Yong VW, Stange CL & McFarlane S (2002) Metalloproteases and guidance of retinal axons in the developing visual system. *J. Neurosci.* **22:** 8091–100

Wehrle R, Camand E, Chedotal A, Sotelo C & Dusart I (2005) Expression of netrin-1, slit-1 and slit-3 but not of slit-2 after cerebellar and spinal cord lesions. *Eur. J. Neurosci.* **22:** 2134–44

Yamashita T & Tohyama M (2003) The p75 receptor acts as a displacement factor that releases Rho from Rho-GDI. *Nat. Neurosci.* **6:** 461–7

Yan C & Boyd DD (2006) Regulation of Matrix Metalloproteinase Gene. *Cell. Physiol.***:** 19–26

Yin Y, Cui Q, Gilbert H, Yang Y, Yang Z, Berlinicke C & Li Z (2009) Oncomodulin links inflammation to optic. *Proc. Natl. Acad. Sci. U. S. A.* **106:** 19587–92

Yin Y, Cui Q, Li Y, Irwin N, Fischer D, Harvey AR & Benowitz LI (2003) Macrophage-Derived Factors Stimulate Optic Nerve Regeneration. *J. Neurosci.* **23:** 2284–93

Yin Y, Henzl MT, Lorber B, Nakazawa T, Thomas TT, Jiang F, Langer R & Benowitz LI (2006) Oncomodulin is a macrophage-derived signal for axon regeneration in retinal ganglion cells. *Nat. Neurosci.* **9:** 843–52

Yong VW, Power C, Forsyth P & Edwards DR (2001) Metalloproteinases in biology and pathology of the nervous system. *Nat. Rev. Neurosci.* **2:** 502–11

Young P, Qiu L, Wang D, Zhao S, Gross J & Feng G (2008) Single-neuron labeling with inducible Cre-mediated knockout in transgenic mice. *Nat. Neurosci.* **11:** 721–8

Zhang X (2004) Kainic Acid-Mediated Upregulation of Matrix Metalloproteinase-9 Promotes Retinal Degeneration. *Invest. Ophthalmol. Vis. Sci.* **45:** 2374–2383

Zhang Y, Klassen HJ, Tucker BA, Perez M-TR & Young MJ (2007) CNS progenitor cells promote a permissive environment for neurite outgrowth via a matrix metalloproteinase-2-dependent mechanism. *J. Neurosci.* **27:** 4499–506

Zheng B, Atwal J, Ho C, Case L, He X, Garcia KC, Steward O & Tessier-lavigne M (2005) Genetic deletion of the Nogo receptor does not reduce neurite inhibition in vitro or promote corticospinal tract regeneration in vivo. *Proc. Natl. Acad. Sci. U. S. A.* **102:** 1205–1210

Zucker S, Drews M, Foda HD, Declerck YA, Langley KE, Bahou WF, Andrew J, Docherty P, Cao J, Conner C & Docherty AJP (1998) Tissue Inhibitor of Metalloproteinase-2 (TIMP-2) Binds to the Catalytic Domain of the Cell Surface Receptor, Membrane Type 1-Matrix Metalloproteinase 1 (MT1-MMP). *J. Biol. Chem.* **273:** 1216–22

ADDENDA

ADDENDUM 1: BUFFERS AND OTHER SOLUTIONS

Citrate buffer 10x (pH=6,0)	100mM citric acid (Chemilab); 0,5% Tween-20; H_2O
DAPI	1x PBS; 0,002% DAPI (DAKO)
Destaining buffer	20ml acetic acid; 100ml ethanol; 80ml AD
Mowiol	12ml 0,2M Tris-HCl; 6g glycerol; 2,4g mowiol; 6ml MQ
PBS 10x (pH=7,4)	80mM $Na_2HPO_4.2H_2O$; 20mM KH_2PO_4; 1,5M NaCl; 30mM KCl
PBST	1x PBS; 0,5% triton X-100 (VWR)
PFA 4% (pH=7,4)	1x PBS; 0,1M PFA (Sigma)
Saline	1x PBS; 0,9% NaCl

SDS lysis buffer	65mM Tris-HCl; 2% SDS; EDTA free protein inhibitor cocktail (Roche Diagnostics)
Staining buffer	100ml methanol; 100ml AD; 0,2g Coomassie blue (R250; Aldrich chemical company)
TBS 10x (pH=7,6)	1M Tris-HCl; 1,5M NaCl; 0,015M triton X-100
TBS 1x (pH=7,4; Benowitz)	0,15M NaCl; 7,58g/l Trizma present crystals
TBS_2T 1x (pH=7,4; Benowitz)	0,30M NaCl; 7,58g/l Trizma present crystals; 2ml of 50% Tween-20
TNB	1x TBS; 0,5% blocking reagent (Perkin Elmer)
Tris 10x (pH=7,4)	0,5M Tris-HCl 1x PBS

ADDENDUM 2: RISK ANALYSIS

Experiments are not always without hazards, often, there is contact with physical, biological and chemical risks. Knowledge of the substances used in the experiments is essential to identify, assess and avoid potential risks. Therefore, it is vital that good laboratory practice is established and guidelines must be known and respected. These are found in the code of good laboratory practices (GLP). Most of the experiments are performed in a level L1 containment laboratory (non-pathogenic). In such facility, no pathogenic micro-organisms are used and there is a minimal risk for the environment. Wearing protective clothing like lab coat and gloves, is required during the procedures. Personal hygiene such as washing your hands after each experiment is of great importance. Eating, drinking or smoking are prohibited in the laboratory.

In the laboratory, a major physical risk is encountered with sharp objects. Needles, capillaries and knives should be disposed in the appropriate sharpsafe containers and recapping of the needles is forbidden. Knives on the cryostat should be handled carefully when replaced or manipulated. Also, working with instruments for surgical procedures should be done with caution. In the case of lacerations due to sharp objects, the wound must be thoroughly disinfected, rinsed and examined.

The only biological/physical risk of this project, is the model organism itself, namely the mouse. Scratch and bite wounds are a real risk for people who work with rodents. There is direct damage but also the risk of infection. Due to the irregular shape, these injuries are an extremely good culture to grow bacteria. The site of the bite (vascularization) and the extent of contamination (composition of mouth flora of rodent and skin flora of victim) determine the chance of infection. Some major infections after a rodent bite are *Streptobacillus moniliformis* and *Spirillium minus,* which can cause serious complications. After a bite, the victim should check the tetanus vaccination, have a doctor check the wound and have a veterinarian check the animal for specific diseases.

The chemical risk factor is the most significant category during this project. Next, the important hazards of the most relevant chemicals used in current study are described. Non-hazardous waste should be separated from hazardous waste. The chemical waste is divided into different waste categories. For each category, the necessary barrels should be present, provided with a label and a color code that indicate the nature of the contents.

To activate the Cre(ER)T2-LoxP system, TXF is administered. TXF is carcinogenic and is a reproductive hazard. It can harm the fertility of an unborn child and is harmful when ingested. It is obligated to wear a lab coat, safety goggles and double gloves. All the work surfaces have to be disinfected after the experiments. Anything that comes into contact with TXF has to be collected separately in waste category 6 and cleaned with javel. TXF is excreted via faeces and urine, therefore dirty bedding has to be disposed separately and cages have to be cleaned with javel.

The use of ketamine, xylazine and nembutal is written up in a logbook. These anesthetics are addictive for humans and can be used as drugs.

For the fixation of tissues, PFA was used. This is toxic and there are some indications that it may be carcinogenic. It can be irritating for the eyes and skin and cause irritation to the airways or lead to acute toxicity when ingested. Procedures must always be performed under the fume hood and PFA is collected separately in waste category 5.

For the optical clearing, THF, BA and BB are used. THF is highly flammable and can penetrate the skin which causes dehydration. After contact with oxygen, THF can form highly explosive peroxides. BABB is known to dissolve plastic, so all procedures with this solution are performed in glass bottles and under the fume hood. The stock solutions should be kept in a safety closet and collected separately in waste category 6.

During the IHC stainings, H_2O_2 is diluted in methanol. H_2O_2 is a strong oxidizing agent that can cause burns or explosions. Both substances are harmful when inhaled or swallowed and have to be kept away from combustible material. Methanol and H_2O_2 always have to be handled under the fume hood. Ethanol and methanol are flammable and can cause toxic effects when inhaled, ingested or during contact with skin or eyes. Also, Triton X-100 can cause serious harm to the eyes and after ingestion.

ADDENDUM 3: ANTIBODIES

Table 1: Overview of the antibodies used in western blotting.

Antibody	Species	Source	Protocol	Dilution (in TNB)
MT1-MMP marker				
RP3	Rabbit	Triple point	Western blotting	1:5000
Ab53712	Rabbit	Abcam	Western blotting	1:1000
MMP-2 marker				
MMP-2	Rabbit	Santa Cruz	Western blotting	1:100

Table 2: Overview of the blocking buffers used in this study.

Pre-immune serum	Host	Dilution (in TNB)
PIR	Rabbit	1:5
PID	Donkey	1:10
PIG	Goat	1:5

Table 3: Overview of the primary antibodies used in the immunohistochemical stainings.

Antibody	Species	Source	Protocol	Dilution (in TNB)
Regenerating axon marker				
GAP-43	Sheep	Novus Biologicals	Special protocol Cryosections ON	1:200
MMP-2 marker				
MMP-2	Rabbit	Millipore	Citrate buffer Long amplification Cryosections ON	1:200
RGC marker				
Brn3a	Goat	Santa Cruz	No pre-treatment Whole mount Retina	1:750

Table 4: Overview of the secondary antibodies used in this study.

Fluorophore	Species	Antigen	Source	Dilution (in TNB)
Anti-rabbit				
Alexa Fluor biotin	Goat	Rabbit	DAKO	1:300
Anti-sheep				
Alexa Fluor 594	Donkey	Sheep	Invitrogen	1:500
Anti-goat				
Alexa Fluor 568	Rabbit	Goat	Invitrogen	1:500

DIERENFYSIOLOGIE EN NEUROBIOLOGIE
Naamsestraat 61, bus B
3000 LEUVEN, BELGIË
tel. + 32 16 32 39 91
fax + 32 16 32 42 60
www.kuleuven.be